MSc Thesis Report

Settlement Predictions of The Noordtunnel
A Numerical Simulation

Prabendra Ardhan Atmakusuma

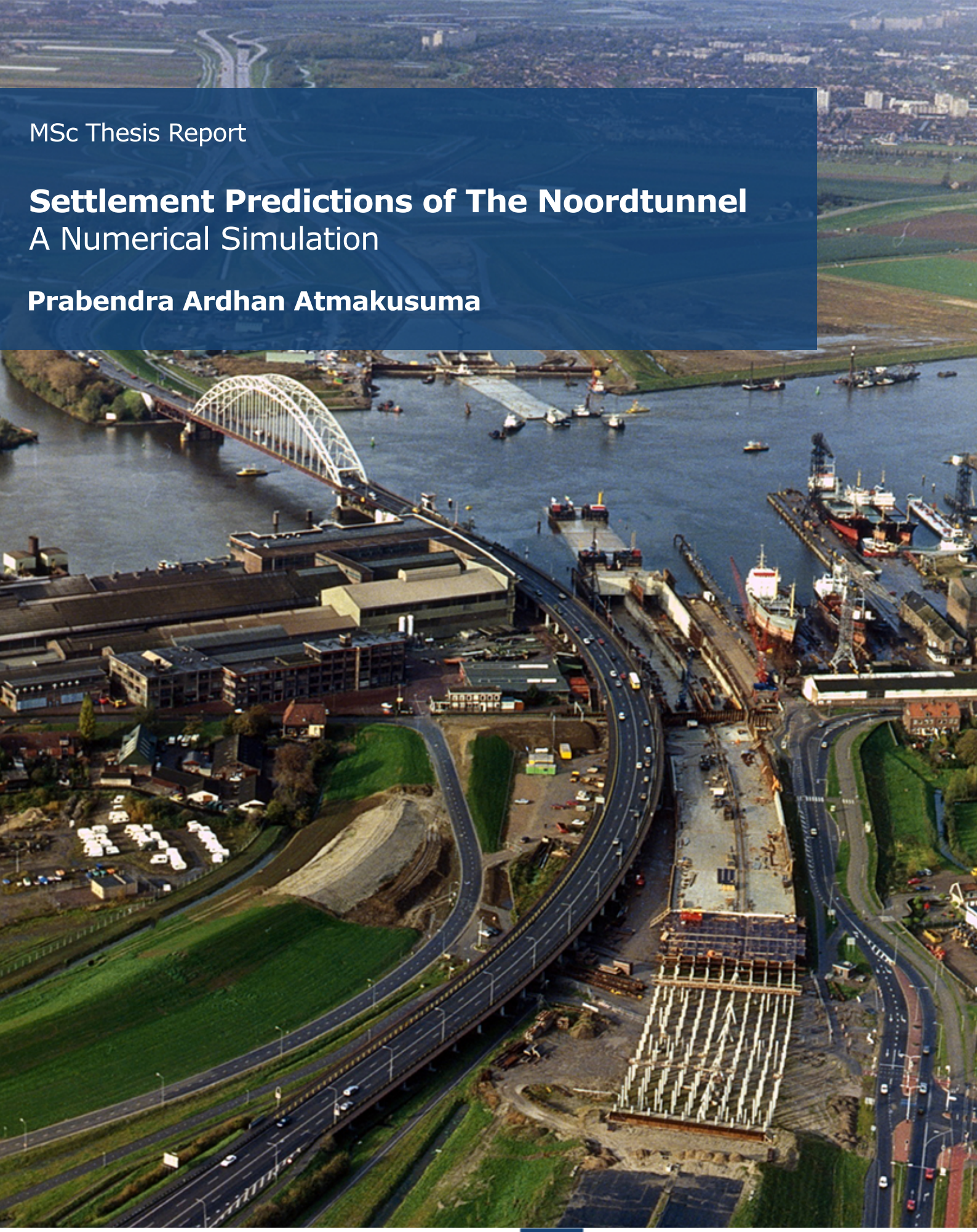

TU Delft

Rijkswaterstaat
Ministerie van Infrastructuur en Waterstaat

SETTLEMENT PREDICTIONS OF THE NOORDTUNNEL: A NUMERICAL SIMULATION

by

Prabendra Ardhan Atmakusuma
4807162

in partial fulfillment
of the requirements for the degree of

Master of Science
in Geo-Engineering
at the
Delft University of Technology

To be defended publicly on Wednesday, 13^{th} September 2023 at 10 : 00 CEST

Supervisors: Dr. ir. Wout Broere — TU Delft
Harry R.E. Dekker, M.Sc. — Rijkswaterstaat
Dr.ing. Mark Z. Voorendt — TU Delft
Xuehui Zhang, Ph.D. — TU Delft

Prabendra Ardhan Atmakusuma: *Settlement Predictions of The Noordtunnel: A Numerical Simulation* (2023)

to obtain the degree of Master of Science at the Delft University of Technology

The work in this thesis was carried out in the:

Geo-Engineering
Faculty of Civil Engineering & Geoscience
Delft University of Technology

This Research was supported by:

Indonesia Endowment Fund For Education
Ministry of Finance of The Republic of Indonesia

Rijkswaterstaat
Ministry of Infrastructure and Water Management

An electronic version of this thesis is available at http://repository.tudelft.nl/
Front cover: The Noordtunnel construction process (www.wegenwiki.nl).

ACKNOWLEDGMENT

Alhamdulillah, I would like to express my gratitude to the almighty Allah SWT for giving me the strength to complete my master's thesis. This report is the outcome of my unwavering efforts over the past eight months within the 'roller-coaster' journey of my master's study. Throughout this period, I committed myself to acquiring new knowledge, establishing valuable networks with some nice colleagues in The Rjikswaterstaat, and consistently working towards attaining the most optimal outcomes from this research project. Eight months may not fully encapsulate the quest for the finest research results. Nevertheless, I adhered to a rigorous schedule, ensuring that I continuously worked towards delivering the best work I could accomplish.

I would like to thank all committee members that directly involved in this research. The completion of this thesis could not have been possible without the expertise of my supervisors, Dr. Wout, Mr. Harry Dekker, Dr. Mark, and Xuehui. I would like to thank my chair supervisor, Dr. Wout Broere, for the supervision and support he provided in my master's research. To Mr. Harry and the Rijkswaterstaat colleague, thank you for opening the doors and providing me with the opportunity to work within their respected organization. Next, I want to express my gratitude to Dr. Mark who has given me valuable feedback to write a well-written report. Moreover, I would like to thank my daily supervisor, Xuehui, for the supervision and support over the last eight months. Thank you for letting me work in your office on the weekend.

Secondly, I wish to convey my boundless gratitude to my family. Thank you to my supportive parents, Bapak, Ibu, Papa, and Mama, who have prayed for me and always pushed me forward to pursue my dream. To my lovely wife and son, Rani and Naeem, thank you for your endless support. You all will always be my home. Also, for my brother and sister, Agung, Rafika, and Gita for your ceaseless support.

I would like to extend my gratitude to my employer The Ministry of Public Works and Housing of Indonesia for all of the support and opportunity. Moreover, it would not be possible to complete this study without financial support from The Indonesia Endowment Fund for Education (LPDP).

Last but not least, I would like to thank all of my colleagues, friends, and everyone who has lent their helping hands to me during my master's study and made it a valuable experience.

Prabendra Ardhan Atmakusuma
Delft, September 2023

ABSTRACT

The Noordtunnel is an immersed tunnel open to roadway service since 1990 in The Netherlands. Over the past thirty years of its operation time, a significant differential settlement behaviour has been observed, and this ongoing settlement potentially imposes safety concerns to the tunnel, such as joint leakage. However, the underlying factor triggering this differential settlement behavior remains unknown. To ensure the tunnel's serviceability, this thesis aims to investigate the underlying causes of the occurring excessive settlement, predict future settlements, and assess its impact on tunnel structural safety within its designed lifetime.

The analysis starts by reconstructing the settlement time history of the Noordtunnel. The process involves determining the most reliable reference point and performing back analysis to estimate the settlement magnitude during the unmeasured period. Further, the settlement history is reconstructed by combining all the settlement data of all the periods. It is found that the settlement history at all immersion joints show a logarithmic trendline, with a maximum estimated settlement of about 94.36 mm occurring at immersion joint 2. Subsequently, the soil profile and geotechnical parameters were determined for the simulation. The provided Cone Penetration Test (CPT)s data and borehole ensure the soil profile depicted in the given situation map. Additionally, in the absence of laboratory data, the Hardening Soil Model (HS Model) and Soft Soil Creep Model (SSC Model) parameters are estimated based on CPT - NEN Table 2b correlations.

Afterward, the Two Dimension (2D) Finite Element Method (FEM) simulations were carried out in PLAXIS (a commercial simulation software), while considering the variations of load acting on top of the subsoil. Two types of soil constitutive law were chosen to simulate the settlement in the Noordtunnel: HS Model and SSC Model. The optimum model, which can simulate the settlement behaviour in the field, was selected by aligning the simulation outcomes to the reconstructed historical settlement. The simulation results show that only settlement at immersion joint 2 has the same tendency as the SSC Model, while the other immersion joints tend to have a similar tendency to the HS Model. The simulation outcomes also indicate that excessive settlement at immersion joint 2 occurs due to the soft soil underneath the tunnel and the natural sedimentation on top of it. The soft soil is responsible for at least 20 mm of settlement, while the sedimentation contributes to a minimum of 8 mm of settlement during 30 years of tunnel operation. Subsequently, the sensitivity analysis is conducted to examine how much the simulation outcomes may deviate when accounting for soil variability in the field. Due to the narrow distribution of the reference values, adjusting the most sensitive parameter will only deviate the results by a maximum of 5.48% at immersion joint 2 and 4% at the other immersion joints. These results indicate that the model is robust enough and expected to generate reasonable future settlement predictions. An additional settlement of 15.13 mm of settlement is predicted to occur at immersion joint 2, while 4 to 5 mm of additional settlement is anticipated at the other immersion joints over the tunnel's remaining lifespan.

The differential settlement at the tunnel longitudinal direction has triggered element tilting and further induced compression and decompression to the GINA gasket at immersion joints. It has been observed that while uneven settlement contributes to joint decompression, the external forces acting on the GINA gasket remain considerably lower in magnitude compared to the overall friction force. Therefore, the impact of uneven settlement on the water tightness is generally minimal. Additionally, considering the limitations of the current monitoring procedure, an optimized monitoring plan based on the Distributed Optical Fiber Sensor (DOFS)

system is proposed. Finally, future recommendations to improve the current thesis are also put forward.

Keywords: Immersed tunnel, settlement, FEM, predictions, immersion joint, leakage

CONTENTS

1 INTRODUCTION

This chapter introduces the research motivation and problem addressed in the thesis, leading to the formulation of research questions. Further, it also details the research approach which describes the steps to answering the research question.

1.1 RESEARCH MOTIVATION

The Noordtunnel is an immersed tunnel that goes under the Noord River in the Netherlands. The tunnel is part of the A15 highway that connects Alblasserdam and Hendrik-Ido Ambacht in South Holland. Previously, before the tunnel was built, travellers crossed the Noord River via the adjacent arch bridge. However, during the 1970*s*, the traffic on A15 became busier, and traffic jams increased considerably. Therefore, the call for an alternative infrastructure to connect the two regions made Rijkswaterstaat decide to build the immersed tunnel. The construction started in 1989 and finished in 1991. During the construction phase, the dyke situated on the western side underwent a relocation towards the west.

Figure 1.1: The Noordtunnel under construction (SWECO, 2020)

The Noordtunnel consists of two traffic tubes with three lanes for each tube. An escape route in the middle of the structure separates the two traffic tubes. The tunnel consists of three main sections: immersed section, the west access ramp, and the east access ramp. The length of the immersed section is approximately 430 m. The west access ramp is 290 m long and was

built in a cofferdam after removing the dyke to the west. Conversely, a 550 m approach was constructed on top of piled foundation. Hence, the total length of the tunnel counting the access ramps is 1270 m. The immersion part of the Noordtunnel consists of 4 tunnel elements, where the westernmost element consists of four segments and the other elements consist of five segments each. A single tunnel section is 31.95 m wide, 8.02 m high, and 26.156 m long. The immersion phase of the tunnel started in October 1990 and finished in December 1990.

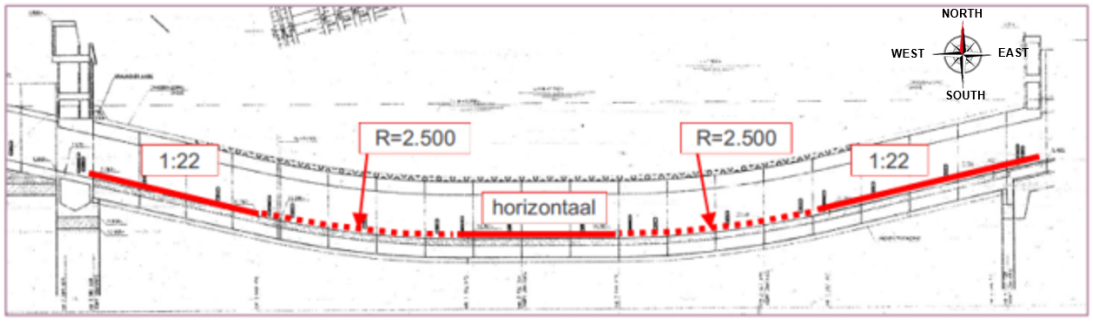

Figure 1.2: Longitudinal profile of the Noordtunnel (SWECO, 2020)

The construction stage of an immersed tunnel begins with excavating the trench. Afterwards, the foundation had installed, and the tunnel elements are placed in the riverbed to their intended position. Considering the unloading effects in the dredging stage, the weight of immersed tunnel and sand backfill above it is generally lighter than the original soil it replaces. Therefore, minimal settlements are expected. However, the Noordtunnel behaviour differs since the tunnel did not settle uniformly with immersion joint two encountering greater settlement than anticipated.

As settlements are often not uniform, excessive settlement increases the risk of uneven settlement. The differential settlement could cause large stress concentrations in tunnel structure, followed by local cracking, leakage, and deterioration of exposed rebar. It should be noted that some settlement is inevitable or inherent since making the soft ground a rigid body which would not cost-effective, if not impossible. Engineers have used numerical modelling to simulate the settlement of geotechnical structure. A good simulation will assist in the analysis so that settlement behaviour can be illustrated and predictions can become more accurate. However, applying numerical simulation to demonstrate immersed tunnel behaviour has been an enormous challenge for engineers. Despite SWECO (2020) initial attempt with limited success, this research aims to simulate the settlement behaviour of the Noordtunnel and compare the outcomes with the monitored settlements. Based on the simulation results, the settlements in the coming years can be predicted.

1.2 PROBLEM ANALYSIS

The settlement of the Noordtunnel was measured by fitting the measuring bolts to the top of the guide construction at the location of the immersion joint. The settlement was measured within two time-frame periods, namely in the first ten months after immersion was completed, and regular measurement from 17 September 1993 to 12 April 2019. Notably, there was no settlement measurement between 1991 and 1993, resulting in a gap in the monitoring data during that period. Moreover, concern has emerged over the reliability of regular measurements due to the uncertainty around the stability of the initial reference point, which is susceptible to fluctuations in temperature (SWECO, 2020).

Figure 1.3 depicts the measured settlement at all immersion joints from 17 September 1993 to 12 April 2019. Along the longitudinal profile of the Noordtunnel, non-uniform settlement patterns were observed, as depicted by the graph. In addition, the measured settlement values exceed the initially anticipated magnitudes, with the second immersion joint being particularly prominent with 31 mm of settlement.

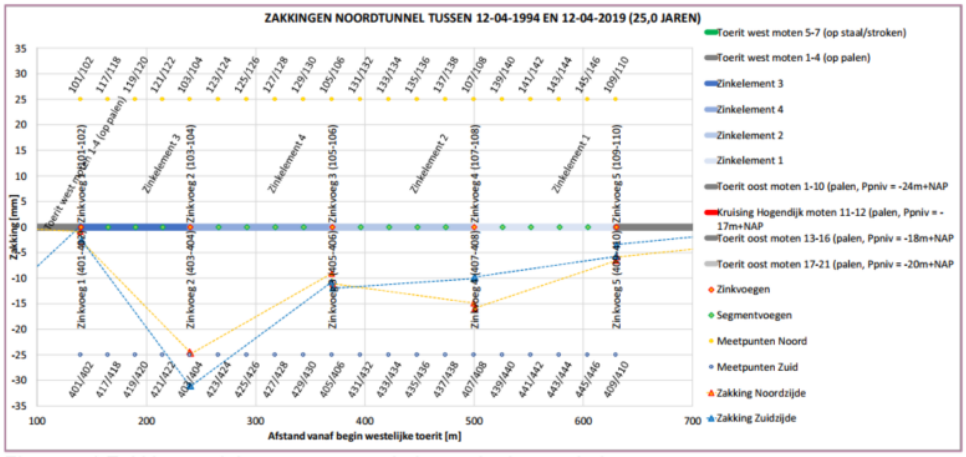

Figure 1.3: The settlements of the Noordtunnel over 25 years of operation (SWECO, 2020)

Figure 1.4 presents the settlement trendline of the second immersion joint investigated previously by SWECO (2020). The yellow dots represent the monitoring data, while the red, green, and purple dashed lines are the logarithmic fit and linear trendline, respectively.

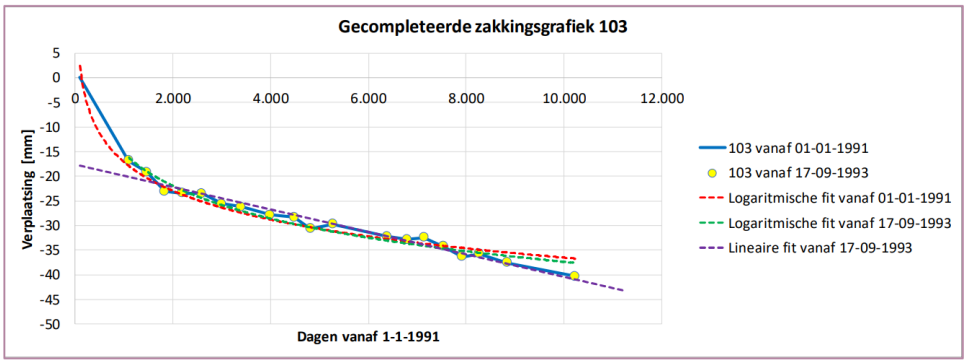

Figure 1.4: Linear settlement trendline at the second immersion joint (SWECO, 2020)

In the report, SWECO (2020) states that the excessive settlement at the second immersion joint fits the linear trendline. However, the cause behind this settlement behaviour remains unidentified, as mentioned in the same report. Therefore, in this research, a numerical simulation is conducted to determine the potential causes of excessive settlement in the Noordtunnel and predict its future settlement.

1.3 RESEARCH QUESTION

Based on the problems described in the prior section, the following main question and subquestions are formulated as follows:

"How to reasonably predict the future settlement of the Noordtunnel and assess its impact on structural safety?"

1. How to interpret the historic settlement of the Noordtunnel?
2. What are the accountable reasons that induced the local excessive settlement observed in the Noordtunnel?
3. Which geotechnical parameter has the most dominant influence on the settlement of the Noordtunnel?
4. How does the ongoing settlement impact the tunnel structural safety? And what measures can be conducted to optimize the present monitoring work and mitigate the structure's deterioration?

1.4 RESEARCH APPROACH

The primary objective of this study is to investigate the settlement behaviour of the Noordtunnel and make a reasonable prediction about its future settlement. To achieve this, several steps are taken:

1. Conduct the literature review.

   Literature reviews provide the foundation for comprehending theories and concepts related to the research subject. This section details the methodology employed to ascertain the soil parameters. Additionally, the fundamental insight into the construction process of the immersed tunnel is described and utilized as a foundation for the selection of subsoil constitutive law employed in the simulation, so that the model can reasonably reproduce the settlement patterns observed in practice.

2. Establish the settlement time-history of the Noordtunnel.

   To accomplish the research objective, it is essential to have a thorough understanding of what occurred with the Noordtunnel. The Noordtunnel's settlement history must be reconstructed. The process involves performing back analysis to determine the unrecorded settlement magnitude using linear regression and combining them with the regular measurement using a logarithmic trendline. The reconstructed measured settlement will serve as valuable insight into the settlement behaviour of the Noordtunnel and will also be used for validating the simulation results.

3. Identify the soil profile and geotechnical parameters for the simulation.

   Due to limited laboratory data in this project, the soil profile is determined by validating the situation map using CPT and borehole data. Certain geotechnical parameters for the soil models are estimated by correlating CPT tip resistance with the corresponding value from NEN (2017) Table 2b. In addition, other soil properties that influence to settlement, such as hydraulic conductivity and void ratio are derived from the Robertson SBT chart or some empirical formula.

4. Create the model and verify its accuracy.

   The numerical simulation uses PLAXIS, a well-known software in geotechnical engineering, for analysing settlements. The tunnel is divided into five cross-sections, each representing the settlement behaviour at an immersion joint. The immersed tunnel construction process involves trench dredging, tunnel immersion, and backfilling. As a result, the

Hardening Soil Model is selected to simulate the unloading-reloading behaviour of the soil. Additionally, the Soft Soil Creep Model is utilized to capture time-dependent deformations during long-term settlement, particularly in areas where soft soil significantly influences the behaviour. The simulation involves three types of models: (1) model 1, constructed based on the as-built drawing; (2) model 2, which considers the traffic load; and (3) model 3, which takes into account the effects of natural sedimentation and additional soil cover.

The models are developed to simulate the settlement, incorporating different construction stages, starting from the trench excavation phase and extending through the tunnel's intended operational lifespan. The resulting settlement data is then compared with the settlement history of the Noordtunnel. By analysing and comparing the measured settlement with the simulation outcomes, the accuracy and reliability of the simulation can be assessed, providing a solid basis for predictions of settlements in the coming years. In addition, the cause of the local excessive settlement is also analysed at this stage. Moreover, given the uncertainty in soil properties on-site, a sensitivity analysis will be conducted to examine the impact of soil variability on settlement. The analysis is carried out by varying the value of soil properties to see which parameters influence settlement the most and how much the settlement will deviate after parameter adjustment.

5. Analyze effects of ongoing settlement on tunnel structural safety and propose an optimized monitoring plan.

   The last step examines two main topics: the effect of the continuing settlement on the tunnel's structural safety and the proposed monitoring procedure for the Noordtunnel. The uneven settlement occurring along the longitudinal axis of the Noordtunnel results in joint opening/closure at the immersion joints. In order to assess the potential risk of leakage, a comparison between the external load subjected to the GINA gasket and its friction force is conducted. Furthermore, considering that the reliability of simulation outcomes hinges on accurate settlement measurements, an optimized monitoring procedure is introduced to address the limitations of the current monitoring procedure.

Step 1 intends to provide the theories related to the problems being investigated. Step 2 aims to answer subquestion 1, while steps 3 and 4 intend to answer subquestions 2 and 3, respectively. Lastly, step 5 aims to answer sub-question 4. By following this systematic approach, the research answers each subquestion, providing valuable insights into the settlement prediction of the Noordtunnel and its impact on the potential risk of leakages at the immersion joints.

1.5 REPORT STRUCTURE

The thesis consists of seven chapters, which are outlined as follows:

1. Chapter 2 (Literature Review) contains a literature study on general information about immersed tunnel and settlements in immersed tunnel. Thus, the settlement mechanism can be understood.
2. Chapter 3 (Settlement History of the Noordtunnel) presents the settlement history of the Noordtunnel measured by the monitoring instrument.
3. Chapter 4 (Soil Profile and Geotechnical Parameters) describes the geological profile of the Noordtunnel and the determination of relevant parameters for numerical simulation purposes.

4. Chapter 5 (Settlement Simulation and Prediction) describes the model made for the simulation and its results.
5. Chapter 6 (Effects of Ongoing Settlement on Structural Safety and Proposed Optimized Monitoring Plan) describes the effects of ongoing settlement on structural safety and proposes an optimized structure health monitoring plan in the Noordtunnel for future safety assurance.
6. Chapter 7 (Conclusions and Recommendations) delivers the conclusions derived from the analysis and further recommendations.

2 LITERATURE REVIEW

This chapter presents an overview of relevant concepts and theories essential for understanding the research problem being studied. To begin with, the general knowledge of immersed tunnel construction process and its potential impact on the subsoil property will aid the selection of the model's constitutive law in the simulation, ensuring that the model aligns with what occurs in practice. Moreover, the concept of Robertson's method and CPT-NEN Table 2b correlation explained in this chapter will serve as the basis for determining the soil profile and its mechanical properties in Chapter 4.

2.1 IMMERSED TUNNEL

2.1.1 Development of Immersed Tunnel

Tunnels and bridges are commonly used for crossing a waterway if a high capacity between different geographical areas is required. If a tunnel is the best option, the type of tunnel must be selected. Generally, there are three types of tunnel construction: bored, immersed, and cut and cover. The difference between the alternatives is the construction method and the depth required. A bored tunnel requires greater depth than other types of tunnels, as its soil cover must be approximately equal to the tunnel's diameter. However, immersed and in situ tunnels only require 2-3 m soil cover on top of their structure to prevent any damage caused by falling anchors or sinking ships. The shallower depth of immersed tunnels is advantageous for water crossings at certain locations because the tunnel element can be constructed shorter, with less backfill and shorter approaches structure (Glerum, 1988; Lunnis and Baber, 2013). Figure 2.1 compares the depth and length of the immersed tunnel, bored tunnel, and bridge.

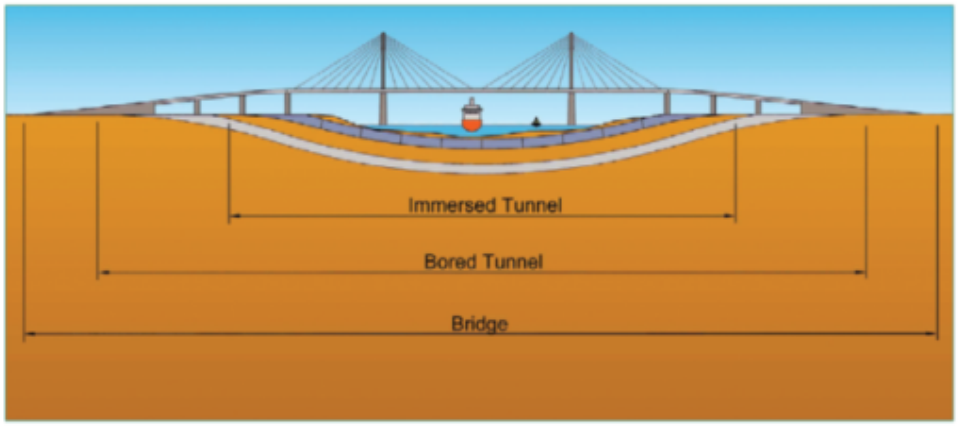

Figure 2.1: The depth and length comparison of the immersed tunnel, bored tunnel, and bridge (Olsen et al., 2022)

Most immersed tunnels are built to traverse rivers, canals, or harbours where the sub-soil conditions are usually soft. In 1893, the first immersed tunnel was constructed in Boston, United States of America. It was a simple system in which a 100-meter-long, 2.7-meter-diameter sewer pipe made of masonry and concrete runs from Boston to Deer Island beneath a 60-meter-wide tidal sea (Lunnis and Baber, 2013). Each tunnel segment ended with timber bulkheads and external steel flanges, allowing them to be bolted together after installation. However, problems with the sewer's water-tightness and functionality arose due to the pipe's permeable structure, which allowed water to enter the interior layers through the cracks between the bricks.

The first immersed tunnel for transportation was constructed between Detroit and Windsor in the United States and Canada in 1910 as a result of advances in technology and construction techniques. Twin watertight steel pipelines serving train passengers were positioned in a dredged trench and encircled with concrete. Other tunnels with steel structures were built in the following years. After the triumph of the first immersed tunnel for transportation, the first tunnel with a rectangular concrete structure was constructed seventeen years later.

After three decades, The Maastunnel in Rotterdam became the first immersed tunnel in The Netherlands. It goes beneath the Meuse River and serves for road transport in Rotterdam. At the time, steel prices in Europe were comparatively higher than in North America, so the tunnel was constructed from concrete. The general construction stages of the immersed tunnel commenced with the prefabricating of the concrete in a dry dock, towing them with tugboats to the tunnel site, and immersing them in an excavated riverbed trench. The advantage of the concrete-immersed tunnel at the time was the ability to increase the number of traffic channels within the tunnel to accommodate the increased traffic demand (Olsen et al., 2022). The tremendous success of the project has made the immersion tunnel system a popular solution for Dutch ground conditions and topography. Until now, no less than 27 immersed tunnels built in the Netherlands (Gavin et al., 2019).

2.1.2 Structure and Construction Process

Immersed tunnels function structurally in the vertical direction as beams or as a series of beams joined together. Engineers considered these beams uniformly supported for most tunnel projects (Grantz, 2001). The immersed tunnel structure is designed to prevent uplift with a design factor of up to 1.1, excluding the backfill's weight (Olsen et al., 2022). Immersed tunnels can be categorized into three categories based on the construction material: conventional reinforced concrete tunnel elements, composite sandwich tunnels, and steel shell tunnel elements (Liu et al., 2022).

Typically, steel shell tunnels have a circular box shape. The tunnels can be distinguished into double or single steel casings. A single steel shell element is embedded with an external steel shell fabricated typically from approximately 10 mm steel plate to ensure strength and water-tightness. A 700 mm thick reinforced concrete lining and other internal equipment are installed inside the steel shell to provide stability while afloat. The double steel shell, on the other hand, consists of two steel skins in cross sections and an outer steel box that encircles the interior steel shell. Construction of a steel shell tunnel begins with the fabrication of a series of regular modular subassemblies of steel shells in a shipyard. The subassemblies are subsequently welded together to produce a continuous element. The elements are launched into the water and then outfitted with concrete while floating.

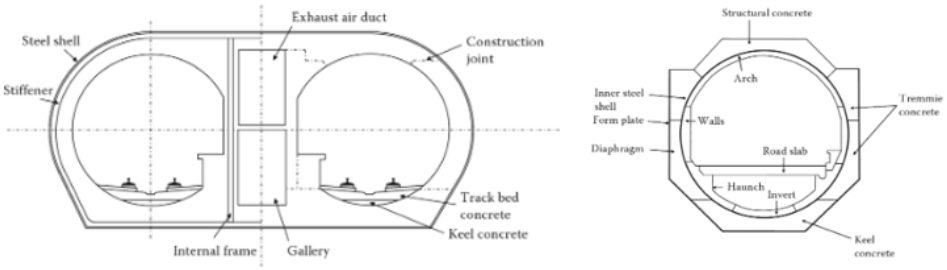

Figure 2.2: The visualization of single steel shell type in BART tunnel San Francisco (left) and double steel shell design in Hampton Roads Tunnel (right) (Lunnis and Baber, 2013)

Unlike steel shell tunnels, concrete tunnels usually have a rectangular box shape. Traditionally, the concrete elements are fabricated in a large open casting basin called a construction dock. The casting process starts from the floor slab, followed by the walls and roof of the tunnel elements. In the past, tunnel elements were constructed as a continuous 100 to 200-m reinforced concrete structure. Nonetheless, this structure is susceptible to cracking due to shrinkage, temperature fluctuations, and differential longitudinal settlements. Consequently, 20 to 25 m segmental elements are utilized more frequently than monolithic elements. Between these segments, expansion joints are installed to enable differential settlements and ensure water tightness (Nagel, 2011).

After the prefabrication phase, the tunnel elements are transported from the construction dock to the tunnel site. Throughout this period, the elements are longitudinally pre-stressed. During the transport and immersion phases, the components function as a single rigid tunnel element that can transmit bending moments. After the elements have been positioned in the desired location, the pre-stressed cables are cut so that the element can follow the differential settlement.

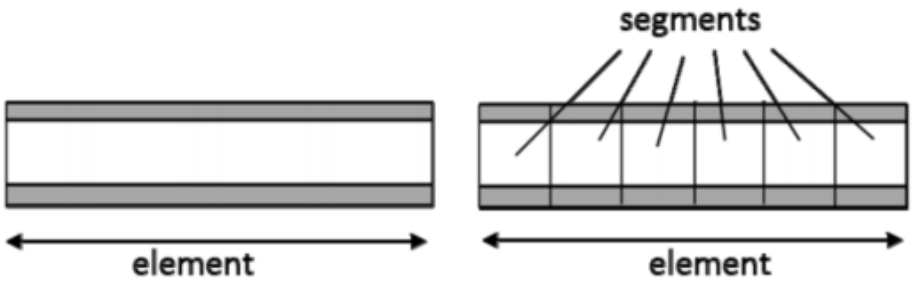

Figure 2.3: The comparison of monolithic tunnel element (left) and segmental tunnel element (right) (Reinders, 2019)

In Japan, a steel-concrete-steel (SCS) sandwich-immersed tunnel has been constructed for the past two decades, as it is deemed to be very advantageous in regions with high seismic activity. Concrete and steel's ability to move and act together distinguishes the composite steel tunnel from the double steel tube elements. The composite action is provided by shear connectors embedded in the interior faces of both steel plates to form a hybrid structure (Reinders, 2019). This tunnel form has a distinct advantage: the overall height of the tunnel element can be reduced compared to reinforced concrete. The inner walls of this tunnel can also be constructed from reinforced concrete, resulting in greater structural capacity and smaller dimensions. However, it requires highly competent workers and extensive quality control during fabrication to ensure reliable results Luttikholt et al. (2022).

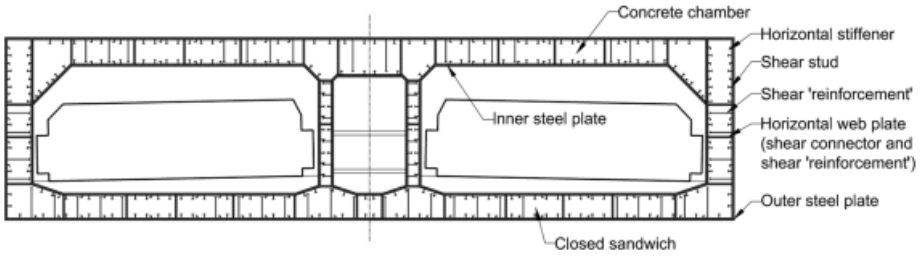

Figure 2.4: Schematic cross-sectional view of a sandwich element (Luttikholt et al., 2022)

Grantz (2001) has observed the general construction phases of the immersed tunnel as follows:

1. Prefabricating tunnel element. The tunnel structure is divided into several shorter elements and prefabricated in a dry dock. Depending on the design requirements, these elements can either be monolithic or segmented.
2. Excavating trench. The excavation process involves creating a trench along the designated alignment.
3. Transporting tunnel element. Usually, the tunnel element is towed with tug boats to the immersion site. Temporary sealing of the two ends of the element is implemented using bulkheads during transportation.
4. Immersing tunnel element. The tunnel element is immersed and subsequently linked to either the approach structure or the preceding immersed element.
5. Constructing the tunnel's foundation. A temporary jack lifts the tunnel before the foundation is applied. The space between the tunnel element and the soil is filled with sand or gravel.
6. Backfilling. The sides and top of the tunnel are filled with either soil or gravel as a backfill material.
7. Finishing work such as walls, road furnishing, and technical installation.

2.1.3 Settlement on Immersed Tunnel

Limiting the subsoil settlement is critical to the performance of immersed tunnel. Although the weight of immersed tunnel is generally lighter than the original soil it replaces, settlement may still be compelling and, in some cases, exceed the expected values derived from the geotechnical prediction (Olsen et al., 2022). Settlement may cause immediate or future issues due to cracking and leakage, resulting in corrosion of structural reinforcing steel, ice on the roadway, lifelong draining costs, and deterioration of tunnel finish.

As for civil engineers, uniform settlements are usually less of being concerned than differential settlements. Generally speaking, uniform settlements refer to the structure's settlement as a rigid body. It occurs when the structure loading lies on an elastic foundation or ground since the stiffness of the soil medium is limited. However, this type of settlement will not cause any cracks rotation to the tunnel structure. In contrast, almost all tunnel experience differential settlement. Differential settlements refer to the varying magnitudes of settlement along the tunnel body. This type of settlement may result in the element rotation, joint opening, cyclic compression and expansion of the rubber gasket, and internal force of the tunnel body (Zhang and Broere, 2019). Damage caused by the differential settlement will diminish the performance of an immersed tunnel (Grantz, 2001).

As pointed out by Grantz (2001) and Wei et al. (2012), the variety of factors that could cause the settlement of immersed tunnel can be summarised as follows:

1. **Ground conditions**. Generally, river beds consisting of consolidated soil layers have a lower settlement value than compressible clayey layers. The clay layer also needs a longer time to reach a stable final settlement.
2. **Traffic Loads**. Although a tunnel has been designed to accommodate a certain load level, the actual load is often greater than anticipated. The increasing traffic, especially in an economically developing area, could cause an outstrip load.
3. **Trench dredging technique**. Typically, hydraulic cutter-head suction dredges or clamshell bucket dredges are utilized to excavate the tunnel trench. However, the latter technique produces a bottom with more irregularities and larger voids. Therefore, the foundation material will fill and stabilize for an extended duration.
4. **Method of tunnel foundation construction**. There are four typical foundation types for immersed tunnels: sand flow, gravel bed, pile, and grouting. Each foundation's treatment shows varying settlement control abilities. The study case in China shows that an immersed tunnel with a pile foundation generally has the lowest accumulative settlement. In contrast, the sand flow foundation in soft ground with serious siltation has the lowest control ability to settlement. (Wang et al., 2020).
5. **Tidal action**. The water elevation determined water pressure during the calculation load. Under certain circumstances, a large amplitude of tidal variation may cause settlement on an immersed tunnel. Considering the soil swelling and recompression characteristics, every swelling and progressive compaction cycle accumulate a small amount of settlement. If the original ground layer consists of a clay layer that needs a longer time to relieve pore pressure, the upper layers of sand may cause an oscillation of supporting ground.
6. **Tunnel geometry**. The contact width of the tunnel element with the ground could cause settlement. The contact width of an octagonal-shaped tunnel is narrower than its projected plan width. A rectangular shape tunnel, on the other hand, has the same contact width as the projection. Typically, a larger contact area corresponds to less pressure on the foundation, resulting in relatively less settlement.

2.2 GEOLOGICAL PROFILE DETERMINATION

2.2.1 Soil Layer Interpretation

The soil profile can be derived from the available CPT data. The Robertson (1990) soil behaviour chart can classify the soil. This method used some empirical relations between friction ratio (R_f) and normalized cone resistance (q_t) to determine the soil behaviour type, as shown in Figure 2.5.

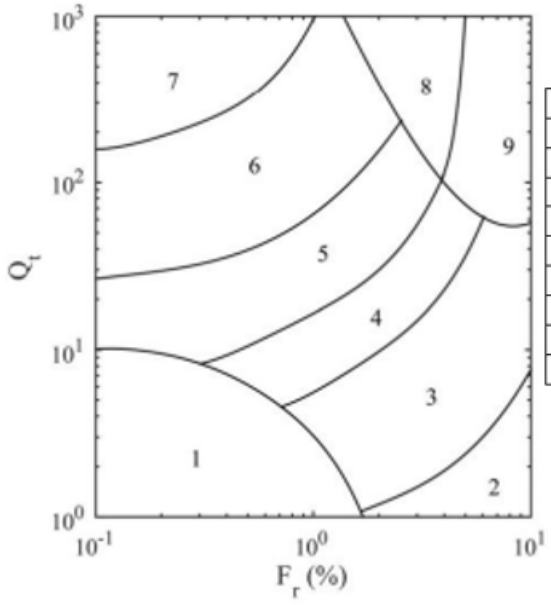

Zone	Soil Behaviour Type (SBT)
1	*Sensitive fine-grained*
2	*Clay - organic soil*
3	*Clays: clay to silty clay*
4	*Silt mixtures: clayey silt & silty clay*
5	*Sand mixtures: silty sand to sandy silt*
6	*Sands: clean sands to silty sands*
7	*Dense sand to gravelly sand*
8	*Stiff sand to clayey sand**
9	*Stiff fine-grained**

** Overconsolidated or cemented*

Figure 2.5: The Robertsons's soil classification chart (Robertson, 2010)

Robertson (2015) determined that friction ratio (R_f) and normalized cone resistance (q_t) cannot be directly measured from the CPT data, but can be indirectly calculated by some parameters measured by CPT as shown in the equation below.

$$Q_t = \frac{q_t - \sigma_{v0}}{\sigma'_{v0}} \tag{2.1}$$

$$F_r = \frac{f_s}{q_t - \sigma_{v0}} x100 \tag{2.2}$$

$$q_t = q_c + u_2(1 - a) \tag{2.3}$$

where,
Q_t is normalized friction ratio, q_t is corrected cone resistance (kPa), σ_{v0} is total in situ vertical stress (kPa), σ'_{v0} is effective in situ vertical stress (kPa), F_r is normalised friction ratio, f_s is measured sleeve friction (kPa), u_2 is measured pore pressure (kPa), and a is net area ratio.

2.2.2 Soil Parameter Determination

NEN9997-1 Table 2b contains the characteristics value of each soil type. The soil properties, strength and stiffness can be determined by correlating the CPT tip resistance (q_c) value with the corresponding soil type listed in Table 2b. The characteristic values of soil properties listed in NEN Table 2b are presented in Table 2.1.

Table 2.1: The characteristic values of soil properties (NEN, 2017)

Grondsoort			Karakteristieke waarde [a] van grondeigenschap																	
Hoofd-naam	Bijmengsel	Consis-tentie [b]	γ [c] kN/m³		γ_{sat} kN/m³		q_c [d g] MPa		C'_p [g]		C'_s		$C_p/(1+e_0)$ [g] [-]		C_α [f] [-]		$C_{sw}/(1+e_0)$ [g] [-]		E_{100} [g h] MPa		φ' [g] Graden		c' kPa		c_u kPa	
Grind	Zwak siltig	Los	17		19		15		500		∞		0,004 6		0		0,001 5		45		32,5		0			
		Matig	18		20		25		1 000		∞		0,002 3		0		0,000 8		75		35,0		0		N.v.t.	
		Vast	19	20	21	22	30		1 200	1 400	∞		0,001 9	0,001 6	0		0,000 6	0,000 5	90	105	37,5	40,0	0			
	Sterk siltig	Los	18		20		10		400		∞		0,005 8		0		0,001 9		30		30,0		0			
		Matig	19		21		15		600		∞		0,003 8		0		0,001 3		45		32,5		0		N.v.t.	
		Vast	20	21	22	22,5	25		1 000	1 500	∞		0,002 3	0,001 5	0		0,000 8	0,000 5	75	110	35,0	40,0	0			
Zand	Schoon	Los	17		19		5		200		∞		0,011 5		0		0,003 8		15		30,0		0			
		Matig	18		20		15		600		∞		0,003 8		0		0,001 3		45		32,5		0		N.v.t.	
		Vast	19	20	21	22	25		1 000	1 500	∞		0,002 3	0,001 5	0		0,000 8	0,000 5	75	110	35,0	40,0	0			
	Zwak siltig, kleiig		18	19	20	21	12		450	650	∞		0,005 1	0,003 5	0		0,001 7	0,001 2	35	50	27,0	32,5	0		N.v.t.	
	Sterk siltig, kleiig		18	19	20	21	8		200	400	∞		0,011 5	0,005 8	0		0,003 8	0,001 9	15	30	25,0	30,0	0		N.v.t.	
Leem [e]	Zwak zandig	Slap	19		19		1		25		650		0,092 0		0,003 7		0,030 7		2		27,5	30,0	0		50	
		Matig	20		20		2		45		1 300		0,051 1		0,002 0		0,017 0		3		27,5	32,5	1		100	
		Vast	21	22	21	22	3		70	100	1 900	2 500	0,032 9	0,023 0	0,001 3	0,000 9	0,011 0	0,007 7	5	7	27,5	35,0	2,5	3,8	200	300
	Sterk zandig		19	20	19	20	2		45	70	1 300	2 000	0,051 1	0,032 9	0,002 0	0,001 3	0,017 0	0,011 0	3	5	27,5	35,0	0	1	50	100
Klei	Schoon	Slap	14		14		0,5		7		80		0,328 6		0,013 1		0,109 5		1		17,5		0		25	
		Matig	17		17		1,0		15		160		0,153 3		0,006 1		0,051 1		2		17,5		5		50	
		Vast	19	20	19	20	2,0		25	30	320	500	0,092 0	0,076 7	0,003 7	0,003 1	0,030 7	0,025 6	4	10	17,5	25,0	13	15	100	200
	Zwak zandig	Slap	15		15		0,7		10		110		0,230 0		0,009 2		0,076 7		1,5		22,5		0		40	
		Matig	18		18		1,5		20		240		0,115 0		0,004 6		0,038 3		3		22,5		5		80	
		Vast	20	21	20	21	2,5		30	50	400	600	0,076 7	0,046 0	0,003 1	0,001 8	0,025 6	0,015 3	5	10	22,5	27,5	13	15	120	170
	Sterk zandig	-	18	20	18	20	1,0		25	140	320	1 680	0,092 0	0,016 4	0,003 7	0,000 7	0,030 7	0,005 5	2	5	27,5	32,5	0	1	0	10
	Organisch	Slap	13		13		0,2		7,5		30		0,306 7		0,015 3		0,102 2		0,5		15,0		0	1	10	
		Matig	15	16	15	16	0,5		10	15	40	60	0,230 0	0,153 3	0,011 5	0,007 7	0,076 7	0,051 1	1,0	2,0	15,0		0	1	25	30
Veen	Niet voorbelast	Slap	10	12	10	12	0,1		5	7,5	20	30	0,460 0	0,306 7	0,023 0	0,015 3	0,153 3	0,102 2	0,2	0,5	15,0		1	2,5	10	20
	Matig voorbelast	Matig	12	13	12	13	0,2		7,5	10	30	40	0,306 7	0,230 0	0,015 3	0,011 5	0,102 2	0,076 7	0,5	1,0	15,0		2,5	5	20	30
Variatiecoëfficiënt v			0,05				–		0,25										0,10				0,20			

[a] De tabel geeft van de desbetreffende grondsoort de lage, respectievelijk de hoge karakteristieke waarde van gemiddelden. Binnen een gebied, vastgesteld door de rij van het bijmengsel en de kolom van de parameter (een cel), geldt:
— als een verhoging van de waarde van een van de grondeigenschappen tot een ongunstiger situatie leidt dan de toepassing van de in de tabel gepresenteerde lagere karakteristieke waarde, moet de rechterwaarde op dezelfde regel zijn gebruikt. Is er rechts geen waarde vermeld, dan moet de waarde er recht onder zijn toegepast;
OPMERKING Dit is bijvoorbeeld het geval bij negatieve kleef op een paal waar een hogere waarde van φ', c' en c_u ook een hogere waarde van de negatieve kleef oplevert.
— voor $C_p/(1+e_0)$, C_α en $C_{sw}/(1+e_0)$ zijn in de tabel de hoge karakteristieke gemiddelde waarden vermeld.

[b] Los: $0 < R_n < 0{,}33$
Matig: $0{,}33 \leq R_n \leq 0{,}67$
Vast: $0{,}67 < R_n < 1{,}00$

[c] De γ-waarden zijn van toepassing bij een natuurlijk vochtgehalte.

[d] De hier gegeven q_c-waarden (conusweerstand) behoren beschouwd te worden als ingang in de tabel en mogen niet in de berekeningen worden gebruikt.

[e] De waarden hebben betrekking op verzadigd leem.

[f] De C_α-waarden zijn geldig voor een spanningverhogingstraject van ten hoogste 100 %.

[g] Voor grind, zand en in beperkte mate ook voor leem en sterk zandige klei zijn q_c, E_{100}, φ' en de samendrukkingsparameters C'_p, $C_p/(1+e_0)$ en $C_{sw}/(1+e_0)$ genormeerd voor een effectieve verticale grondspanning σ'_v van 100 kPa. Om voor de in het terrein gemeten waarden van q_c een juiste ingang in de tabel te krijgen moeten deze waarden zijn geconverteerd naar het niveau van de effectieve verticale grondspanning σ'_v van 100 kPa. In dat kader moet de formule $q_{c;tabel} = q_{c;terrein} \times C_{qc}$ worden gebruikt, waarbij C_{qc} moet zijn ontleend aan $C_{qc} = (100/\sigma'_v)^{0{,}67}$. Voor de hoek van inwendige wrijving φ' en de cohesie c' geldt dat deze afhankelijk zijn van de consistentie van de grond. Dit betekent dat deze conversie ook nodig is voor φ' en c'. Als $q_{c;tabel}$ groter wordt dan de in de tabel gegeven waarde geldt de onderste regel voor de desbetreffende grondsoort.

[h] De elasticiteitsmodulus bij belastingsherhalingen mag zijn aangenomen als zijnde driemaal de aangegeven waarde.

It is worth noticing that for coarse-grained soils, q_c must be corrected to the comparable level of 100 kPa vertical effective stress via the equation below.

$$q_{c,table} = C_{qc}(q_c) \tag{2.4}$$

$$C_{qc} = (\frac{100}{\sigma'_v})^{0.67} \tag{2.5}$$

where,
$q_{c,table}$ is the modified cone resistance value under 100 kPa of effective stress, C_{qc} is the cone resistance correction factor, q_c is the cone resistance measured from CPT (kPa), and σ'_v is the effective vertical stress (kPa).

2.3 SOIL CONSTITUTIVE LAW

PLAXIS is a finite element program which is powerful for analysing deformation, stability and groundwater flow in geotechnical engineering. In this research, the reliability of the results highly depends on the input parameters and the chosen constitutive law for the soil model.

2.3.1 Hardening Soil Model

The construction stage of the immersed tunnel begins by dredging the trench. During this stage, the upper soil layer is being removed. This activity causes unloading to the underlying soil layer. Afterwards, the soil was reloaded by the placement of the foundation, tunnel element, and backfilling of soil. Therefore, the HS Model is being used for the simulation to capture the unloading and reloading behaviour during the construction stages (Schanz et al., 2019). Brinkgreve (2022) has pointed out the characteristics of this model as follows:

1. It is characterised by a more general stress-dependent stiffness behaviour based on a power-law formulation.
2. In axial compression, the stress-strain relationship is hyperbolic.
3. It involves the generation of plastic deviatoric strains by mobilising the materials internal friction. This is termed 'shear hardening'.
4. It involves the generation of plastic volumetric strains in primary compression. This is termed 'compaction hardening', similar to the Soft-Soil model's hardening.
5. The behaviour in unloading and reloading is elastic.
6. The failure behaviour is according to the Mohr-Coulomb failure criterion.

There are two yield contours: shear hardening and compaction (cap) hardening. Shear hardening is used to model irreversible strains due to primary deviatoric loading. In contrast, compaction (cap) hardening models irreversible plastic strains due to primary compression in Oedometer and isotropic loading.

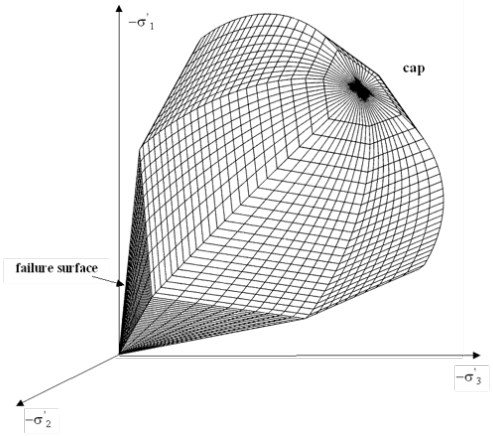

Figure 2.6: The yield contour of Hardening Soil model (Brinkgreve, 2022)

In this model, soil behaviour is nonlinear before it fails. After it reaches the failure contour (indicated by the cone in Figure 2.6), soil behaviour is determined based on Mohr-Coulomb strength parameters (cohesion and angle of internal friction). The overall behaviour of the stress-strain relationship, along with various stiffness parameters, is shown in Figure 2.7.

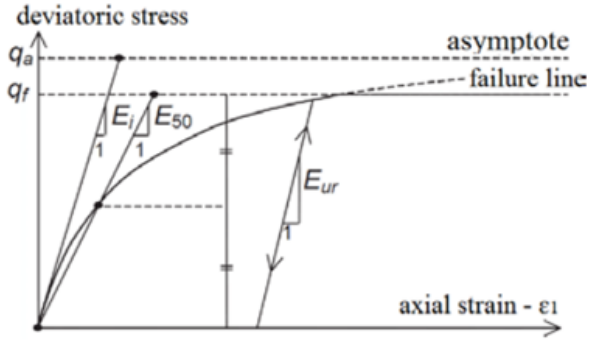

Figure 2.7: The hyperbolic stress-strain relationship used in the Hardening Soil model (Celik, 2017)

For numerical analysis in PLAXIS, the hardening soil model uses three types of stiffness: secant stiffness in the triaxial test at reference pressure (E_{50}^{ref}), tangent stiffness in the Oedometer test at p_{ref} (E_{oed}^{ref}), and reference stiffness in unloading/reloading (E_{ur}^{ref}).

The value of secant stiffness (E_{50}^{ref}) also depends on the type of soil. For coarse-grain soil, E_{50}^{ref} is roughly equals to Oedometer stiffness (E_{oed}^{ref}). In contrast, the value of E_{50}^{ref} is twice the Oedometer stiffness (E_{oed}^{ref}) for pure normally consolidated clay soil. Lastly, the unloading/reloading stiffness (E_{ur}^{ref}) for both types of soil is in a range from three to five times E_{50}^{ref} (PLAXIS, 2020).

$$E_{oed}^{ref} = E_{50}^{ref} \quad \text{for sand} \tag{2.6}$$

$$E_{oed}^{ref} = 0.5E_{50}^{ref} \quad \text{for soft soil} \tag{2.7}$$

$$E_{ur}^{ref} = (3to5)E_{50}^{ref} \quad \text{for sand and clay} \tag{2.8}$$

2.3.2 Soft Soil Creep Model

Despite the ability of the HS Model to capture unloading and reloading behaviour, it could not accurately represent the long-term settlement of soft soil. Therefore, the SSC Model is employed to capture better the long-term settlement behaviour of tunnel elements situated on soft soil. According to Brinkgreve (2022), the SSC Model exhibits the following characteristics:

1. It involves a logarithmic stress-strain relationship.
2. The model demonstrates elastic behaviour during both unloading and reloading.
3. The model retains the pre-consolidation stress as part of its memory.
4. It generates irreversible volumetric strain during primary loading.
5. The failure behaviour in the model follows the Mohr-Coulomb failure criterion.
6. The model can generate time-dependent deformations, known as 'secondary compression'.
7. Irreversible strains in the model are formulated using visco-plasticity principles instead of plasticity theory.

The SSC Model has eight model parameters. In PLAXIS numerical analysis, three stiffness parameters are relevant, namely: modified compression index (λ*), modified swelling index (κ*), and modified creep index (μ*). The comparison of those parameters is visualised in

Figure 2.8. The stress-strain behaviour resulting from increasing stresses, followed by decreasing stress towards the end, is depicted in the left diagrams. On the other hand, the right diagrams illustrate the time-strain behaviour resulting from initial loading, with subsequent stress remaining constant. In the latter scenario, the initial part of the curve represents the consolidation process, followed by pure creep. Hence, the determination of the C_α and μ^* parameters is based on the "straight" segment of the curve.

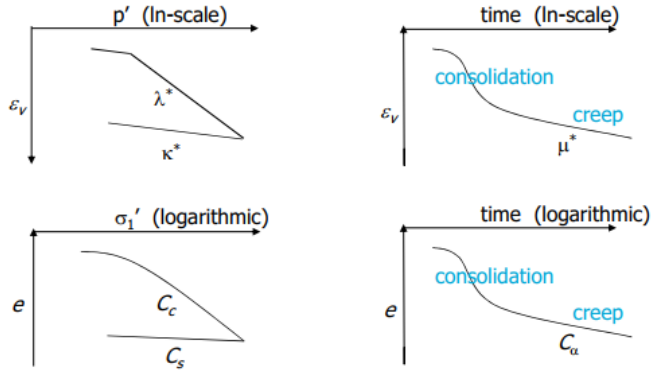

Figure 2.8: The visualisation of primary and secondary compression parameters in the Soft Soil Creep model (Brinkgreve, 2022)

PLAXIS (2021) has pointed out the relationship between SSC Model's stiffness parameters to internationally normalized parameters, as shown in the equation below.

$$\lambda^* = \frac{C_c}{2.3(1+e)} \tag{2.9}$$

$$\kappa^* = \frac{2C_r}{2.3(1+e)} \tag{2.10}$$

$$\mu^* = \frac{C_\alpha}{2.3(1+e)} \tag{2.11}$$

3 SETTLEMENT HISTORY OF THE NOORDTUNNEL

This chapter aims to reconstruct the settlement time-history of the Noordtunnel. The work starts by determining a 'new' reference point, because the 'initial' reference point is considered questionable since it is most subjected to temperature changes, and some measurement data shows inconsistent settlement tendencies. The new reference point, with its new settlement trendline, will serve as a baseline for estimating settlement magnitude within the unrecorded monitoring period. After the settlement in all time frames, from tunnel immersion until the latest regular measurement, is known, the historical settlement of the Noordtunnel is reconstructed by summing them up. This reconstructed historical settlement is critical to get a complete picture of the settlement tendency of the Noordtunnel.

3.1 AVAILABLE SETTLEMENT DATA

As previously mentioned, the settlement of the Noordtunnel is measured in two time periods: the initial ten months following the completion of the immersion, and a regular settlement started from 17 September 1993 to 12 April 2019. In the initial timeframe, the measurement frequency varies, ranging from weekly to monthly intervals. Figure 3.1 depicts the measured settlement in the first ten months after immersion at tunnel element 3. The solid line, written as the primary end, represents the end of the tunnel that connected to the previous structures. Whereas the dashed line, labeled as the secondary end, represents the end of the tunnel that is not connected to any structures during immersion.

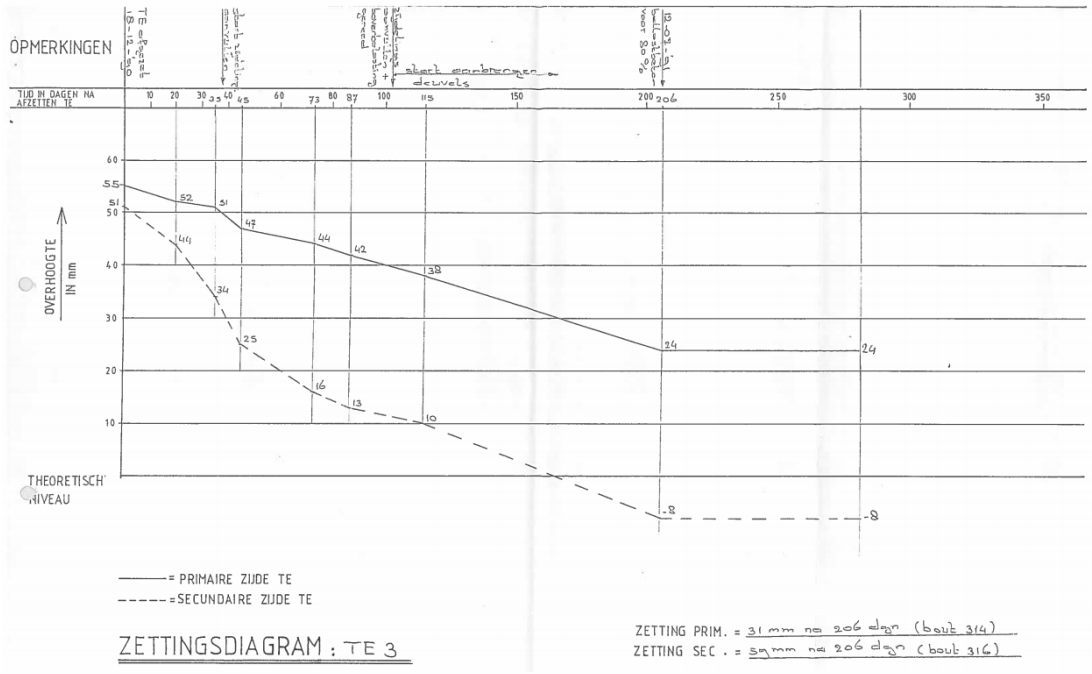

Figure 3.1: The measured settlement on the first ten months at tunnel element 3 (TEC, 1992)

Furthermore, the regular measurement is conducted by fitting the measuring bolts to the top of the road barrier at the immersion joints. The measurement is observed manually and conducted over a yearly period. The measuring bolts are installed at the north and southern parts of the tunnel, as depicted in Figure 3.2. It should be noted that the settlement history of the segment joints cannot be reconstructed since only two measurements are provided during the regular measurement.

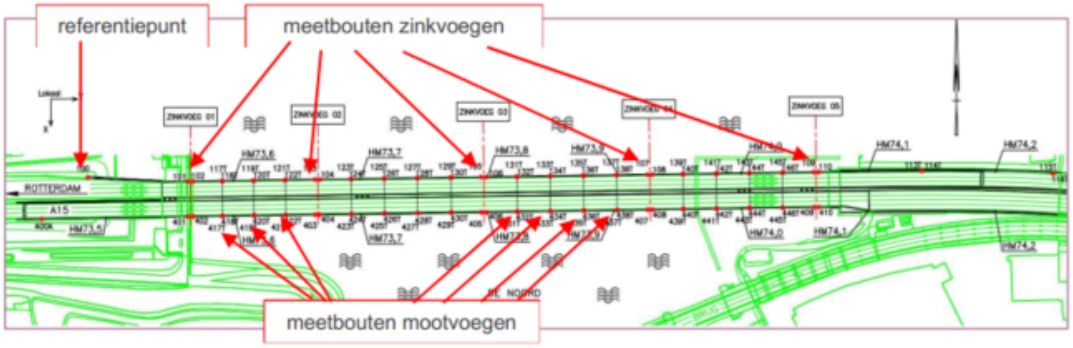

Figure 3.2: Overview of measuring points of the Noordtunnel (SWECO, 2020)

3.2 SELECTION OF SUITABLE REFERENCE POINT

The historical settlement of the Noordtunnel is reconstructed by first choosing the 'reliable' reference point. The initial reference point is point 100, located at the west access ramp and labeled as *'referentiepunt'* in Figure 3.2. The height of this initial reference point has yet to be checked since the zero measurements and is assumed to be fixed. However, although this point is located in the piled section of the ramp, the stability of this point is questionable since the previous study states that it is sensitive to temperature changes. It is important to note that a 'reliable' reference point should generate a consistent tendency, for instance, a continuous settlement curve in the long tendency. Therefore, the stability of the 'initial' reference point is validated by observing the settlement tendency of other measuring points. Points 101, 401, 110, and 410, located at the ramp founded in piles with an ideally limited settlement, are chosen to verify the reference point. The settlement tendency of all monitoring bolts is compared to those five reference points (please see Appendix A). However, in this chapter, the settlement at points 102 and 402 are chosen as examples to evaluate.

From Figure 3.3, it can be observed that the settlement of points 102 and 402 depict an irregular pattern when points 100/110/410 serve as reference points. The settlement graph demonstrates alternating trends of settlement, uplift, and settlement when plotted against those points. Although the magnitude of the alternating trend is 'only' 4 to 5 mm, the observed trend does not align with the initial expectation of a continuous settlement in the long term. Thus, using points 100, 110, and 410 as reference points could lead to deviations and biased settlement trends. Conversely, the reference point 101/401 exhibits the most consistent tendency in the settlement curve. Although there are occasional fluctuations in the settlement trend, they occur less frequently, and the magnitude is relatively low.

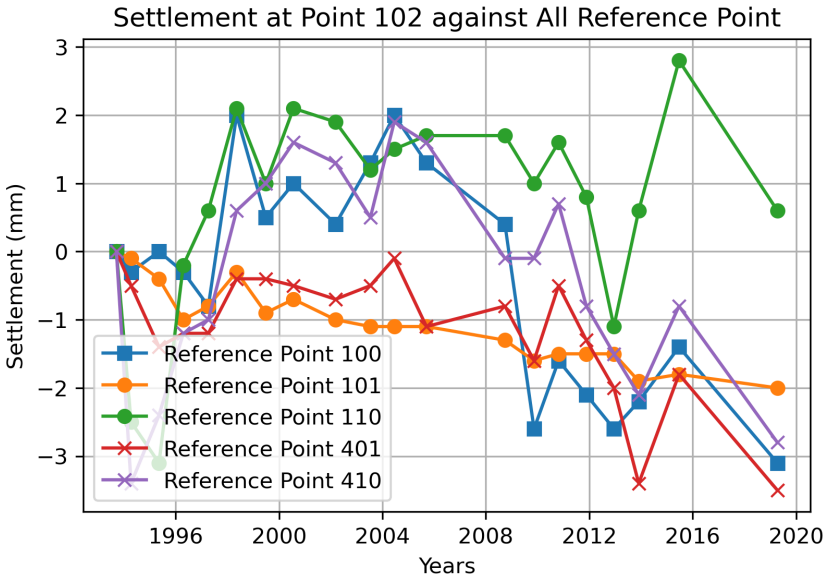

(a) Point 102

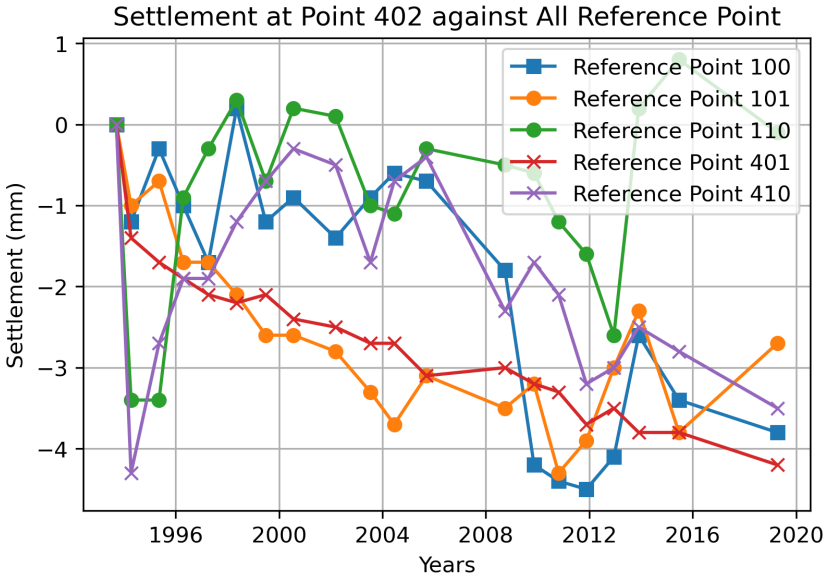

(b) Point 402

Figure 3.3: The settlement tendency of point 102 and 402 comparison at all reference points

The details in Figure 3.3 show that using point 101 provides the most stable downward trend for point 102, whereas point 401 gives the most stable downward trend for point 402. However, when all the settlement tendencies outlined in Appendix A are taken into account, it is observed that point 101 exhibits the most consistent tendency for 62.5% of the (10 out of the 16) measuring points. On the contrary, using reference point 401 maintains a consistent tendency for only 37.5% of the measuring points. Therefore, point 101 is determined as the new reference point in this research.

3.3 RECONSTRUCTION OF THE SETTLEMENT TIME-HISTORY OF THE NOORDTUNNEL

It has become apparent that no settlement is recorded in the second and third years after immersion, resulting in a gap in the monitoring data. Consequently, the actual historical settlement of the Noordtunnel remains to be discovered. Settlement of the tunnel is caused by primary and, to some extent, secondary compression within the soil. Primary compression, known as 'consolidation', refers to the reduction in soil volume or mass that directly responds to natural or human-made loadings. After the loads are applied on top of the subsoil, excess pore water pressure is generated and by the time it dissipated, settlement occurs. On the other hand, secondary compression, also known as 'creep' involves the time-dependent settlement behaviour of the subsoil.

According to TEC (1992) data depicted in Figure 3.1, the settlement rate is generally lower after seven months of tunnel element immersion, indicating that consolidation was mostly complete within the first ten months. On the other hand, the regular measurement data exhibits a consistent settlement trend. Therefore, a backward calculation is performed based on regular measurements to estimate the settlement magnitude during the period without measurements. The regular measurement is plotted, and a trendline is fitted to estimate the magnitude of settlement. Point 103, located at the second immersion joint, is selected as an example for evaluation.

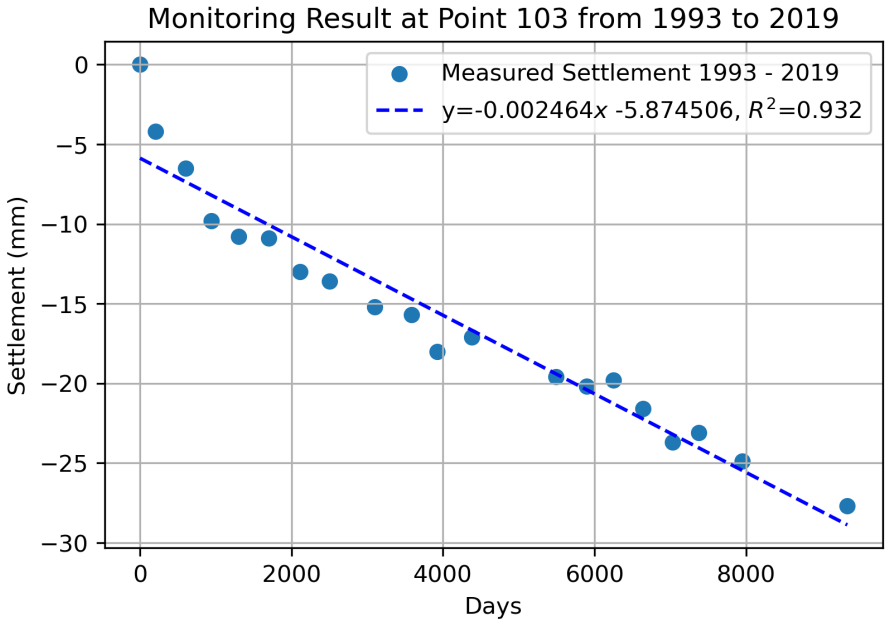

Figure 3.4: The regular measurement result at point 103

It is noted that settlement was not measured for 723 days. Based on the equation derived from the trendline in Figure 3.4, it is estimated that 7.7 mm of settlement occurred during this unmeasured period. The settlement estimation for other immersion joints is determined using the same approach. Table 3.1 presents the estimated settlement values during the period with no measurements for the respective immersion joints. It is worth noticing that the immersion joint 2 is a closure joint made of rigid structures. Moreover, since four measurement points can represent the settlement at an immersion joint, then in this research the highest settlement value that occurs is chosen for considering the worst-case scenarios.

Table 3.1: The estimated settlement during no-measuring period

Location	Magnitude of Settlement (mm)
Immersion Joint 1 (Point 102)	0.5
Immersion Joint 2 (Point 103)	7.7
Immersion Joint 3 (Point 106)	0.8
Immersion Joint 4 (Point 107)	2.8
Immersion Joint 5 (Point 109)	1.9

The settlement history is reconstructed after collecting and compiling all the gathered data. Figure 3.5 depicts the measured settlement trendline of point 103, showcasing the settlement pattern at the second immersion joint. From Figure 3.5, it is evident that the settlement behaviour of point 103 shows a logarithmic trendline. A higher settlement magnitude is observed within the first 300 days after tunnel immersion. This has become a valuable finding depicting the primary consolidation in the subsoil. Moreover, it can also be observed that the settlement rate is lower during the regular measurement, indicating that the regular measurement captures the secondary compression in the subsoil.

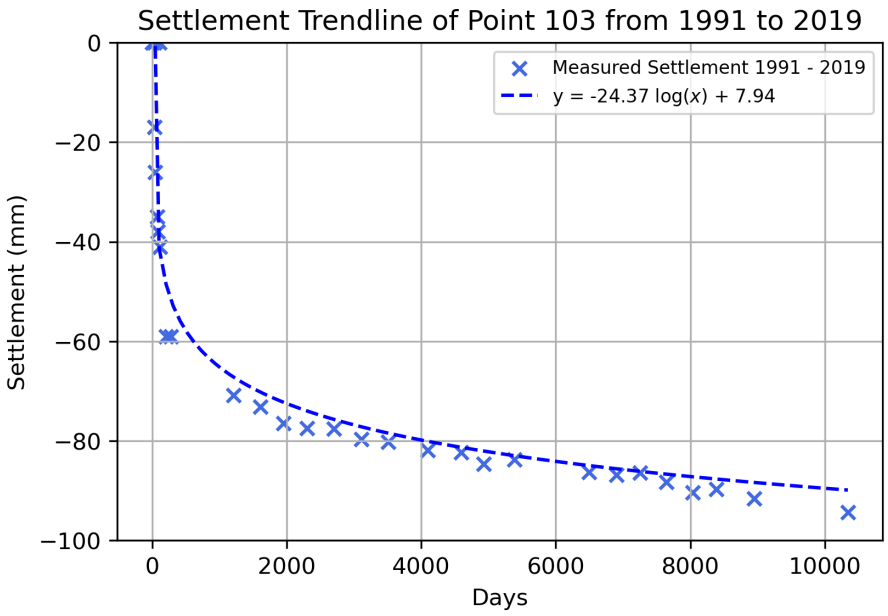

Figure 3.5: The settlement history at point 103

Furthermore, the settlement tendencies at the other immersion joints are determined by applying the same approach. The results show that all immersion joints show logarithmic trendlines of settlement (as depicted in Appendix A). Overall, the reconstructed historic settlement at all immersion joints shows that a higher settlement magnitude is recorded within ten months after tunnel immersion and flattening curve afterward.

3.4 DISCUSSIONS

In this chapter, the settlement history of the Noordtunnel is reconstructed based on the initial and regular settlement measurement. The initial measurement, conducted in the first ten months after tunnel immersion, generally shows a higher settlement magnitude than the reg-

ular measurement. Subsequently, the settlement rate decreased after 206 days, and the graph gradually flattened, indicating the creep effects. This phenomenon shows that the primary compression, or consolidation, mainly occurred during the first seven months after immersion. Thus, it is reasonable to estimate the unmeasured settlement by performing back calculations of the regular monitoring trendline. Table 3.2 shows the generated settlement magnitude for all sets of settlement data. However, it should be noted that immersion joints 1 and 5, located at the westernmost and easternmost of the tunnel, are connected to the approach structure founded on piles. A high magnitude of primary compression is possible to occur at this location before the tunnel is connected to the approach structure. Afterward, ideally/limited settlement is expected in this particular area.

Table 3.2: The generated settlement magnitude for all sets of settlement data

Data set	Magnitude of Settlement (mm)				
	IJ 1	IJ 2	IJ 3	IJ 4	IJ 5
Initial measurement (1990-1991)	31	59	31	25	41
Estimated settlement (1991-1993)	0.5	7.7	0.8	2.8	1.9
Total settlement occurred until 2019	33.45	94.36	42.72	42.52	47.63
Settlement rate per year (1991-2019)	0.09	1.26	0.42	0.63	0.24
*)Note:	IJ: Immersion Joint				

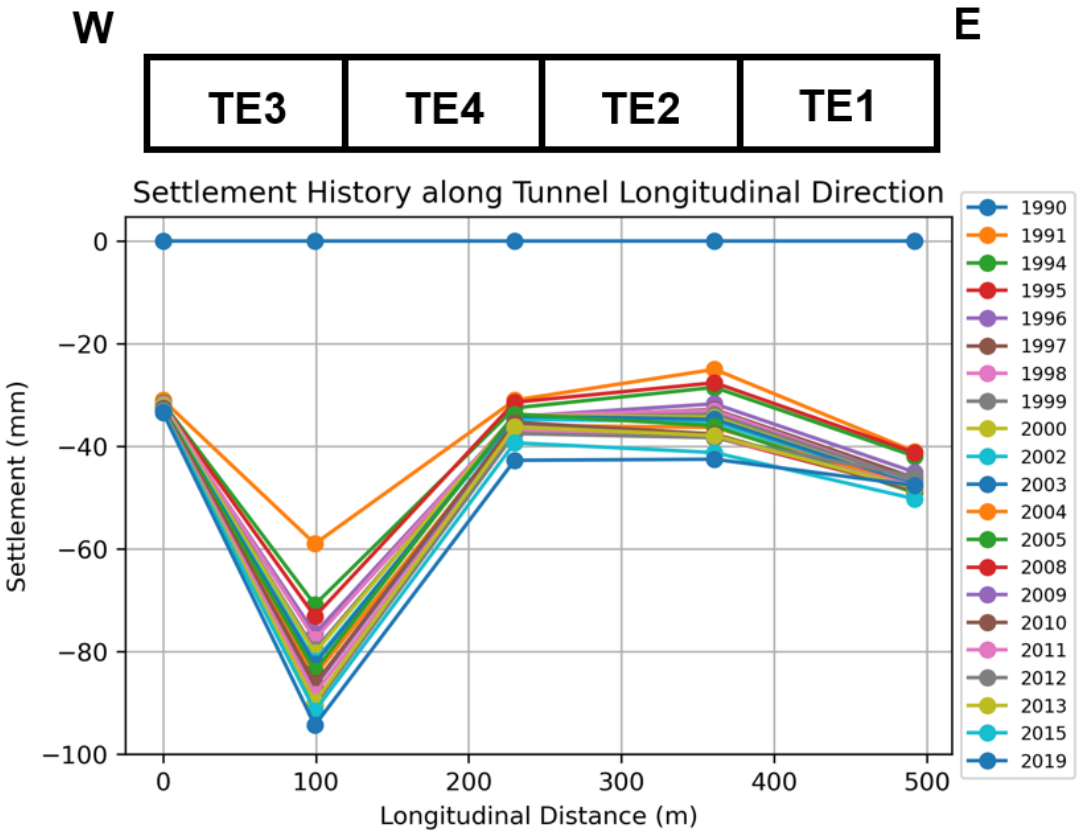

Figure 3.6: The settlement history of The Noordtunnel along longitudinal direction

The settlement history of all immersion joints (presented in Figure 3.6) shows that uneven settlement occurred along Noordtunnel's longitudinal direction, with immersion joint two being prominent by 94.36 mm of settlement in 2019. On the other hand, the settlement at the other immersion joints occurred within a range of 34 to 48 mm in 2019.

Moreover, the settlement history in Appendix A shows that all settlement trendlines fit the logarithmic trend, indicating that the settlement that occurred in the Noordtunnel is mainly derived by geotechnical mechanism and thus challenges the findings derived from prior research by SWECO (2020). In addition, Table 3.2 reveals that immersion joint two shows higher compared to the other immersion joints, indicating that the creep effect is more pronounced in this specific location. Considering the same weight of the tunnel element, this phenomenon is likely to occur due to the geological conditions in the field and probably the applied construction method. In order to investigate the cause of excessive settlement at the second immersion joint, further analysis will be conducted using numerical simulation.

3.5 CONCLUSIONS

The following points are the important findings of this chapter, which also could be used to answer the sub-research questions given in Chapter 1:

- The settlement history reveals that all immersion joints have a logarithmic trendline of settlement tendencies, indicating that the settlement that occurred in the Noordtunnel is derived by geotechnical mechanism.
- The settlement history data indicates that consolidation primarily occurs within the initial seven months following immersion. Subsequently, a phase of secondary compression or creep is observed.
- The settlement at all immersion joints show a flattening trend of settlement, except for immersion joint two. Considering the equivalent of loads (caused by the tunnel weight and the soil cover) applied on top of the subsoil along the tunnel longitudinal direction, the varying settlement magnitude between the immersion joints is highly likely due to the field's geological condition.

4 SOIL PROFILE AND GEOTECHNICAL PARAMETERS

This chapter examines the classification of geological profiles and determining geotechnical parameters for numerical simulation in PLAXIS in the next Chapter 5.

4.1 SOIL PROFILE

4.1.1 Data Available

Usually, before constructing an immersed tunnel, the geological profile along the designed tunnel alignment could be determined by boreholes, CPT, and laboratory tests. However, in this project, laboratory tests for determining soil strength and stiffness are missing. Only CPT, borehole, and reports of soil properties are available. However, a site map depicting the soil profile along the tunnel's longitudinal direction is provided. Thus, the site map will serve as a basis to determine the subsoil profile. At the same time, the borehole and CPT from SWECO (2020) and TEC (1992) report will be used to ensure the geological profile depicted in the map. From the CPT, one can immediately see a clearly defined boundary between some soft soil layer(s) and a coarse-grained soil layer. Typically, the soil is identified as peat when the cone resistance (q_c) is less than 1 MPa, and the friction ratio (R_f) is greater than 5%. Conversely, when the friction ratio is less than 5%, and the cone resistance remains relatively low ($q_c < 1$ MPa), it is highly likely that the soil layer is composed of clay (Robertson, 2010). Therefore, the CPT data can confirm the presence of clay, peat, and sandy soil, as indicated in the site map. The geological profile of the tunnel in the longitudinal direction is depicted in Figure 4.1.

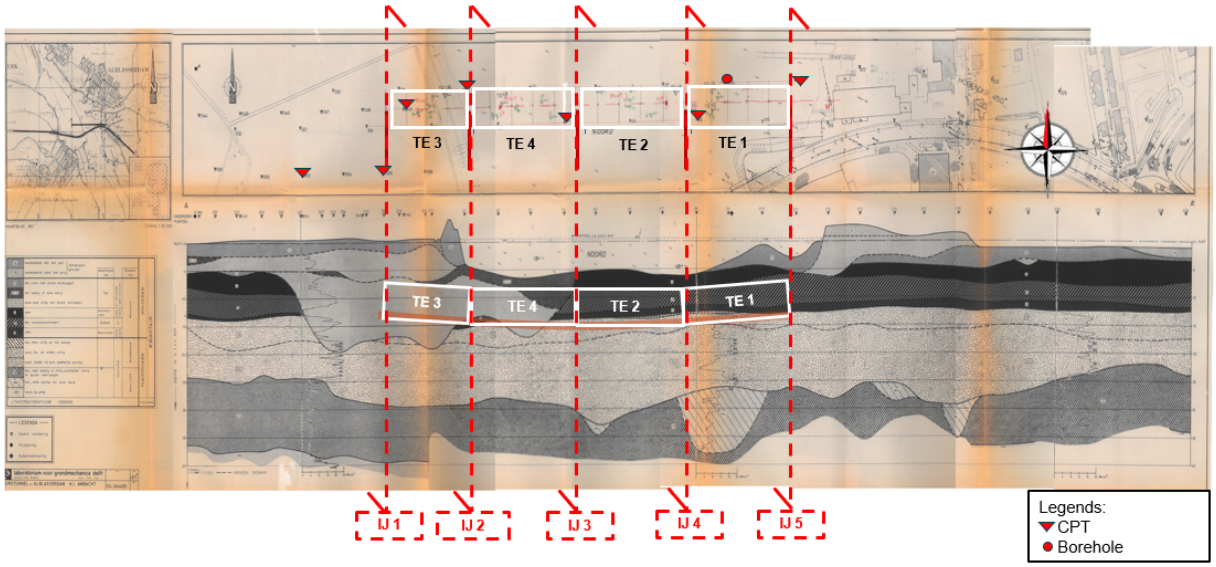

Figure 4.1: The soil profile along longitudinal direction

Moreover, DINOloket is used to estimate the soil profile in the transverse direction, as shown in Figure 4.2.

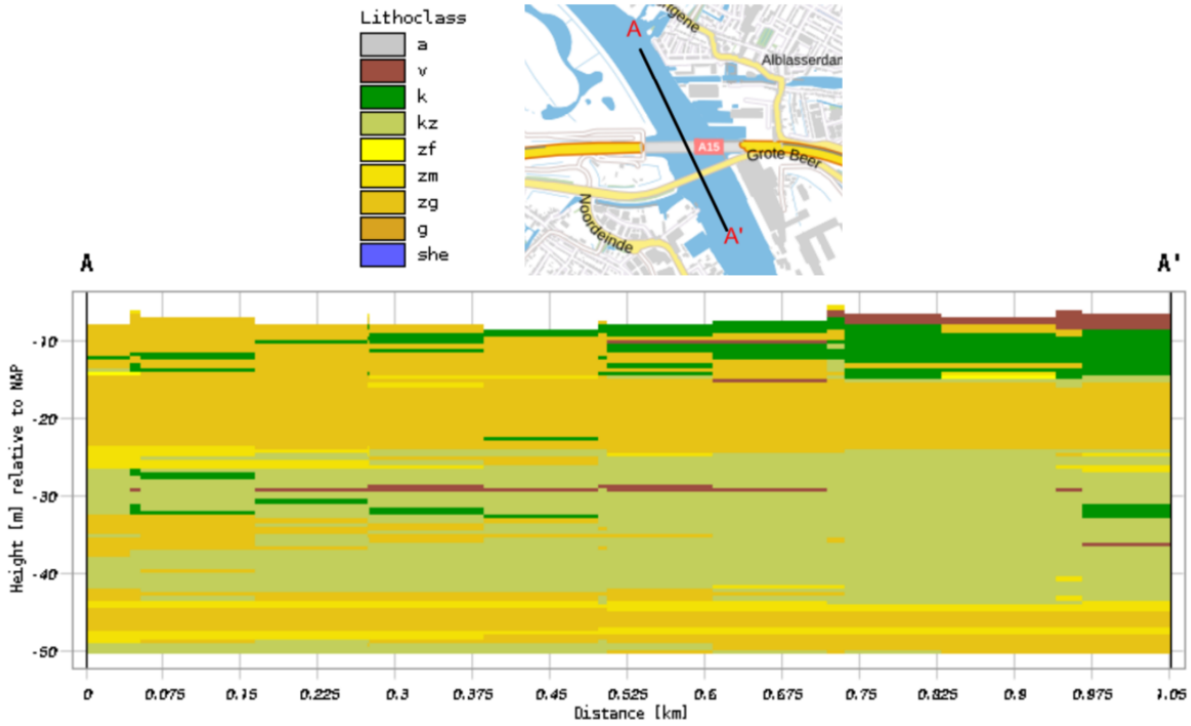

Figure 4.2: The soil profile along transverse direction (DINOloket, 2023)

Figure 4.1 shows a localized layer of peat and clay along the tunnel route. This topographic characteristic aligns with Figure 4.2, which displays a thin layer of clay and peat in the transverse direction of the tunnel. Furthermore, the SWECO (2020) report provides 22 CPT data points. However, only eight of these CPTs were conducted along the longitudinal alignment of the tunnel. Figure 4.3 illustrates the CPT data obtained from the tunnel longitudinal profile. CPT numbers 01, 04, 08, and 11 were collected in the river near the immersion joints 2, 3, 4, and 5, respectively. Whereas CPT numbers 47, 49, 53, and 55 were acquired prior to the removal of the west dike. However, it should be noted that for the CPT taken in the west dike, only tip resistance data is available.

Based on the site map and CPT data, the water level is observed to be at +0.5 m Normal Amsterdam Peil (NAP). Furthermore, analysis of the DINOloket graph and CPT data reveal minimal soil heterogeneity in the transverse direction. Therefore, the soil profile is considered homogenous in the transverse direction.

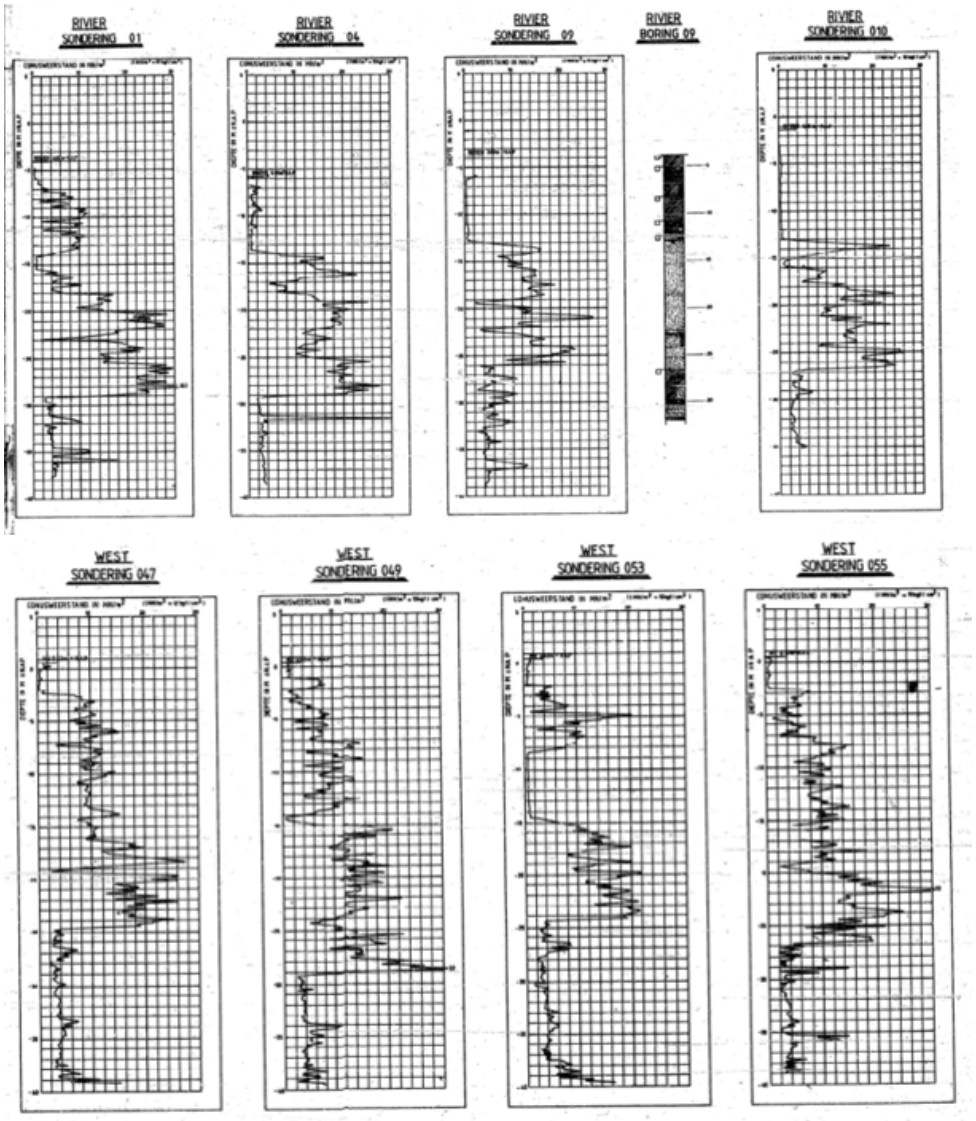

Figure 4.3: CPT profile taken in the river and west dike (SWECO, 2020)

4.1.2 Soil Profile Interpretation

The soil profile at the westernmost immersion joint is determined based on the information provided by the site map. CPT measurements from numbers 49 and 55, which are closest to the site, are considered to ensure the soil stratigraphy. Based on the CPT tip resistance measurement, the upper layer of the soil profile is identified as soft soil, with a thickness of 2.5 m. Then, a layer of stronger soil extends to a depth of 7.0 m, followed by a weaker layer of 0.5 m thickness. Below that, there are granular soils until -29 m, followed by clay layers. However, as the CPT was taken at approximately -39.5 m, the subsequent layer is determined solely based on the situation map, which indicate there is a sandy layer below the clay layer. Table 4.1 shows the resulting soil profile at immersion joint one.

Table 4.1: The soil layer intepretation at immersion joint 1

Depth (m)	Soil Type	Soil Code	Description
0.5 to -2.0	Clay	12	Clay sometimes with sand
-2.0 to -7.0	Sand	14	Sand often silty with thin clay layers
-7.0 to -7.5	Clay	12-14	Sandy clay
-7.5 to -17.0	Sand	14	Sand often silty with thin clay layers
-17.0 to -29.0	Sand	32A	Sand, medium grains, locally gravelly
-29.0 to -39.5	Clay	38	Clay, often sandy or silty, locally peaty or thin peat layer
-39.5 to -75.0	Sand	38B	Sand, find and silty

CPT 01, located near immersion joint 2, is chosen to establish the geological profile in that specific area. The CPT measurement with q_c up to 1 MPa and R_f around 1% indicates a 2.5 m thick layer of clay starting at a depth of -4.5 m. Below it, there is a 7 m thick layer of coarse-grained soil, followed by a 1.5 m thick layer of soft soil with 8% of friction ratio, and finally, a 12.5 m thick layer of strong soil. The weaker subsoil is detected from a depth of -29 m to the end of the CPT data at -38 m. Considering the relatively consistent soil profile based on DINOloket data, a sandy soil type is assumed for simulation purposes between depths of -38 m and -75 m, following the soil type identified at the first immersion joint. Table 4.2 presents the resulting soil profile at immersion joint two.

Table 4.2: The soil layer interpretation at immersion joint 2

Depth (m)	Soil Type	Soil Code	Description
-4.5 to -7.0	Clay	$12-14$	Clay sandy or sandy clay
-7.0 to -14.0	Sand	14	Sand often silty with thin clay layers
-14.0 to -14.5	Clay	15	Clay with plant remains
-14.5 to -15.5	Base peat	9	-
-15.5 to -18.0	Sand	32	Sand, fine to medium, silty
-18.0 to -28.0	Sand	32A	Sand, medium grains, locally gravelly
-28.0 to -38.0	Clay	38	Clay, often sandy or silty, locally peaty or thin peat layer
-38.0 to -75.0	Sand	38B	Sand, find and silty

Moreover, CPT 04, located at the midpoint of the tunnel length, is evaluated to confirm the soil layers indicated in the site map. The CPT tip resistance is less than 1 MPa which indicates a soft soil layer from -5.5 m to -8.5 m. While the friction ratio of 6.25% confirms the upper layer is made of peat. Afterward, soft soil with qc less than 1 MPa is identified within the depth range of -8.5 to -14.0 meters. The sleeve friction values of 5% and 6% correspond to the presence of clay and peat layers, respectively. Subsequently, a strong layer measuring 16.5 m thick is encountered, followed by a relatively weaker layer of clay from -30.5 m to -38.5 m, where the data collection concludes. In addition, coarse-grained soil is assumed for the remaining layers for the simulation. Table 4.3 presents the resulting soil profile at immersion joint three.

Table 4.3: The soil layer interpretation at immersion joint 3

Depth (m)	Soil Type	Soil Code	Description
-5.5 to -8.5	Peat	4	-
-8.5 to -13.0	Clay	15	Clay with plant remains
-13.0 to -14.0	Base peat	9	-
-14.0 to -18.0	Sand	32	Sand, fine to medium, silty
-18.0 to -30.5	Sand	32*A*	Sand, medium grains, locally gravelly
-30.5 to -38.5	Clay	38	Clay, often sandy or silty, locally peaty or thin peat layer
-38.0 to -75.0	Sand	38*B*	Sand, find and silty

Furthermore, the soil profile in the fourth immersion joint can be readily verified as the CPT value is indicated on the site map. The resulting soil profile is presented below.

Table 4.4: The soil layer interpretation at immersion joint 4

Depth (m)	Soil Type	Soil Code	Description
-6.5 to -8.5	Peat	4	-
-8.5 to -12.5	Clay	15	Clay with plant remains
-12.5 to -13.5	Base peat	9	-
-13.5 to -16.0	Sand	32	Sand, fine to medium, silty
-16.0 to -27.5	Sand	32*A*	Sand, medium grains, locally gravelly
-27.5 to -34.0	Clay	38*A*	Clay, strongly sandy to sandy clay
-34.0 to -38.5	Clay	38	Clay, often sandy or silty, locally peaty or thin peat layer
-38.5 to -75.0	Sand	38*B*	Sand, find and silty

The nearest recorded measurement for the final immersion joint is CPT 11. According to the CPT data, the upper layer starts at a depth of -2.5 m and is characterized as soft soil with a thickness of 10.5 m. It should be noted that a thin peat layer is detected at a depth of -12 to -13 m, as evidenced by a friction ratio of 6%. friction ratio of 6% indicates This is followed by a layer of stronger soil extending to a depth of -27.0 m, then a 7 m thick clay layer. However, since the CPT was taken at approximately -34.0 m, the remaining subsequent layer is considered coarse-grained soil for the simulation. Table 4.5 presents the resulting soil profile at the easternmost immersion joint.

Table 4.5: The soil layer interpretation at immersion joint 5

Depth (m)	Soil Type	Soil Code	Description
-2.5 to -5.5	Clay	12	Clay sometimes with sand
-5.5 to -6.0	Peat	4	-
-6.0 to -12.0	Clay	15	Clay with plant remains
-12.0 to -13.0	Base peat	9	-
-13.0 to -15.0	Sand	32	Sand, fine to medium, silty
-15.0 to -27.0	Sand	32*A*	Sand, medium grains, locally gravelly
-27.0 to -34.0	Clay	38	Clay, often sandy or silty, locally peaty or thin peat layer
-34.0 to -75.0	Sand	38*B*	Sand, find and silty

4.2 GEOTECHNICAL PARAMETERS

The geotechnical parameters are determined using two different approaches. The soil properties, including unit weight, cohesion, and friction angle, are obtained from the report of GrondmechanicaDelft (1984, 1986). On the other hand, the stiffness parameters are estimated by correlating CPT tip resistance values with NEN (2017) Table 2b.

4.2.1 Soil Properties

The soil properties obtained from the GrondmechanicaDelft (1984, 1986) reports, collected before the tunnel construction, are presented in Table 4.6 below.

Table 4.6: The soil layer interpretation at immersion joint 5

Soil Type	Soil Code	γ_{sat} (kN/m^3)	c (kN/m^2)	Friction Angle (°)
Clay	12	16	5	22
Clay	$12-14$	16	5.4	21.6
Peat	4	11	5	25
Base peat	9	12	5	28
Clay	15	14	7	20
Clay	38	20	13	22.5
Clay	$38A$	18	0	27.5
Sand	32	20	0	35
Sand	$32A$	20	0	35
Sand	$38B$	21	0	35

Additionally, the void ratio could influences the settlement, but no specific void ratio data was available in this case. To estimate the void ratio (e), the relative density (D_r) is first calculated using the Robertson (2013) method.

$$D_r^2 = \frac{Q_{tn}}{305 \cdot C_c \cdot C_{OCR} \cdot C_{AGE}} \tag{4.1}$$

$$D_r = \frac{e - e_{min}}{e_{max} - e_{min}} \tag{4.2}$$

where,

Q_{tn}	= normalized tip resistance	$= [(q_t - \sigma_v)/\sigma'_v]^n$
n	= compressibility factor	
C_{OCR}	= overconsolidation factor	$= OCR^{0.18}$
C_{AGE}	= aging factor	$= 1.2 + 0.05 \cdot log(t/100)$
e	= void ratio	
e_{min}	= minimum void ratio	
e_{max}	= maximum void ratio	

In the analysis, the q_t value and the vertical stress (σ) are differentiated by considering the collected CPT data and the soil profile at the site. In this scenario, it is assumed that the soil is under normally consolidated conditions, resulting in an Over Consolidated Ratio (OCR) value of one. Since the construction began in 1989, a 34-year ageing period has been assigned. However, it should be noted that this method applies only to coarse-grained soils. The default value of the void ratio will be used for fine-grained soils in the simulation, which is expected to have a minimal impact on the final results. The impact on clay soils should be even less, as the main relationship in the HS Model involves the increase of internal friction with changes

in volumetric strain or void ratio. It is essential to mention that clay has a lower friction angle than sand, and the variation of friction angle with the void ratio is expected to be low. The typical values of the void ratio are determined based on USCS, as shown in Figure 4.4.

Description	USCS	Void ratio [-]		
		min	max	Specific value
Well graded gravel, sandy gravel, with little or no fines	GW	0.26	0.46	
Poorly graded gravel, sandy gravel, with little or no fines	GP	0.26	0.46	
Silty gravels, silty sandy gravels	GM	0.18	0.28	
Gravel	(GW-GP)	0.30	0.60	
Clayey gravels, clayey sandy gravels	GC	0.21	0.37	
Glatial till, very mixed grained	(GC)	-	-	0.25
Well graded sands, gravelly sands, with little or no fines	SW	0.29	0.74	
Coarse sand	(SW)	0.35	0.75	
Fine sand	(SW)	0.40	0.85	
Poorly graded sands, gravelly sands, with little or no fines	SP	0.30	0.75	
Silty sands	SM	0.33	0.98	
Clayey sands	SC	0.17	0.59	
Inorganic silts, silty or clayey fine sands, with slight plasticity	ML	0.26	1.28	
Uniform inorganic silt	(ML)	0.40	1.10	
Inorganic clays, silty clays, sandy clays of low plasticity	CL	0.41	0.69	
Organic silts and organic silty clays of low plasticity	OL	0.74	2.26	
Silty or sandy clay	(CL-OL)	0.25	1.80	
Inorganic silts of high plasticity	MH	1.14	2.10	
Inorganic clays of high plasticity	CH	0.63	1.45	
Soft glacial clay	-	-	-	1.20
Stiff glacial clay	-	-	-	0.60
Organic clays of high plasticity	OH	1.06	3.34	
Soft slightly organic clay	(OH-OL)	-	-	1.90
Peat and other highly organic soils	Pt	-	-	
soft very organic clay	(Pt)	-	-	3.00

Figure 4.4: Typical values of void ratio

Settlement of the tunnel is caused by primary and, to some extent, secondary compression experienced by the soil. Consolidation refers to the reduction in volume of the soil due to natural or human-induced loading. This loading will generate excess pore water pressure within the soil, leading to settlement. The consolidation rate is determined by the soil's hydraulic conductivity (k) and, to a large extent, by the drainage path length (Puzrin et al., 2010). However, in this project, no recorded data on hydraulic conductivity is available. Therefore, the CPT SBT chart developed by Robertson (2010) is utilized to estimate the value of k for each soil layer. Figure 4.5 depicts the characteristic values of k for each type of soil.

SBTn Zone	SBTn	Range of k (m/s)
1	Sensitive fine-grained	$3x10^{-10}$ to $3x10^{-8}$
2	Organic soils - clay	$1x10^{-10}$ to $1x10^{-8}$
3	Clay	$1x10^{-10}$ to $1x10^{-9}$
4	Silt mixture	$3x10^{-9}$ to $1x10^{-7}$
5	Sand mixture	$1x10^{-7}$ to $1x10^{-5}$
6	Sand	$1x10^{-5}$ to $1x10^{-3}$
7	Dense sand to gravelly sand	$1x10^{-3}$ to 1
8	*Very dense/ stiff soil	$1x10^{-8}$ to $1x10^{-3}$
9	*Very stiff fine-grained soil	$1x10^{-9}$ to $1x10^{-7}$

**Overconsolidated and/or cemented*

Figure 4.5: Typical values of hydraulic conductivity (Robertson, 2010)

The void ratio is estimated using equation (4.2), while the hydraulic conductivity value is determined as an average value within the range of Robertson (2010) table. Table 4.7 presents the resulting soil profile at all immersion joints.

Table 4.7: The resulting void ratio and hydraulic conductivity at all immersion joint

Location	Depth (m)	Soil Type	Soil Code	$Q_{tn}(MPa)$	D_r^2	D_r	e	$k(m/day)$
	0.5 to -2.0	Clay	12	-	-	-	0.5	8.6×10^{-4}
	-2.0 to -7.0	Sand	14	134.96	0.38	0.61	0.58	8.6×10^{-2}
	-7.0 to -7.5	Clay	12-14	-	-	-	0.5	4.3×10^{-3}
Joint 1	-7.5 to -17.0	Sand	14	86.51	0.24	0.49	0.66	8.6×10^{-2}
	-17.0 to -29.0	Sand	$32A$	91.88	0.25	0.51	0.52	0.86
	-29.0 to -39.5	Clay	38	-	-	-	0.5	4.3×10^{-4}
	-39.5 to -75.0	Sand	$38B$	29.63	0.08	0.29	0.62	0.86
	-4.5 to -7.0	Clay	$12-14$	-	-	-	0.5	4.3×10^{-3}
	-7.0 to -14.0	Sand	14	58.62	0.16	0.4	0.33	8.6×10^{-2}
	-14.0 to -14.5	Clay	15	-	-	-	0.5	8.6×10^{-5}
Joint 2	-14.5 to -15.5	Base peat	9	-	-	-	0.5	8.6×10^{-4}
	-15.5 to -18.0	Sand	32	67.98	0.19	0.43	0.55	0.86
	-18.0 to -28.0	Sand	$32A$	95.65	0.27	0.52	0.52	0.86
	-28.0 to -38.0	Clay	38	-	-	-	0.5	4.3×10^{-4}
	-38.0 to -75.0	Sand	$38B$	30.99	0.09	0.29	0.62	0.86
	-5.5 to -8.5	Peat	4	-	-	-	0.5	8.6×10^{-4}
	-8.5 to -13.0	Clay	15	-	-	-	0.5	8.6×10^{-5}
	-13.0 to -14.0	Base peat	9	-	-	-	0.5	8.6×10^{-4}
Joint 3	-14.0 to -18.0	Sand	32	115.43	0.32	0.57	0.49	0.86
	-18.0 to -30.5	Sand	$32A$	108.43	0.30	0.55	0.50	0.86
	-30.5 to -38.5	Clay	38	-	-	-	0.5	4.3×10^{-4}
	-38.0 to -75.0	Sand	$38B$	34.4	0.1	0.31	0.61	0.86
	-6.5 to -8.5	Peat	4	-	-	-	0.5	8.6×10^{-4}
	-8.5 to -12.5	Clay	15	-	-	-	0.5	8.6×10^{-5}
	-13.0 to -14.0	Base peat	9	-	-	-	0.5	8.6×10^{-4}
Joint 4	-14.0 to -18.0	Sand	32	96.42	0.27	0.52	0.52	0.86
	-18.0 to -30.5	Sand	$32A$	115.53	0.32	0.57	0.50	0.86
	-27.5 to -34.0	Clay	$38A$	-	-	-	0.5	3.9×10^{-4}
	-34.0 to -38.5	Clay	38	-	-	-	0.5	4.3×10^{-4}
	-38.5 to -75.0	Sand	$38B$	34.52	0.1	0.31	0.61	0.86
	-2.5 to -5.5	Clay	12	-	-	-	0.5	8.6×10^{-4}
	-5.5 to -6.0	Peat	4	-	-	-	0.5	8.6×10^{-4}
	-6.0 to -12.0	Clay	15	-	-	-	0.5	8.6×10^{-5}
Joint 5	-12.0 to -13.0	Base peat	9	-	-	-	0.5	8.6×10^{-4}
	-13.0 to -15.0	Sand	32	112.99	0.31	0.56	0.50	0.86
	-15.0 to -27.0	Sand	$32A$	126.23	0.35	0.59	0.48	0.86
	-27.0 to -34.0	Clay	$38A$	-	-	-	0.5	4.3×10^{-4}
	-34.0 to -75.0	Sand	$38B$	36.1	0.1	0.32	0.61	0.86

4.2.2 Soil Stiffness

Specific laboratory test data regarding soil stiffness are unavailable in this study. Consequently, the soil stiffness for the HS Model is determined by establishing a correlation between CPT

cone resistance and NEN (2017) Table 2b. Equations (2.4) and (2.5) are applied to calculate the $q_{c,table}$ specifically for sandy soil. Following the acquisition of the q_c value, an interpolation method is utilized to compute the soil stiffness. Furthermore, equations (2.6) and (2.7) are utilized to determine the soil's secant stiffness and the Oedometer stiffness for coarse and fine-graned soil, respectively. Lastly, unloading-reloading stiffness is chosen to be three times higher than E_{50}^{ref}, as recommended in the PLAXIS (2021) manual book. Table 4.8 presents the calculated E_{100} at all immersion joints, while Table 4.9 shows the derived stiffness at all immersion joints.

Table 4.8: The stiffness determination at all immersion joint

Location	Depth (m)	Soil Type	Soil Code	$q_c(MPa)$	$\sigma'(kPa)$	C_{qc}	$q_{c,table}$	$E_{100}(MPa)$
	0.5 to -2.0	Clay	12	0.2	7.5	1	0.2	1
	-2.0 to -7.0	Sand	14	6	40	1.85	11.09	30.43
	-7.0 to -7.5	Clay	12-14	1	66.5	1	1	2
Joint 1	-7.5 to -17.0	Sand	14	10	115.5	0.91	9.08	20.40
	-17.0 to -29.0	Sand	32A	18	223	0.58	10.5	31.55
	-29.0 to -39.5	Clay	38	2.7	335.5	1	2.7	6
	-39.5 to -75.0	Sand	38B	18	583.25	0.36	5.5	16.57
	-4.5 to -7.0	Clay	$12-14$	1	57.5	1	1	2
	-7.0 to -14.0	Sand	14	6	100	1	6	5
	-14.0 to -14.5	Clay	15	0.5	136	1	0.5	1
Joint 2	-14.5 to -15.5	Base peat	9	0.5	138	1	0.5	1
	-15.5 to -18.0	Sand	32	10	151.5	0.76	7.57	12.85
	-18.0 to -28.0	Sand	32A	18	214	0.60	10.81	32.43
	-28.0 to -38.0	Clay	38	2.7	314	1	2.7	6
	-38.0 to -75.0	Sand	38B	18	567.5	0.31	5.6	16.87
	-5.5 to -8.5	Peat	4	0.2	61.5	1	0.2	0.5
	-8.5 to -13.0	Clay	15	0.5	72	1	0.5	1
	-13.0 to -14.0	Base peat	9	0.5	82	1	0.5	1
Joint 3	-14.0 to -18.0	Sand	32	12	103	0.98	11.76	33.82
	-18.0 to -30.5	Sand	32A	18	185.5	0.66	11.90	35.70
	-30.5 to -38.5	Clay	38	2.5	288	1	2.5	5
	-38.0 to -75.0	Sand	38B	18	528.75	0.33	5.9	17.70
	-6.5 to -8.5	Peat	4	0.2	71	1	0.2	0.5
	-8.5 to -12.5	Clay	15	0.5	80	1	0.5	1
	-13.0 to -14.0	Base peat	9	0.5	89	1	0.5	1
Joint 4	-14.0 to -18.0	Sand	32	10	102.5	0.98	9.84	24.18
	-18.0 to -30.5	Sand	32A	18	172.5	0.69	12.49	37.48
	-27.5 to -34.0	Clay	38A	8	256	1	8	10
	-34.0 to -38.5	Clay	38	2.5	304.5	1	2.5	5
	-38.5 to -75.0	Sand	38B	18	527.75	527.75	5.9	17.72
	-2.5 to -5.5	Clay	12	0.5	39	1	0.5	1
	-5.5 to -6.0	Peat	4	0.2	48.25	1	0.2	0.5
	-6.0 to -12.0	Clay	15	0.5	60.5	1	0.5	1
Joint 5	-12.0 to -13.0	Base peat	9	0.5	73.5	1	0.5	1
	-13.0 to -15.0	Sand	32	10	84.5	1.12	11.19	30.97
	-15.0 to -27.0	Sand	32A	18	154.5	0.75	13.45	40.35
	-27.0 to -34.0	Clay	38	2.5	249.5	1	2.5	5
	-34.0 to -75.0	Sand	38B	18	510	0.34	6.04	18.13

Table 4.9: The Hardening Soil parameters at all immersion joint

Location	Depth (m)	Soil Type	Soil Code	$E_{50}^{ref}(MPa)$	$E_{oed}^{ref}(MPa)$	$E_{ur}^{red}(MPa)$
Joint 1	0.5 to -2.0	Clay	12	1	0.5	3
	-2.0 to -7.0	Sand	14	30.43	30.43	91.29
	-7.0 to -7.5	Clay	12-14	2	1	6
	-7.5 to -17.0	Sand	14	20.40	20.40	61.20
	-17.0 to -29.0	Sand	32A	31.55	31.55	94.66
	-29.0 to -39.5	Clay	38	6	3	18
	-39.5 to -75.0	Sand	38B	16.57	16.57	49.70
Joint 2	-4.5 to -7.0	Clay	$12-14$	2	1	6
	-7.0 to -14.0	Sand	14	5	5	15
	-14.0 to -14.5	Clay	15	1	0.5	3
	-14.5 to -15.5	Base peat	9	1	0.5	3
	-15.5 to -18.0	Sand	32	12.85	12.85	38.5572
	-18.0 to -28.0	Sand	32A	32.43	32.43	97.31
	-28.0 to -38.0	Clay	38	6	3	18
	-38.0 to -75.0	Sand	38B	16.87	16.87	50.62
Joint 3	-5.5 to -8.5	Peat	4	0.5	0.25	1.5
	-8.5 to -13.0	Clay	15	1	0.5	3
	-13.0 to -14.0	Base peat	9	1	0.5	3
	-14.0 to -18.0	Sand	32	33.82	33.82	101.47
	-18.0 to -30.5	Sand	32A	35.69	35.69	107.08
	-30.5 to -38.5	Clay	38	5	2.5	15
	-38.0 to -75.0	Sand	38B	17.69	17.69	53.08
Joint 4	-6.5 to -8.5	Peat	4	0.5	0.25	1.5
	-8.5 to -12.5	Clay	15	1	0.5	3
	-13.0 to -14.0	Base peat	9	1	0.5	3
	-14.0 to -18.0	Sand	32	24.18	24.18	72.54
	-18.0 to -30.5	Sand	32A	37.48	37.48	112.43
	-27.5 to -34.0	Clay	38A	10	5	30
	-34.0 to -38.5	Clay	38	5	2.5	15
	-38.5 to -75.0	Sand	38B	17.72	17.72	53.15
Joint 5	-2.5 to -5.5	Clay	12	1	0.5	3
	-5.5 to -6.0	Peat	4	0.5	0.25	1.5
	-6.0 to -12.0	Clay	15	1	0.5	3
	-12.0 to -13.0	Base peat	9	1	0.5	3
	-13.0 to -15.0	Sand	32	30.97	30.97	92.92
	-15.0 to -27.0	Sand	32A	40.35	40.35	121.04
	-27.0 to -34.0	Clay	38	5	2.5	15
	-34.0 to -75.0	Sand	38B	18.13	18.13	54.38

Furthermore, in this study, the model will also be simulated with SSC Model to better capture the time-dependent behaviour where the soft soil is dominant. However, similar to HS Model, due to missing laboratory data on soil compressibility (C_c), swelling (C_{sw}), and creep index (C_α), those parameters of this constitutive law are determined solely by correlating CPT tip resistance with NEN (2017) Table 2b. The estimated indices were subsequently transformed into SSC Model parameters using equations (2.9), (2.10), and (2.11), where λ^* represents the modified compression index; κ^* represents the modified swelling index; and μ^* represents the modified creep index. A factor, 2.3 of equations (2.9) and (2.10) comes from the difference

between the 10-log and natural log scale. Those soil parameters are closely related to the one-dimensional parameters In addition, Table 4.10 presents the resulting SSC Model parameters for all immersion joints.

Table 4.10: The resulting indices at all immersion joint

Location	Soil Type	Soil Code	$C_c/(1+e_0)$	C_α	$C_{sw}/(1+e_0)$	λ^*	μ^*	κ^*
Joint 1	Clay	12	0.329	0.013	0.110	0.143	0.004	0.095
	Clay	12-14	0.153	0.006	0.051	0.067	0.002	0.044
	Clay	38	0.071	0.003	0.023	0.031	0.001	0.021
Joint 2	Clay	$12-14$	0.153	0.006	0.051	0.067	0.002	0.044
	Clay	15	0.23	0.012	0.077	0.100	0.003	0.067
	Base peat	9	0.23	0.012	0.077	0.100	0.003	0.067
	Clay	38	0.071	0.003	0.023	0.031	0.001	0.021
Joint 3	Peat	4	0.307	0.015	0.102	0.133	0.004	0.089
	Clay	15	0.23	0.012	0.077	0.100	0.003	0.067
	Base peat	9	0.23	0.012	0.077	0.100	0.003	0.067
	Clay	38	0.077	0.003	0.026	0.033	0.001	0.023
Joint 4	Peat	4	0.307	0.015	0.102	0.133	0.004	0.089
	Clay	15	0.23	0.012	0.077	0.100	0.003	0.067
	Base peat	9	0.23	0.012	0.077	0.100	0.003	0.067
	Clay	$38A$	0.046	0.002	0.015	0.020	0.001	0.0135
	Clay	38	0.077	0.003	0.026	0.033	0.001	0.023
Joint 5	Clay	12	0.329	0.013	0.110	0.143	0.004	0.095
	Peat	4	0.307	0.015	0.102	0.133	0.004	0.089
	Clay	15	0.23	0.012	0.077	0.100	0.003	0.067
	Base peat	9	0.23	0.012	0.077	0.100	0.003	0.067
	Clay	38	0.077	0.003	0.026	0.033	0.001	0.023

4.3 DISCUSSIONS

In this chapter, the subsoil's profile and geotechnical parameters of the subsoil are determined using the CPT, borehole, correlation with NEN (2017) Table 2b, and empirical formula. Identifying the soil profile involves aligning the soil types indicated in the site map with the data from CPT and borehole tests. The tip resistance values from CPT can be employed to differentiate between coarse-grained and fine-grained soils, while the CPT friction ratio aids in distinguishing clay and peat layers. The results reveal relatively consistent soil characteristics along the tunnel's longitudinal direction. The upper layer consists of clay and peat, followed by sandy soil. After that, there are thick clay and sandy soil. The CPT data further confirms the presence of localized soft soil at immersion joint two and a strong sandy clay layer at immersion joint five, as depicted in the site map.

Furthermore, the geotechnical parameters for the simulation are determined using CPT and their correlation with NEN (2017) Table 2b. This approach is considered to be a conservative approach but can be used as a foundation for simulation purposes. The correlations reveal that both the upper layer of soft soil and the lower clay layer have low stiffness values, signifying their compressible nature. In contrast, the sandy layers are classified as moderate sand, showcasing a relatively higher stiffness.

Lastly, other soil properties such as void ratio and hydraulic conductivity, can be derived from Robertson's SBT chart and empirical formula. To determine the void ratio for coarse-grained soil, it is necessary to initially calculate the relative density using equation (4.1). In the case of fine-grained soil, a default value of void ratio can be chosen since its influence on clay soils is expected to be minimal. This is due to the primary relationship in the HS Model involving the increase of internal friction with changes in volumetric strain or void ratio, while the relationship between the friction angle and void ratio of clay exhibits minimal to negligible variation.

4.4 CONCLUSIONS

The following points illustrate the key findings of this chapter:

- The soil profile depicted in the sitemap is aligned with the CPT and borehole data. Thus, the site map can be used as the basis for determining the soil profile in tunnel longitudinal directions. In addition, the correlation between CPT and the DINOloket (2023) shows that the subsoil is generally homogeneous in the tunnel's transverse direction.
- Beneath the Noordtunnel, the underlying soil profile is characterized by an upper layer comprising clay and peat, followed by a layer of moderate sand. Further below a ± 10 m thick of clay layer is situated atop sandy layers.
- The CPT and the DINOloket (2023) confirm the localized soft soil underneath immersion joint two depicted in the sitemap.
- The CPT and NEN Table 2b correlation is being used to determine the geotechnical parameters for the HS Model and SSC Model. The results reveal that both the upper and lower layers of clay have lower stiffness than the sandy soil.

5 SETTLEMENT SIMULATION AND PREDICTION

This chapter works to understand the settlement behaviour and reasonably predict the future settlement of the Noordtunnel through numerical simulation, following the fourth step of the approach presented in Chapter 1. In this simulation, five transverse cross-sections along the longitudinal direction are considered, with each representing the section at immersion joint. Each cross-section is modeled with considering three conditions, namely: (1) model 1, in which the simulation is based on the as-built drawing; (2) model 2, which considers the traffic load; and (3) model 3, which takes into account the effects of natural sedimentation and additional soil cover, respectively. The model was then simulated using two constitutive laws: HS Model and SSC Model, resulting in two corresponding outcomes. The accuracy and reliability of the simulation are further evaluated by a comparison of the simulation result and the reconstructed monitoring data described in Chapter 3, providing a basis for investigating the underlying cause of the excessive settlement. Moreover, sensitivity analysis is conducted to assess which soil parameter influences the most settlement and to examine the extent of deviation after adjusting the parameter. Therefore, the robustness of the model can be evaluated and provide a basis for determining future settlement predictions.

5.1 THE NOORDTUNNEL MODEL DESCRIPTION

The main idea of the simulation is to understand the settlement behaviour and reasonably predict the future settlement of the Noordtunnel. The accuracy of the simulation results is highly dependent on the input parameters and the chosen constitutive laws. The input parameters are determined based on the soil profile and geotechnical parameters, while the construction stages and the geotechnical profile along the tunnel longitudinal direction are used as a basis to select the most suitable constitutive law. As previously explained in Chapter 2, the construction process of an immersed tunnel involves unloading-reloading activity. Thus, the HS Model is chosen as the first constitutive law for the simulation. On the other hand, as the analysis in Chapter 4 confirms the presence of presence of soft soil underneath the tunnel, thus the SSC Model is also employed to capture the time-dependent behaviour of the soft soil.

Since the reconstructed monitoring data is measured in the immersion joints, then the tunnel is divided into five transverse models. Each model represents the five immersion joints. This model approach is selected because modeling the tunnel longitudinally in 2D FEM will need some tricks. For instance, the concrete properties should be adjusted to prevent uplift; and the concrete should be set as non-porous material, as the activation of the tunnel structure will block the upstream flow into the subsoil, resulting in no excess pore water pressure generated. On the other hand, modeling the tunnel on each cross-section does not require any modification of tunnel properties. Thus, the model could better represent the actual situation in practice. Furthermore, the simulation results will be used as the basis for determining the causes of excessive settlement and will be used as the basis for predicting future settlements.

The basic model utilizes the as-built drawing of the Noordtunnel as the foundation for reconstructing the 2D FEM model. The location and elevation of the tunnel element is assumed to be the same as that stated in the as-built drawing document, as depicted in Figure 5.1.

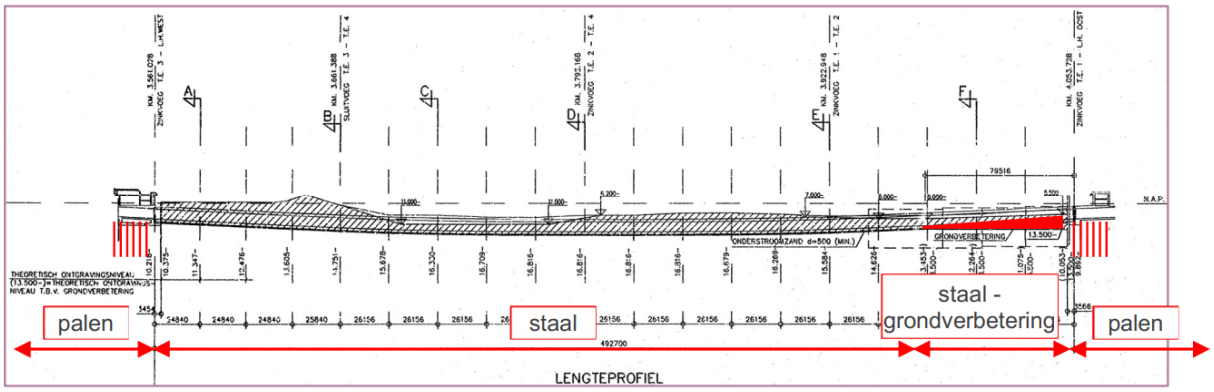

Figure 5.1: Tunnel elevation along longitudinal direction (SWECO, 2020)

The tunnel comprises four tunnel elements, each consisting of five segments, except for element three, which only contains four segments. The tunnel has transverse dimensions of 31.95 m in width, 8.02 m in height, and a wall thickness of 1 m. It is constructed on a foundation consisting of sand flow. The SWECO (2020) and TEC (1992) reports show that the thickness of sand flow is 50 cm. However, there is no report containing the exact properties of the foundation. Thus, it is assumed that the sand flow behave as loose sand. Additionally, it is noted that soil improvement was carried out in the eastern part of the tunnel. However, due to the lack of specific data, it is assumed that the soft soil in this area is replaced by loose sand. Lastly, a 0.65 m thick layer of ballast concrete and a 0.07 m thick layer of asphalt are installed inside the traffic tubes after immersion was completed. The transverse model is built based on the entire tunnel specification.

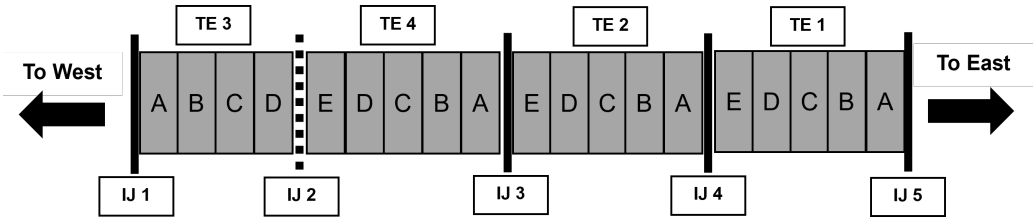

Figure 5.2: Tunnel segmented tunnel element overview (SWECO, 2020)

Table 5.1: The properties of foundation, soil cover, and ballast concrete

Material Type	Thickness (m)	γ_{sat} (kN/m^3)	c (kN/m^2)	ϕ (°)	E (MPa)
Sandflow foundation	0.5	19	0	30	15
Soil Improvement	0.5	19	0	30	15
Soil cover	0.5	19	0	32.5	45
Ballast concrete	0.65	24	0.03	-	$30x10^6$

In this research, a Python-Plaxis interface has been developed to enhance the efficiency of the simulation process. This code streamlines the workflow by automating repetitive tasks and reducing the manual effort required for input preparation and result extraction. The detail of the Python code is presented in Appendix C.

Moreover, in PLAXIS, it is recommended to have a model size that is three to five times the size of the tunnel. Using a sufficiently large model will ensure that the soil can deform within the domain, leading to more realistic results. Therefore, the domain size for the PLAXIS model is set to 250 m in width and 75 m in depth. Listing 5.1 shows the code snippet for creating a soil domain with Python-PLAXIS interface. In addition, Figure 5.3 (the different colours indicate different soil layers as listed in Table 4.2) depicts the model representing immersion joint two, which was selected as a sample for evaluation purposes.

The model also introduces the interface to simulate the soil-structure interaction. Since the tunnel element is built precast, it is necessary to ensure that the structure and soil remain non-composite during simulation. The parameter R_{inter} is set to 0.7 for the soil layer that directly interfaces with the structure. The R_{inter} acts as a factor to reduce the stiffness and strength of the soil.

```
# Set Boundaries
xmax = 125
xmin = -xmax
ymax = 5
ymin = -75
g_i.SoilContour.initializerectangular(xmin, ymin, xmax, ymax)

# Define Soil Thickness
water_level = 0.5 #m, NAP
soil1_topelevation = -4.5   #m, the top of upper layer
soil1_bottomelevation = -7  #m, the bottom of upper layer
soil2_thickness = 7         #thickness soil layer 2
soil3_thickness = 0.5       #thickness soil layer 3
soil4_thickness = 1         #thickness soil layer 4
soil5_thickness = 2.5       #thickness soil layer 5
soil6_thickness = 10        #thickness soil layer 6
soil7_thickness = 10        #thickness soil layer 7
soil8_thickness = 37        #thickness soil layer 8

# Create borehole and define the thickness of each soil layer
borehole1 = g_i.borehole(0)
borehole1.Head = 0.5 # water level
g_i.soillayer(0) #1st layer from top
g_i.soillayer_1.Zones[0].Top = soil1_topelevation
g_i.soillayer_1.Zones[0].Bottom = soil1_bottomelevation #1st layer
g_i.soillayer(soil2_thickness) #2nd layer
g_i.soillayer(soil3_thickness) #3rd layer
g_i.soillayer(soil4_thickness) #4th layer
g_i.soillayer(soil5_thickness) #5th layer
g_i.soillayer(soil6_thickness) #6th layer
g_i.soillayer(soil7_thickness) #7th layer
g_i.soillayer(soil8_thickness) #8th layer

#Example to Set Soil Properties
g_i.gotosoil()
clay_sandy = g_i.soilmat() #clay (clay sandy or sandy clay), code: 12-14
if softsoil_model == "HS":  #select the soil constitutive law
    #Clay with sand or sandy clay (code: 12-14) properties:
    #General
    clay_sandy.setproperties(("MaterialName", "clay_sandy"), ("SoilModel", 3), ("
    DrainageType","Undrained (A)")) #HS
    g_i.clay_sandy.gammaUnsat = 16  #gamma Unsat
    g_i.clay_sandy.gammaSat = clay_sandy_gammasat  #gamma sat
    #Parameters
    E_clay_sandy = 2 * 1000 #kPa (E100 in kPa)
    g_i.clay_sandy.E50ref = E_clay_sandy  #E_50_ref
```

```
    g_i.clay_sandy.EoedRef = 0.5 * E_clay_sandy    #E_oed_ref
    g_i.clay_sandy.EurRef = 3 * E_clay_sandy #Eur_ref
    g_i.clay_sandy.powerm = 0.8  #power m
    g_i.clay_sandy.cref = 5.4    #cohession
    g_i.clay_sandy.phi = 21.6    #phi, friction angle
    g_i.clay_sandy.nu = 0.2   #nu, Poisson's ratio
    #Groundwater
    g_i.clay_sandy.SoilTypeFlow = "Medium Fine" #groundwater soil type flow
    g_i.clay_sandy.perm_primary_horizontal_axis = 0.00432
    g_i.clay_sandy.perm_vertical_axis = 0.00432
    #Interfaces
    g_i.clay_sandy.InterfaceStrength = "Manual" #Interfaces Strength
    g_i.clay_sandy.Rinter = 0.7 #Rinter

#Assign soil properties to the soil layers
g_i.setmaterial((g_i.Soillayers[0]), clay_sandy)
g_i.setmaterial((g_i.Soillayers[1]), sand_silty)
g_i.setmaterial((g_i.Soillayers[2]), clay_withplant)
g_i.setmaterial((g_i.Soillayers[3]), peat_base)
g_i.setmaterial((g_i.Soillayers[4]), sand_32)
g_i.setmaterial((g_i.Soillayers[5]), sand_32A)
g_i.setmaterial((g_i.Soillayers[6]), clay_38)
g_i.setmaterial((g_i.Soillayers[7]), sand_38b)
```

Listing 5.1: Python code snippet for creating soil geometry in PLAXIS

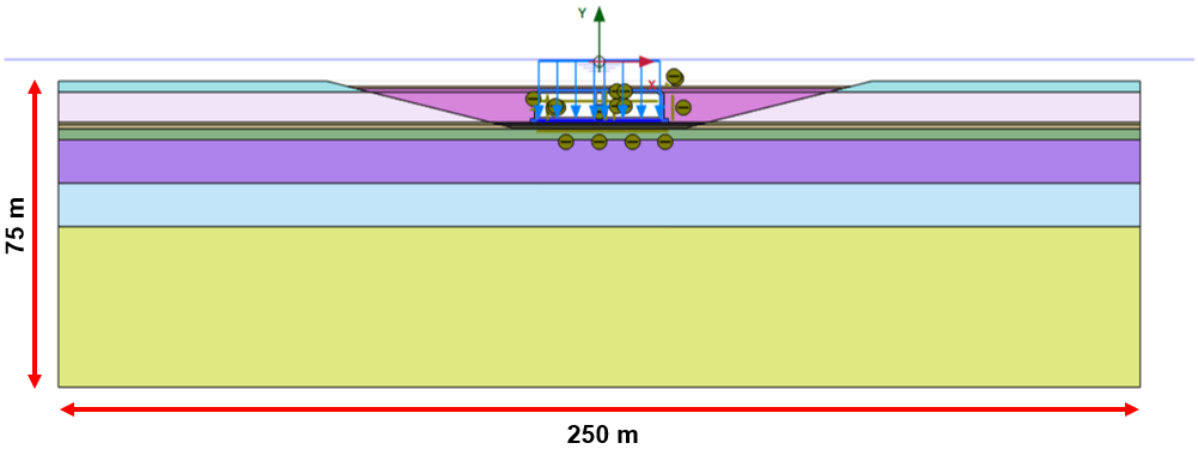

Figure 5.3: The tunnel model - soil domain

Furthermore, two methods are available for simulating the structure of an immersed tunnel: using a solid elastic material without pores or utilizing plate elements. In this research, the plate element is introduced, as it provides the advantage of obtaining internal forces within the structure. The outer contour of the immersed tube can be applied at the bottom and on both sides during the simulation. The plate material properties are set as one-thousandth of the normal value to make the concrete material plays a predominant role and avoid double counting. Table 5.2 show the plate properties of the materials used in the simulation.

Table 5.2: The properties of plate

Material Type	EA (kN/m)	EI (kNm^2/m)	w ($kN/m/m$)
Plate at floor	$42x10^3$	6860	0
Plate at wall	$30x10^3$	2500	0
Plate at center tube	$15x10^3$	312.5	0

5.2 SETTLEMENT SIMULATION OF MODEL 1

5.2.1 Description of Model 1

In this first model type, no additional load is applied to the tunnel. The subsoil's settlement was simulated by only considering the tunnel weight and the soil backfilling. The construction stages have to be determined first before the simulation is conducted. As explained in Chapter 2, the construction phases of the immersed tunnel begin by excavating the trench, then immersing the tunnel element and applying the sand foundation. Afterward, backfilling is conducted until the intended thickness of the soil cover is met. Lastly, the ballast concrete and utility instruments are installed before the tunnel opens for traffic. However, there are no specific details regarding the time required to excavate the trench until immersing the tunnel. Therefore, the plastic calculation type is selected in the simulation for the first three stages. Afterward, consolidation calculation is chosen as the calculation type for the remaining stages. Regarding the flow conditions, the boundary contours are defined as seepage, except for the lowest boundary line.

As an illustration, the following phase explanation utilizes immersion joint 2 (corresponding to point 103), where the most significant settlement was observed. Moreover, it is important to mention that the phase details for the HS Model and the SSC Model are identical.

Phase 1: Trench Excavation
The trench is excavated to a depth of -14,751 meters relative to the NAP, considering the sandflow foundation. The slope of the channel begins at a distance of 4 meters from the base of the tunnel, with a vertical height of 10.251 meters and a slope ratio of 1 : 4. The trench excavation stage involves unloading the soil underneath the trench, resulting in a rebounding phenomenon. The magnitude of rebounding is controlled by the unloading/reloading stiffness modulus, E_{ur} for the HS Model, and $\kappa*$ in the SSC Model. As shown in Figure 5.4, the contour represents the variation in vertical effective stress. Noticeably, the stress initially becomes positive and then transitions to negative, indicating a rebounding trend.

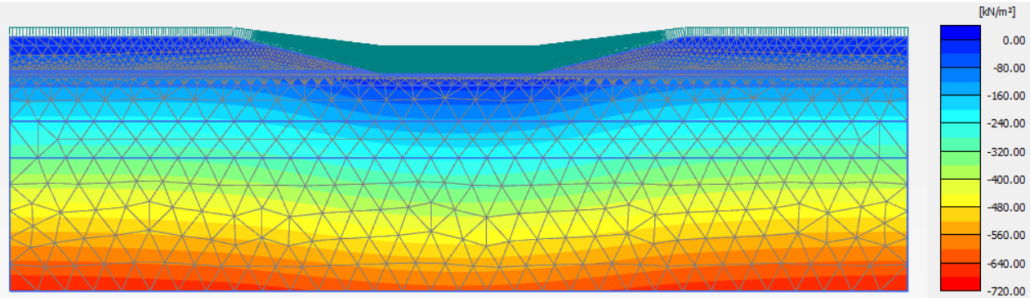

Figure 5.4: The vertical effective stress after dredging the trench

Figure 5.5 illustrates the deformation caused by the unloading phenomenon, with different colours indicating the extent of deformation. It is evident that the maximum unloading occurs at the centre and gradually weakens as it spreads outward of the trench for both HS Model and SSC Model.

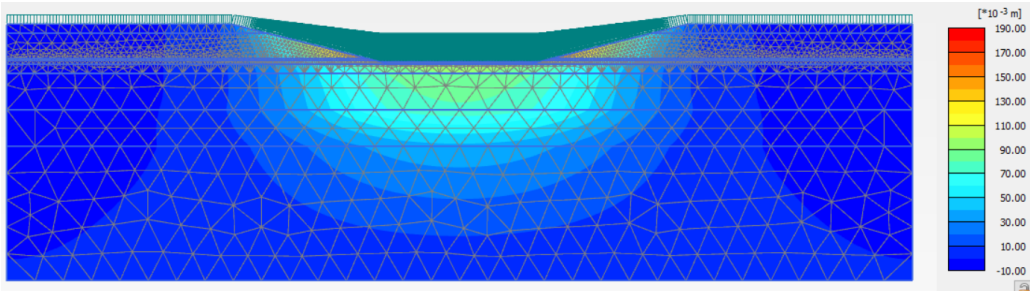

(a) HS Model

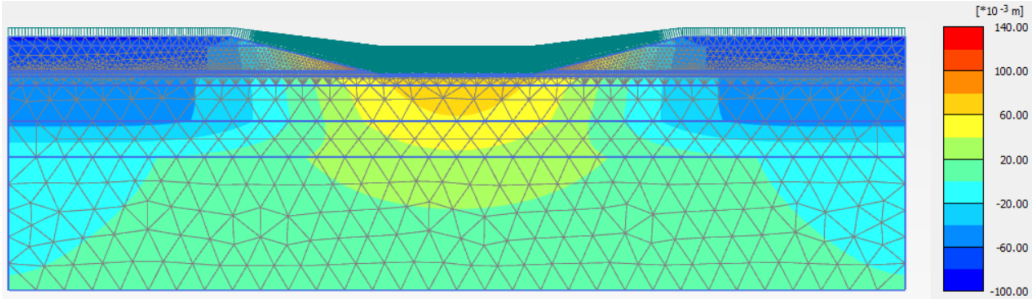

(b) SSC Model

Figure 5.5: The settlement contour dredging the trench

The comparison between the HS model and the soft soil model reveals that the magnitude of rebound in the HS model is slightly higher than that in the soft soil model due to the yield contour difference. The yield contour defines the stress level at which soil deformation transitions from elastic behavior to plastic behaviour. The HS Model has stress-dependent behaviour according to a power law fromulation, while the SSC Model involves a logarithmic stress-strain relationship (where stiffness is linearly dependent on the pre-consolidation stress), resulting in a higher rebound magnitude in the former constitutive law.

Phase 2: Applied Sandflow Foundation

In practice, the sand flow foundation is installed after the tunnel elements have been immersed. During this procedure, the tunnel elements are supported temporarily by lifting jacks while the sand flow foundation is applied beneath the tunnel element. Once the foundation is placed, the temporary jack is removed. However, it is not possible to model this construction process in PLAXIS as the soil body would collapse. Therefore, the application of the sand flow needs to be advanced in time to prevent failure.

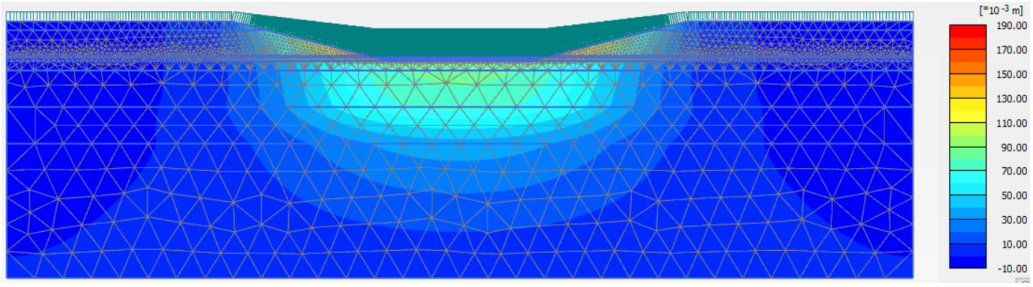

(a) HS Model

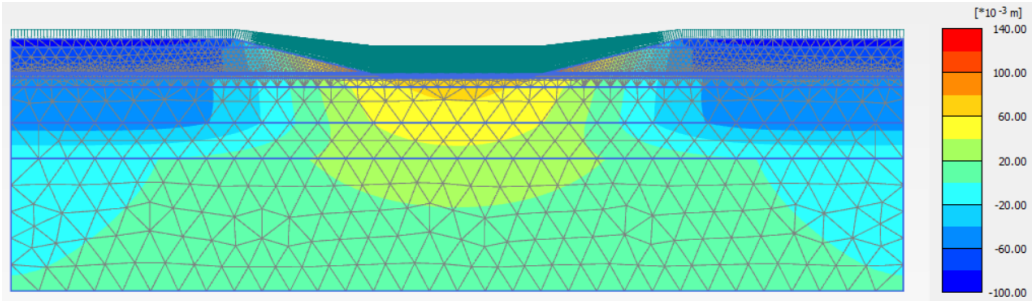

(b) SSC Model

Figure 5.6: The settlement contour after applying sand flow foundation

Figure 5.6 shows that the rebound magnitude during the sand-flow foundation construction is reduced compared to the previous stages. Although the net weight of the sand flow foundation is relatively smaller than the weight of the excavated soil, the subsoil begins to settle.

Phase 3: Immersion Phase

The second immersion joint is situated at a depth of -14.25 m NAP. During immersion, a buoyancy safety factor of 1.05 is implemented to prevent uplift. In practical applications, water tanks are placed inside the tunnel as a counterforce. These water tanks are represented as line loads in the simulation for simplification purposes. During the immersion process, it is assumed that the voids inside the tunnel tubes are set as dry, meaning there is no water present.

As the tunnel element is placed and the increased load is applied, effective stress is significantly increased in the surrounding soil. This change in stress distribution leads to additional settlement of the soil. The simulation shows that the settlement increment for both the HS Model and the SSC Model is almost identical. The HS Model predicts a settlement increment of 22.2 mm, while the SSC Model predicts a slightly higher settlement increment of 23.2 mm. This similarity in settlement increments suggests that both models capture the essential aspects of the settlement behaviour and provide consistent results. The settlement increase in SSC Model is slightly higher than the HS Model because it considers the time-dependent behaviour. Figure 5.7 depicts that the settlement distribution in sandy soil is predominantly vertical, whereas it exhibits a curved pattern in fine-grained soil for both soil models.

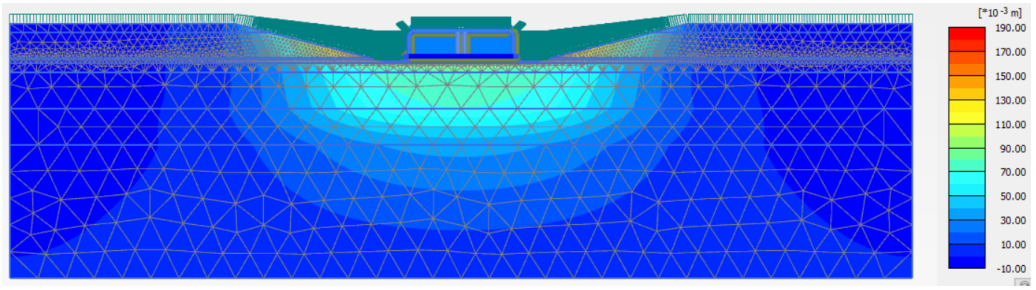

(a) HS Model

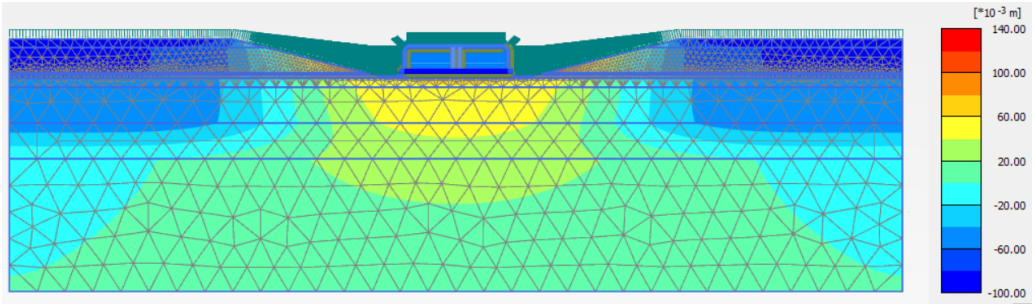

(b) SSC Model

Figure 5.7: The settlement contour after tunnel immersion

Phase 4: Backfilling

In the backfilling process, two types of soil are used: loose sand for the side backfill of the tunnel and gravel for the soil cover on top. The height of the soil cover is 0.5 m. Regarding the settlement behaviour depicted in Figure 5.8, it is observed that the settlements in the backfill soil spread outward from both sides of the tunnel. The settlement amounts gradually change as the distance from the tunnel increases. Notably, the highest settlement increase was observed in the soil beneath the trench, which indicates that the soil under the trench experiences the most significant settlement. This is due to the excavation process during the trenching stage that caused unloading to the soil, then the reloading increase the vertical stress, resulting in soil settlement. As the distance from the trench increases, the settlement amounts gradually decrease. This is because the soil farther away from the trench experiences less disturbance and unloading, resulting in comparatively smaller settlements.

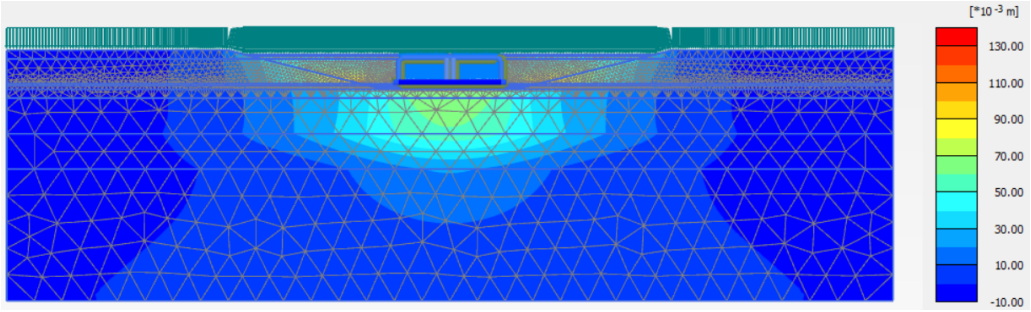

(a) HS Model

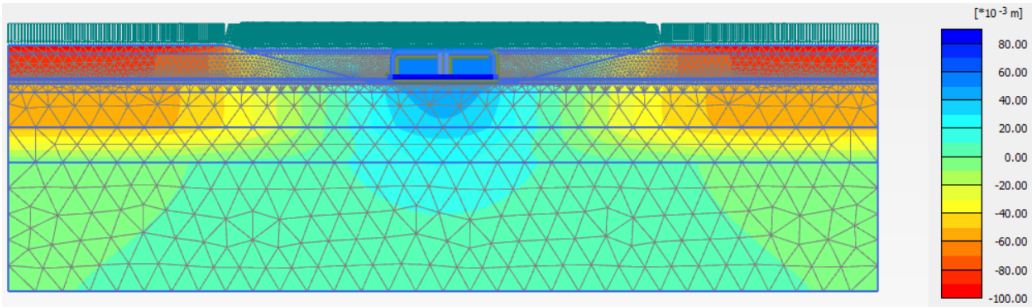

(b) SSC Model

Figure 5.8: The settlement contour after backfilling

Figure 5.9 depicts the accumulation of excess pore pressure in the fine-grained layers. During this phase of consolidation, the sandy layers function as drainage. Thus, the excess pore water pressure generated in the fine-grained soil dissipates to the sandy layer and the seepage boundary line.

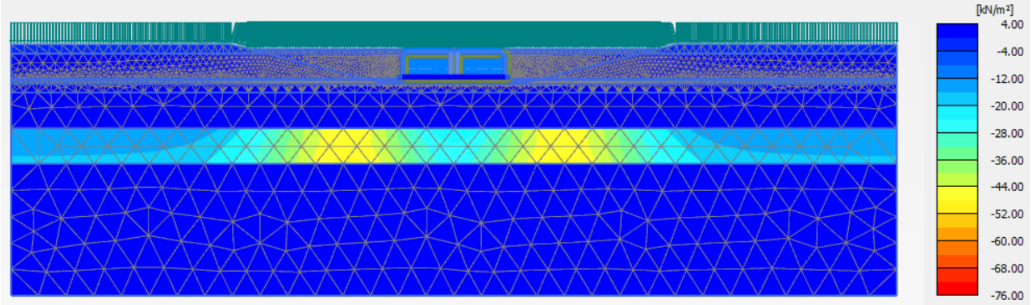

(a) HS Model

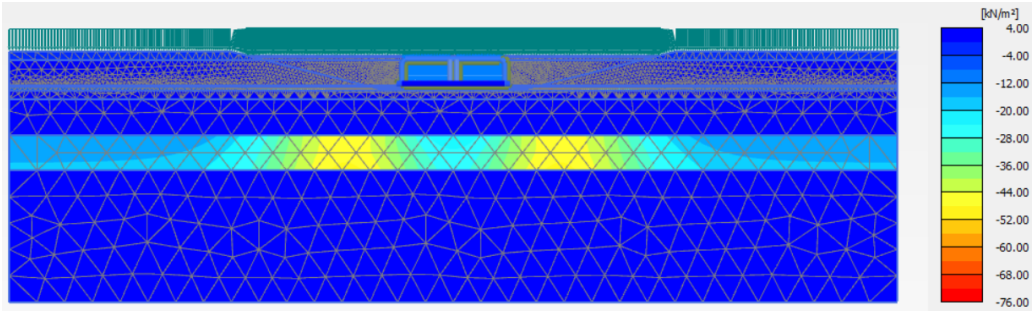

(b) SSC Model

Figure 5.9: The generated excess pore water pressure after backfilling

Phase 5: Ballast Concrete

In practice, once the tunnel elements are connected, the next step is the installation of ballast concrete and asphalt layers. The ballast concrete layer has a thickness of 0.65 m, while the asphalt layer has a thickness of 0.07 m. The simulation implements these layers as static distributed loads applied to both traffic tubes. At this stage the calculation type changes from plastic calculation to consolidation, taking into account the undrained behaviour of fine-grained soils. Furthermore, applying the ballast concrete also means adding more load to the tunnel, resulting in an increase of buoyancy safety factor from 1.05 to 1.1. It also indicates increased resistance to uplift to ensure the structure's stability.

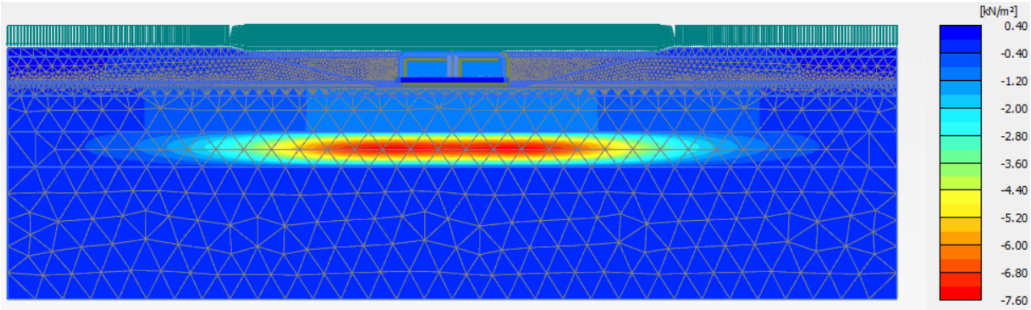

(a) HS Model

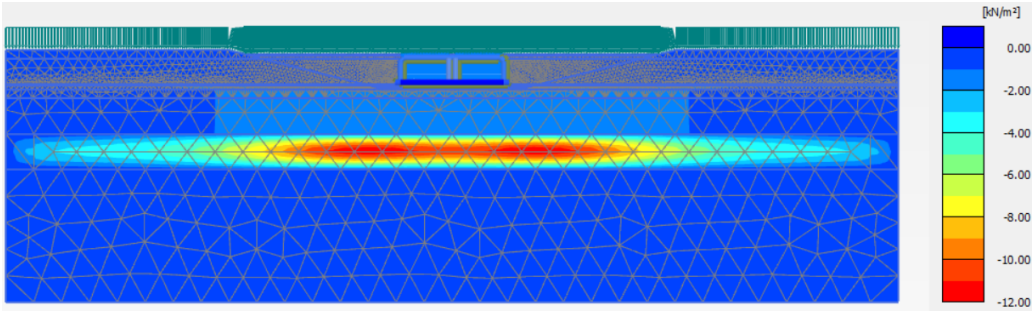

(b) SSC Model

Figure 5.10: The generated of excess pore water pressure after installing ballast concrete and asphalt layer

Figure 5.10 shows that the increase in excess pore water pressure is more pronounced in the SSC Model compared to the HS Model. It is because the SSC Model considers the creep effect. Thus, the settlement increment during this stage is also higher in the SSC Model than HS Model, as shown in Figure 5.11. In the area where soft soil is dominant, the SSC Model captures the long-term settlement behaviour more accurately by accounting for the time-dependent consolidation process, whereas the HS Model focuses on the immediate settlement response due to the additional loads caused by the ballast concrete and asphalt layer.

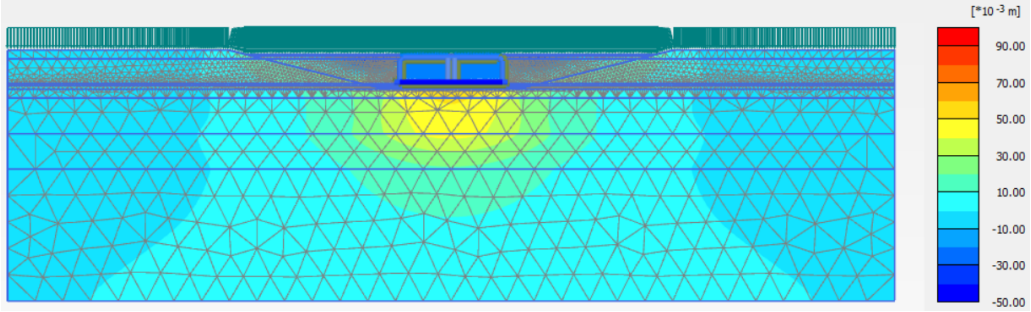

(a) HS Model

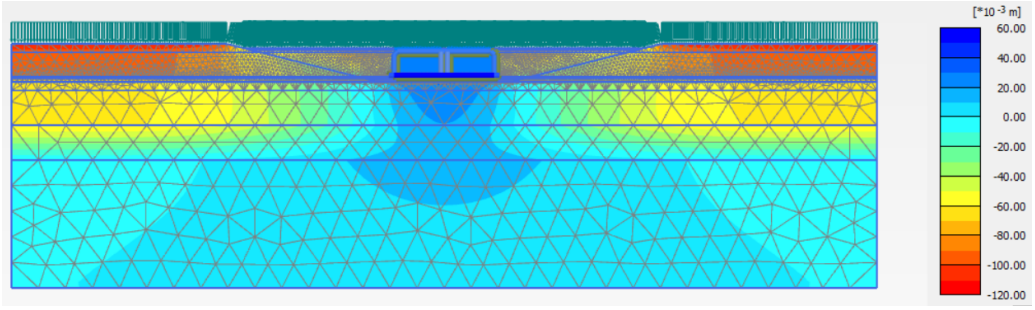

(b) SSC Model

Figure 5.11: The settlement contour after ballast concrete and asphalt layer installation

Phase 6: Open For Traffic

The tunnel opened to traffic on September 25, 1991, so there was seventy five days gap between applying ballast concrete and the opening to traffic. During this period, no additional load is applied to the model. Therefore, Figure 5.12 depicts a decrease in excess pore water pressure compared to the previous stage. It is evident that the excess pore water pressure is relatively small and shows a vertical distribution in the sandy layers. On the other hand, in the clay

layer, the excess pore water pressure takes on a curved shape, spreading towards the sides, up, and bottom. This behaviour occurs due to the dissipation of excess pore water pressure into the upper and lower sandy soils and towards the side boundaries of the clay layer, as it is set as a seepage in the simulation.

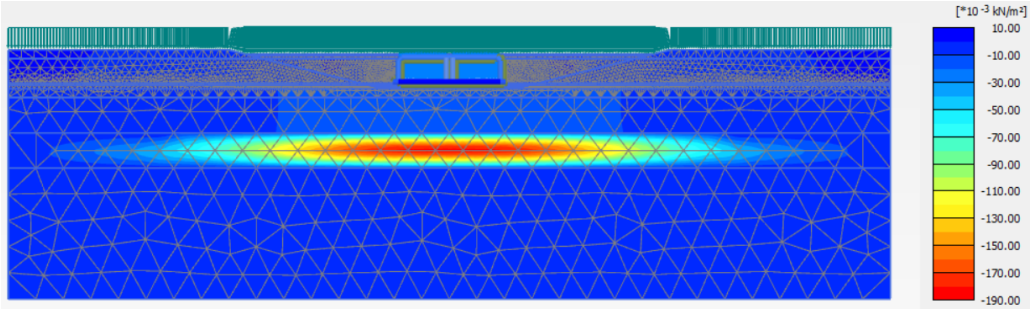

(a) HS Model

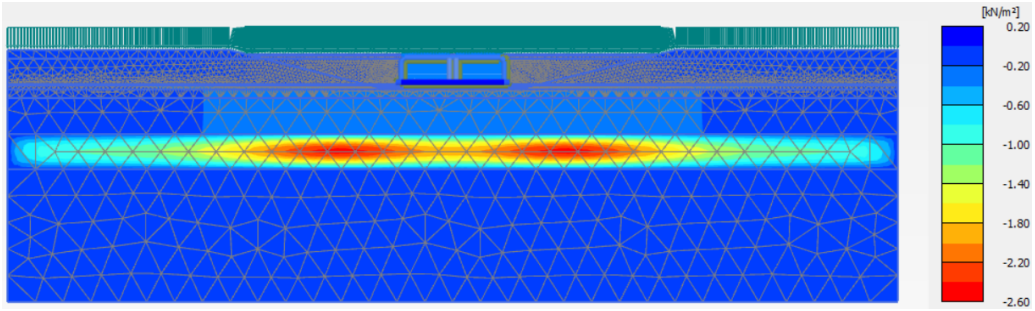

(b) SSC Model

Figure 5.12: The excess pore pressure generated after the tunnel was opened for traffic

Moreover, the ongoing settlement depicted in Figure 5.13 can be attributed to two main factors: the dissipation of excess pore water pressure in the HS Model and the time-dependent settlement behaviour of the soft soil in the SSC Model. Higher settlement magnitude is observed in the SSC Model due to the inclusion of creep effects.

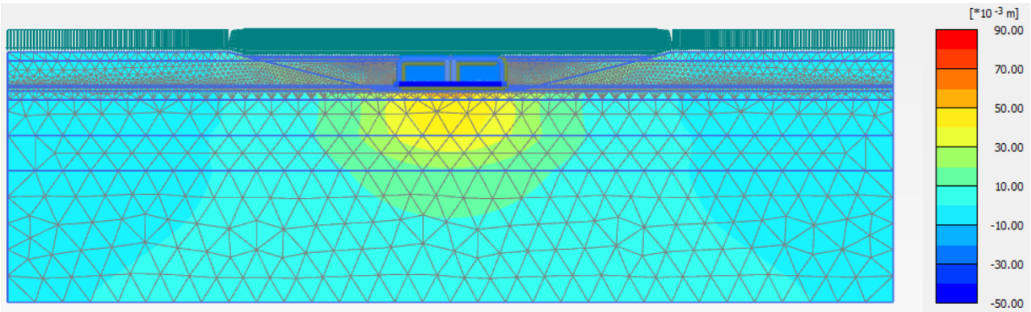

(a) HS Model

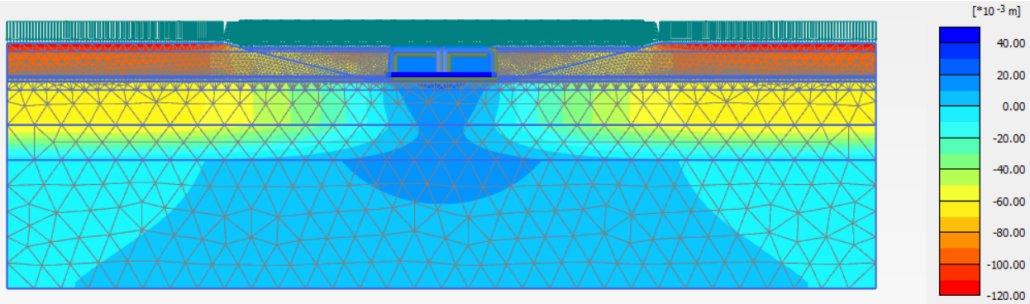

(b) SSC Model

Figure 5.13: The settlement occurred after the tunnel was opened for traffic

Phase 7 - 16: Tunnel Operation after 90 Years

The settlement prediction in this model extends to ninety years after tunnel construction. In this first simulation, no additional load is applied to the model. As a result, the settlement magnitude in the HS Model shows minor changes over time. On the other hand, the SSC Model, which considers creep behaviour, shows ongoing settlement during the tunnel operation but at a slower rate compared to the construction stages. Listing 5.2 shows the code snippet for creating the consolidation phase with the Python-PLAXIS interface.

```
for n in range(9):
    g.i.phase(g.i.Phases[-1])
    g.i.Phases[-1].DeformCalcType = "Consolidation"
    g.i.Phases[-1].PorePresCalcType = "Phreatic"
    g.i.Phases[-1].TimeInterval = 3650 #per 10 years
    g.i.Phases[-1].Deform.ForceFullyDrainedOnActivation = False
    g.i.GroundwaterFlow.BoundaryYMin[g.i.Phases[-1]]= "Closed"
```

Listing 5.2: Python code snippet for tunnel consolidation phase during tunnel operation

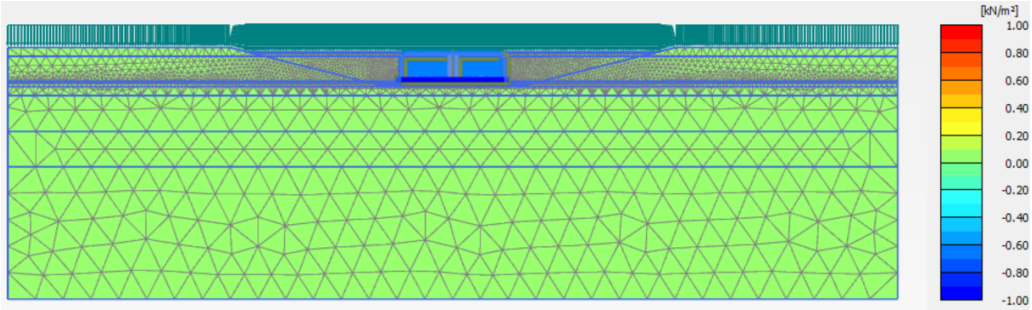

(a) HS Model

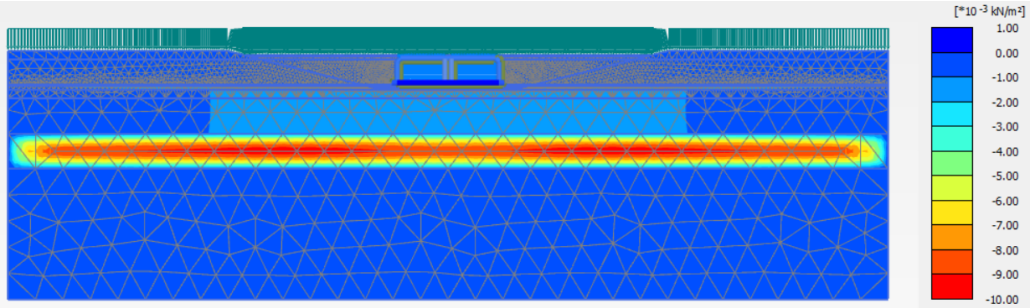

(b) SSC Model

Figure 5.14: The excess pore water pressure after 90 years of tunnel operation

Figure 5.14 above shows no excess pore water pressure generated in the HS Model, which is expected due to the absence of additional load during tunnel operation. In contrast, the SSC Model shows low excess pore water pressure, with a maximum value of only 0.01 kN/m^2. Therefore, although there is no significant increase in settlement in the HS Model, the SSC Model still experiences settlement due to creep effects.

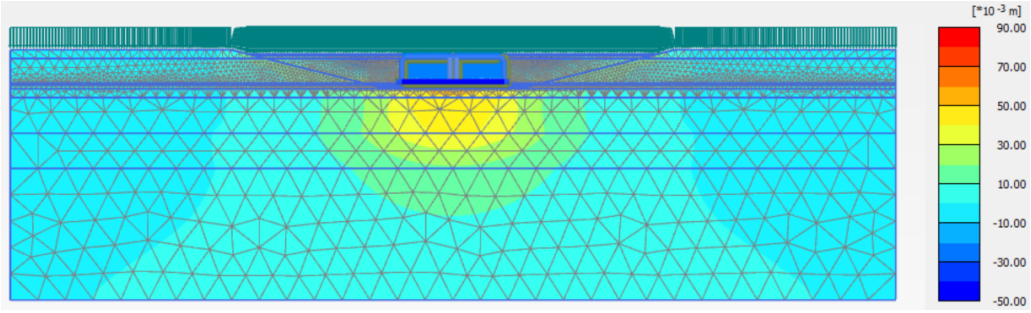

(a) HS Model

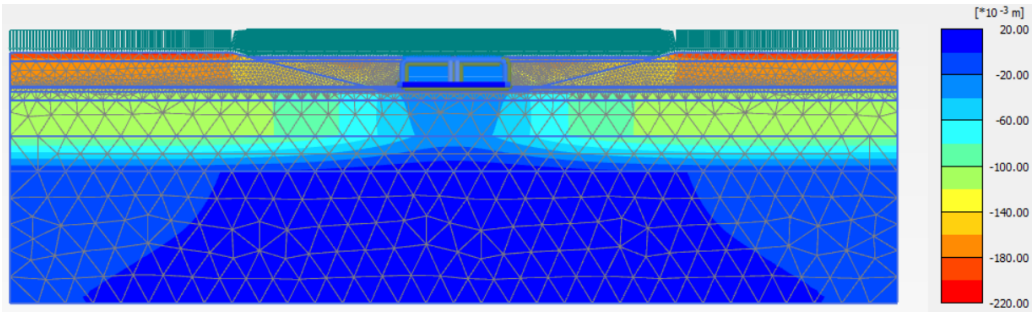

(b) SSC Model

Figure 5.15: The vertical deformation after 90 years of tunnel operation

5.2.2 Simulation Results of Model 1

In the simulation, all immersion joints' construction phases are similar as explained in Subsection 5.2.1, except for the easternmost immersion joint, where soil improvement occurs by replacing the soft soil beneath the tunnel with loose sand. However, since the specific timeline of soil improvement in the particular area is missing, it is assumed that the soil improvement is applied simultaneously with the sand foundation.

The simulation results are compared to the monitoring data for validation and to figure out the settlement tendency at all immersion joints. The settlement tendency of all immersion joints is simulated using two soil models: the HS Model and the SSC Model. Listing 5.3 presents the Python code for extracting the settlement results in the PLAXIS output interface, while Figure 5.16 depicts the comparison of the monitored settlement with the PLAXIS results. However, it is important to note that the following settlement results use the immersion phase as the baseline since the reconstructed historic settlement of the Noordtunnel started after the immersion phase.

```
#Retrieve settlement at selected node
def getnodeid'result(phase, resulttype, nodeid):
    nodeindex = None
    resultLocation = 'Node'
    'resulttypeID = g'o.ResultTypes.Soil.NodeID
    'nodeids = g'o.getresults(phase, 'resulttypeID, resultLocation)
    nodeindex = 'nodeids[:].index(nodeid)
```

```
    if nodeindex is not None:
        resultvalues = g_o.getresults(phase, resulttype, resultLocation)
        requestedvalue = resultvalues[nodeindex]
        return requestedvalue
    print('Could not find the requested node number in the results of this phase')
    return None
def getnodeid_x(phase, nodeid):
    """
    returns the result for X-coordinate for the specific phase and node number
    """
    return getnodeid_result(phase, g_o.ResultTypes.Soil.X, nodeid)
def getnodeid_y(phase, nodeid):
    """
    returns the result for Y-coordinate for the specific phase and node number
    """
    return getnodeid_result(phase, g_o.ResultTypes.Soil.Y, nodeid)
def getnodeid_uy(phase, nodeid):
    """
    returns the result for Uy for the specific phase and node number
    """
    return getnodeid_result(phase, g_o.ResultTypes.Soil.Uy, nodeid)

node_number = 48021 #node selected for data extraction
uy_0 = 0
print("Node -" Phase_0: uy_0 = -" m".format(node_number, uy_0))
```

Listing 5.3: Python code snippet for extracting settlement results in the PLAXIS output

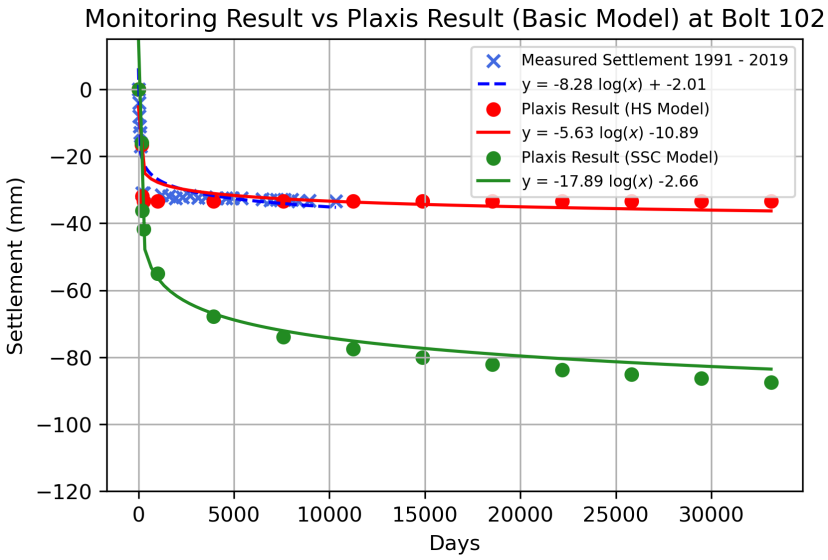

(a) Immersion Joint 1

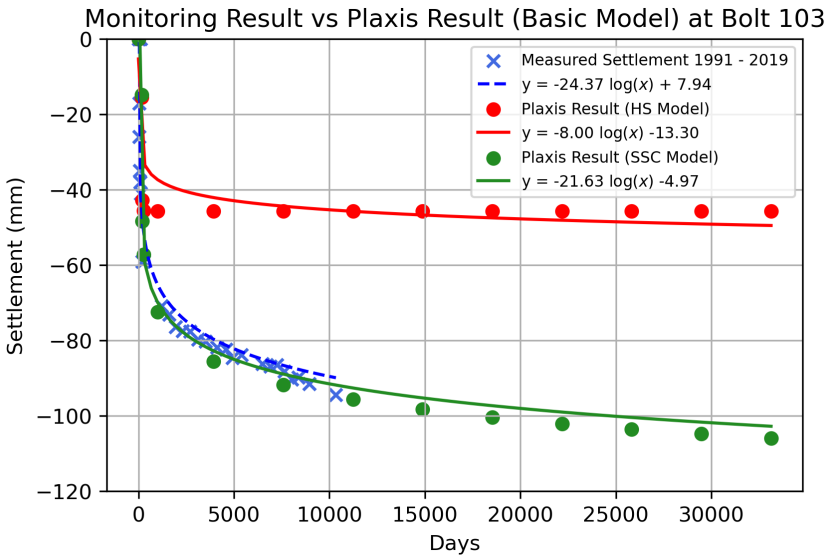

(b) Immersion Joint 2

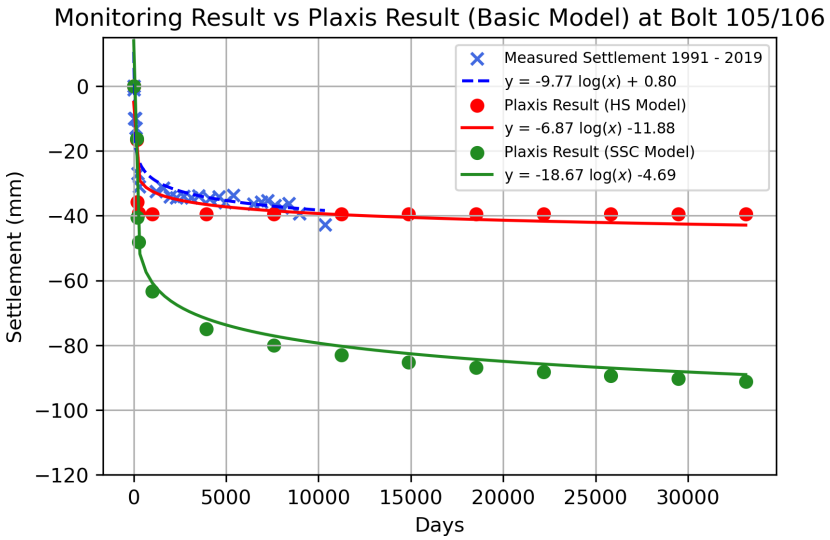

(c) Immersion Joint 3

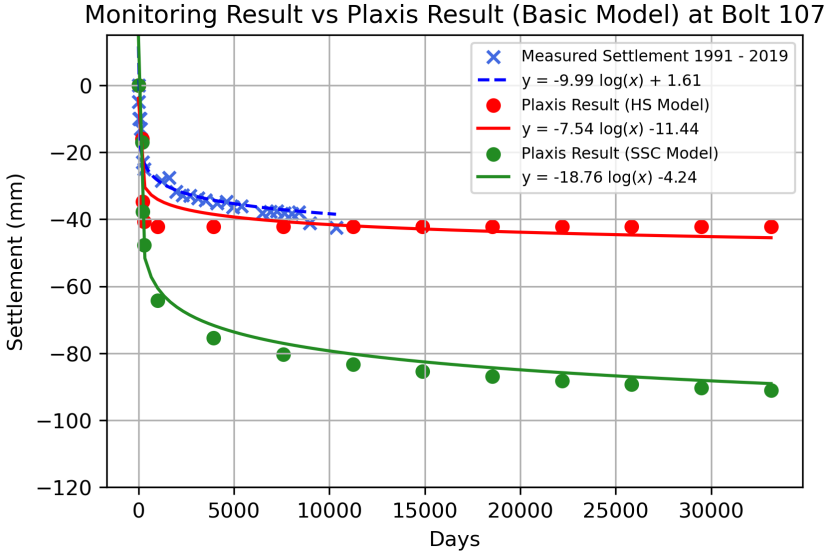

(d) Immersion Joint 4

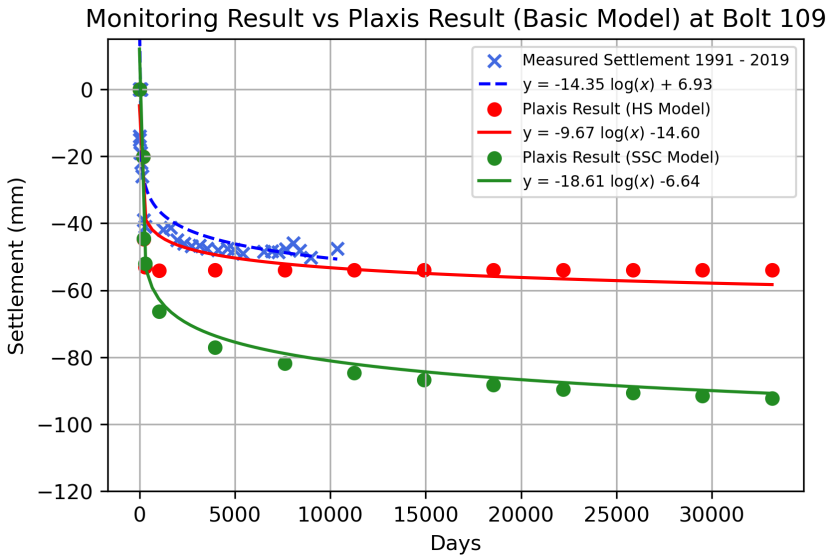

(e) Immersion Joint 5

Figure 5.16: The simulation results against monitoring results at all immersion joints

Figure 5.16 depicts the settlement trendlines for all immersion joints in the HS and SSC models (indicated in red and green trendlines, respectively). The two models show similar settlement tendencies during the initial 206 days, indicating primary compression occurred in the first seven months. The slight difference in settlement magnitude between the models during this period occurs because of the difference in the yield contour. After seven months of immersion, the HS Model shows no further settlement increment, while the SSC Model continues to experience incremental settlement. This is because no additional load is applied to the model, and all excess pore water pressure has been dissipated in the HS Model. On the other hand, the creep effect in the SSC Model leads to ongoing settlement.

Looking at the monitoring data (indicated in blue trendlines), the settlement pattern at all immersion joints indicates a flattening trend. It somewhat fits the HS Model tendency, except for the second immersion joint. This phenomenon is highly likely due to the presence of localized peat and clay underneath the second immersion joint. Soft soil typically has high compressibility, making them susceptible to volume reduction and settlement under applied loads. Consequently, creep behaviour becomes prominent in the second immersion joint, leading to ongoing settlement after the primary compression stage.

Another interesting thing is that besides the second immersion joint, a higher magnitude of settlement is recorded at immersion joint 5, where the ground improvement occurs. The soil is improved by removing and replacing the soft soil with loose sand. Due to this construction method, the combined weight of the soil foundation, tunnel, and soil cover becomes much greater than the removed soft soil. As a result, the subgrade experiences an increase in stress, reaching its pre-consolidation stress level and undergoing elastoplastic deformation. This leads to primary compression during reloading, resulting in a higher settlement magnitude. In PLAXIS, this phenomenon is depicted by the generated compaction hardening as depicted in Figure 5.17 represented in dark blue point.

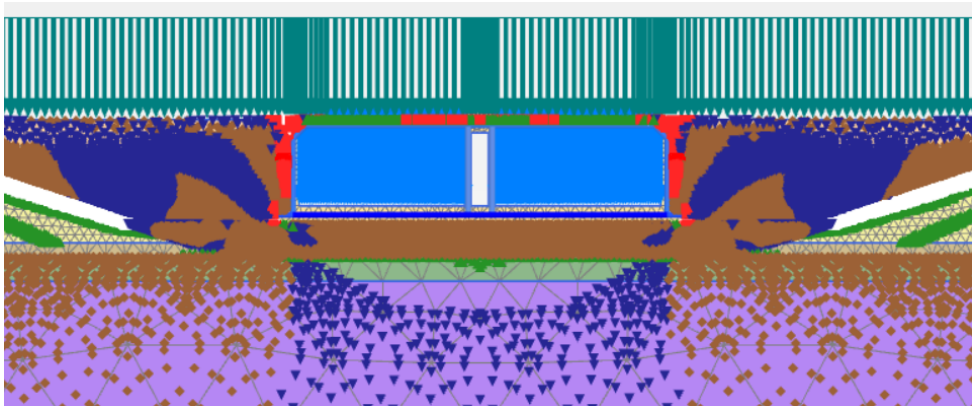

Figure 5.17: The generated compaction hardening at Immersion Joint 5 indicated in dark blue point

Moreover, model 1 demonstrates settlement magnitudes that closely align with the field data. Table 5.3 the deviation between the simulation and monitoring outcomes is relatively minimal, with the highest deviation reaching just 12.15%.

Table 5.3: The comparison of simulation and monitoring results for Model 1

Years	Settlement (mm)				
	IJ 1	IJ 2	IJ 3	IJ 4	IJ 5
2019 (Simulation)	-33.49	-91.81	-39.46	-41.71	-53.42
2019 (Monitoring)	-33.45	-94.36	-42.72	-42.52	-47.63
Deviation	0.12%	2.70%	7.63%	1.9%	12.15%
*)Note:	IJ: Immersion Joint				

5.3 SETTLEMENT SIMULATION OF MODEL 2

5.3.1 Description of Model 2

In the second model type, the traffic load is introduced to the simulation. The traffic load is approximated using (Eurocode, 1991) guidelines. Since the Noordtunnel is part of the national road network, LM 1 (LM 1) is selected. This model is the most suitable as the traffic load is modeled as distributed load and applied on the entire tunnel length. LM 1 is comprised of two partial systems: double-axle concentrated loads, also known as Tandem System (TS), and Uniform Distributed Load (UDL) system, which encompasses the majority of the effects of trucks and cars. Table 5.4 presents the characteristic values for LM 1.

Table 5.4: The characteristic values of LM 1 (Eurocode, 1991)

Location	TS - Axle Loads (kN)	UDL System (kN/m^2)
Lane number 1	300	9
Lane number 2	200	2.5
Lane number 3	100	2.5
Other lanes	0	2.5

In order to obtain the most accurate estimate of traffic load, it is necessary to determine how many vehicles are concurrently inside the tunnel. After its opening, it is anticipated that approximately 67.000 vehicles will go the tunnel daily. If the design speed is 90 kilometers per hour, it only needs 20 seconds or 0.3 minutes for a car to pass the tunnel. Thus, there are approximately 16 vehicles inside the tunnel simultaneously. Considering that it is known

that the tunnel has six lanes, there are approximately three vehicles per lane at any given time. Table 5.5 presents the estimated TS and UDL for one tube when the tunnel opens for traffic.

Table 5.5: The calculated loads for one tunnel tube

Location	Tandem load (kN)	Tandem load / area (kN/m^2)	Total UDL (kN/m^2)
Lane number 1	1800	0.29	4.67
Lane number 2	1200	0.19	
Lane number 3	600	0.1	
Total Load (kN/m^2)	5.24		

As the exact traffic growth through the Noordtunnel is unknown, a 10% increase in traffic per decade is assumed in this research. This assumption serves as a basis to model the potential impact of traffic load on the tunnel's settlement behavior over time. Moreover, the traffic load increase is assumed linear with the weight of cars, meaning that the increasing weight of tandem and uniform distributed loads are the same. The traffic loads increase over time for the simulation is presented in Table 5.6.

Table 5.6: The traffic loads increment over time for one tube

Duration (Years)	Opening	10	20	30	40	50	60	70	80	90
Load (kN/m^2)	5.24	5.76	6.34	6.97	7.67	8.44	9.28	10.21	11.23	12.35

In PLAXIS, the traffic load is represented as line load and applied to both traffic tubes. This traffic load is incorporated in the specific stages of the simulation, namely Phase 7: Tunnel Opening for Traffic to Phase 16: Settlement 90 Years described in Subsection 5.2.1.

5.3.2 Simulation Results of Model 2

The outcomes of the simulation are depicted in Figure 5.18. It can be observed that, unlike the results in the previous subsection, the HS Model shows an increase in settlement in this simulation in each phase of tunnel operation. The reason for this is the inclusion of additional traffic load in each phase, meaning an increase in effective stress resulting in an increase in strain or settlement. Comparing the SSC Model result from this section with the previous section; the results also show a larger settlement magnitude. The subsoil settles more due to the increased effective stress caused by increased traffic volume.

In general, introducing traffic load into the simulation gives a larger settlement magnitude at all immersion joints for both constitutive models, resulting in a higher deviation between the simulation and monitored settlement over time, , as presented in Table 5.7. It is because, in the simulation, the traffic load acts as a static uniform distributed load, meaning that the load stands inside the tunnel at all times. Whereas in reality, it works dynamically. As a result, neither the HS Model nor the SSC Model could fit the settlement tendency of the monitoring data. Thus, modeling settlement with this approach gives an overestimated result.

Table 5.7: The comparison of simulation and monitoring results for Model 2

Years	**Settlement (mm)**				
	IJ 1	**IJ 2**	**IJ 3**	**IJ 4**	**IJ 5**
2019 (Simulation)	-37.28	-100.79	-46.04	-48.94	-61.66
2019 (Monitoring)	-33.45	-94.36	-42.72	-42.52	-47.63
Deviation	11.44%	6.82%	7.77%	15.10%	29.44%
*)Note:	IJ: Immersion Joint				

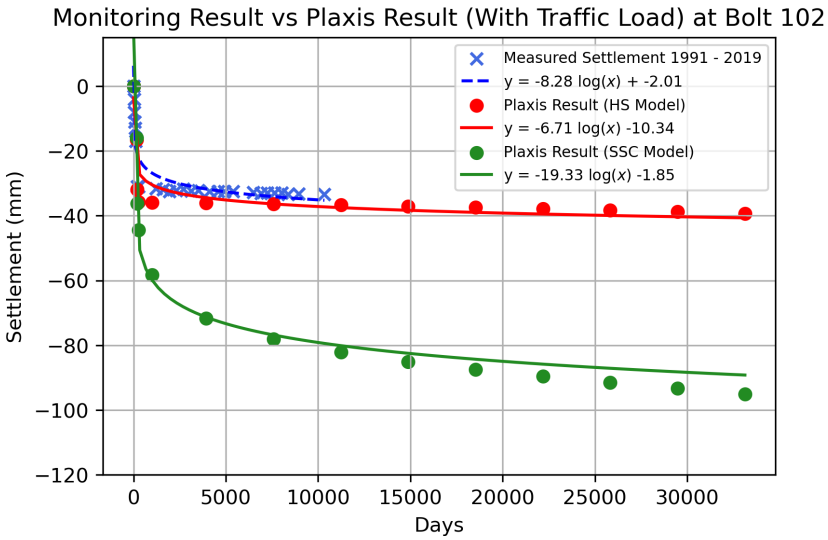

(a) Immersion Joint 1

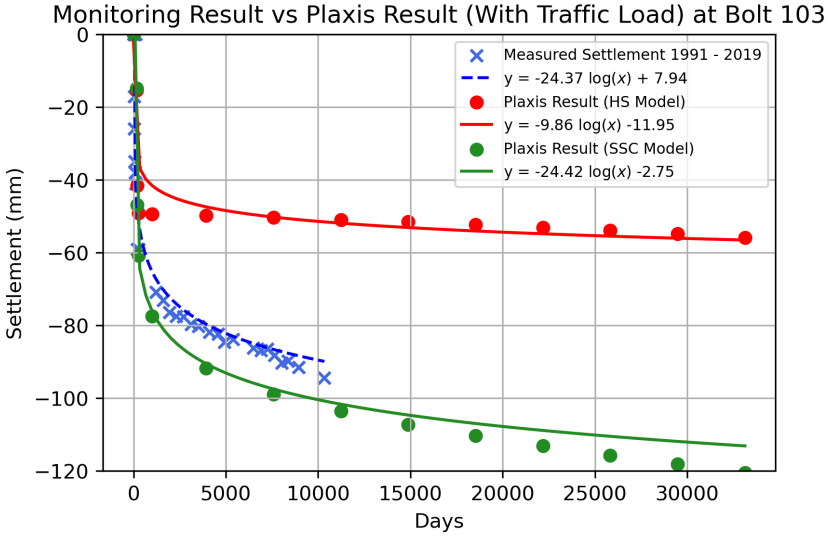

(b) Immersion Joint 2

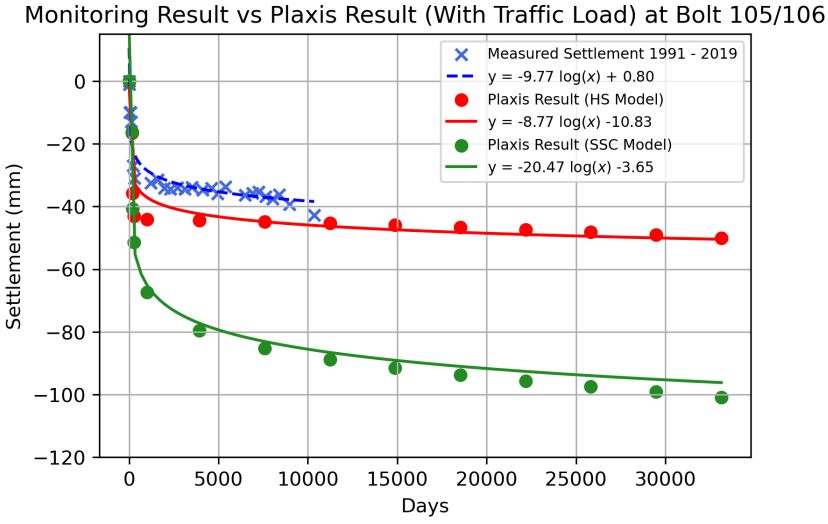

(c) Immersion Joint 3

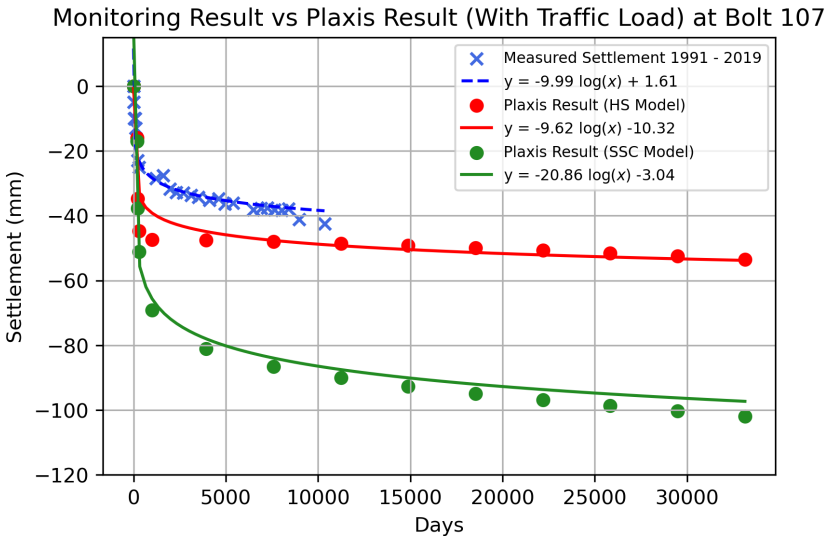

(d) Immersion Joint 4

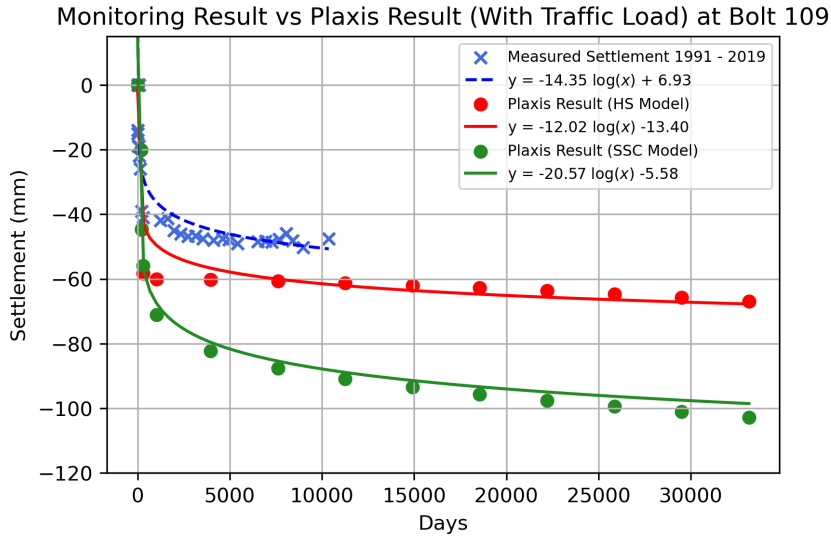

(e) Immersion Joint 5

Figure 5.18: The settlement results after adding traffic loads into the simulation

5.4 SETTLEMENT SIMULATION OF MODEL 3

5.4.1 Description of Model 3

Waterway maintenance was conducted in the Noord River 30 years after the tunnel opening. The maintenance is conducted since there is a lack of coverage due to erosion (de Vries and van de Wiel, 2022). The maintenance is carried out by dumping gravel over the tunnel to the area with less than 1.0 m soil cover. Gravel class 10-60 kg is chosen as backfilling material. Looking at the details of Figure 5.19, it can be observed that two phenomena occurred until 2021: sedimentation and erosion with respect to the intended soil cover. However, the figure does not depict the thickness of soil cover at the first and fifth immersion joints before the maintenance is conducted. Although the data is incomplete, it can be observed that the sedimentation mostly occurs on the west side of the tunnel. The sediment is 100 to 200 cm

higher than the intended level of soil cover, which means there is 1.5 to 2.5 meters thick soil cover on top of the tunnel, while 5 to 10 cm of erosion mostly occurs in the middle of the waterway.

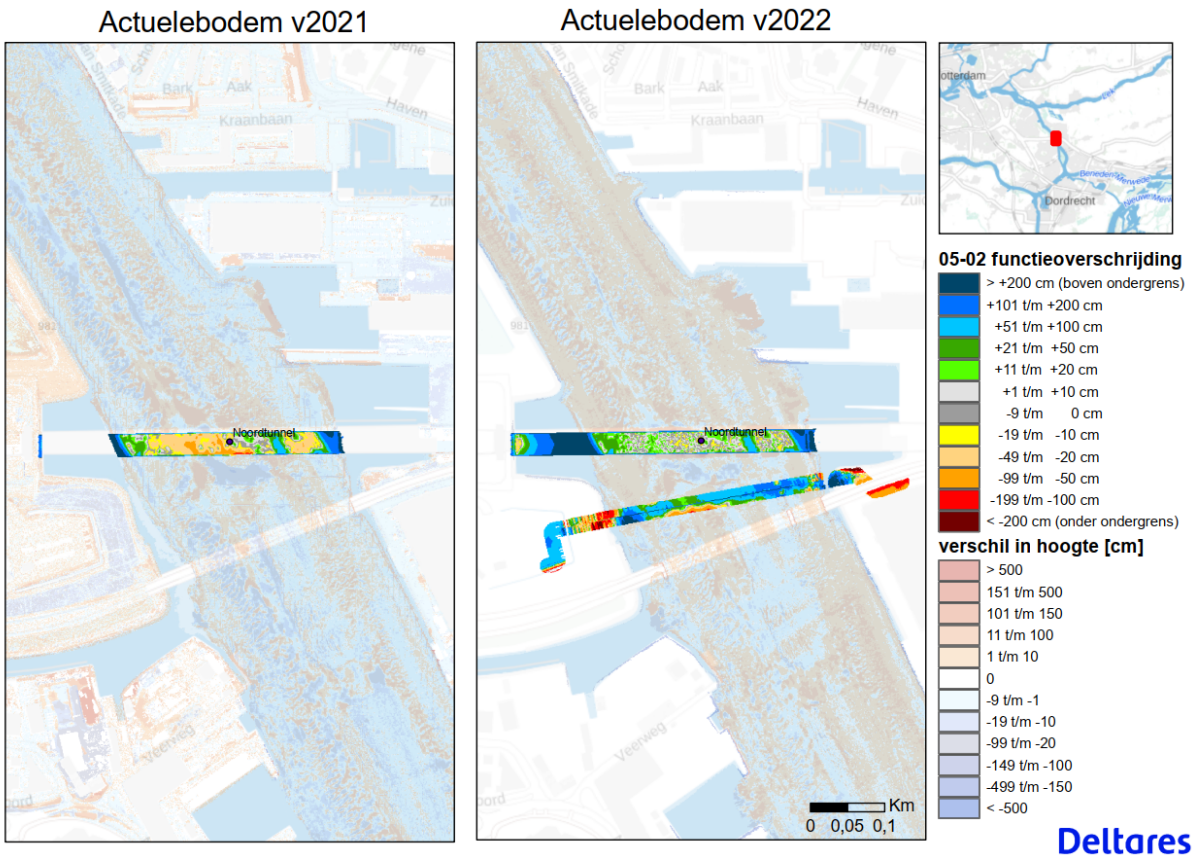

Figure 5.19: The waterway condition before (left) and after (right) adding the soil cover over the tunnel (Deltares, 2022)

In this research, only sedimentation at the second immersion joint is being considered. Meanwhile, the soil cover at the other locations are assumed to be the same during the first 30 years of tunnel operation. However, given the constraints of the available data, it is postulated that the sediment consists predominantly of natural clay. Moreover, in the simulation, the sedimentation rate for simulation purposes is assumed to be linear from the tunnel opening to 2022. Following 2022, it is assumed that maintenance activities will be carried out every year, with the expectation that neither sedimentation nor erosion will occur.

On the other hand, since the erosion is uneven and the magnitude is relatively small, it is assumed that the soil cover in other areas remains 0.5 m thick before the waterway maintenance. In PLAXIS, the sedimentation and the waterway maintenance is modelled by adding layers on top of the tunnel to its intended thickness. The sedimentation is modelled by adding natural clay layer on top of the tunnel, while the waterway maintenance is modelled by adding gravel layer on top of the tunnel. The sedimentation and gravel thickness are 1.5 m and 0.5 m, respectively. It should be noted that no additional cover is applied in the fifth immersion joint.

5.4.2 Simulation Results of Model 3

The simulation results after considering sedimentation and waterway maintenance are presented in Figure 5.20. As expected that sedimentation and maintenance activity increases the effective vertical stress to the subgrade. Thus, both the HS Model and SSC Model show an increase in settlement. Looking at the second immersion joint, the settlement increased almost linearly from the ten and thirty years after immersion for both HS Model and SSC Model. This is because the sedimentation is assumed to occur linearly over time. However, at the other immersion joints, an increase of settlement is expected at day 11231 when 0.5 m of gravel is added on top of the existing soil cover.

As depicted in Figure 5.20, it is evident that only the SSC Model displays an increasing trend in settlement attributed to the creep effect. In contrast, settlement increments are observed exclusively during maintenance activities for the HS Model. Subsequently, it is projected that no further settlement will take place, indicating that all excess pore water pressure has been dissipated. Furthermore, the increase in settlement after the waterway maintenance in 2022 contributes to a slight divergence between the simulation settlement trendline and the monitoring data, resulting in a greater deviation, as presented in Table 5.8.

Table 5.8: The comparison of simulation and monitoring results for Model 3

Years	Settlement (mm)				
	IJ 1	IJ 2	IJ 3	IJ 4	IJ 5
2019 (Simulation)	-36.66	-96.51	-45.85	-48.44	-53.42
2019 (Monitoring)	-33.45	-94.36	-42.72	-42.52	-47.63
Deviation	9.59%	2.28%	7.34%	13.91%	12.15%
*)Note:	IJ: Immersion Joint				

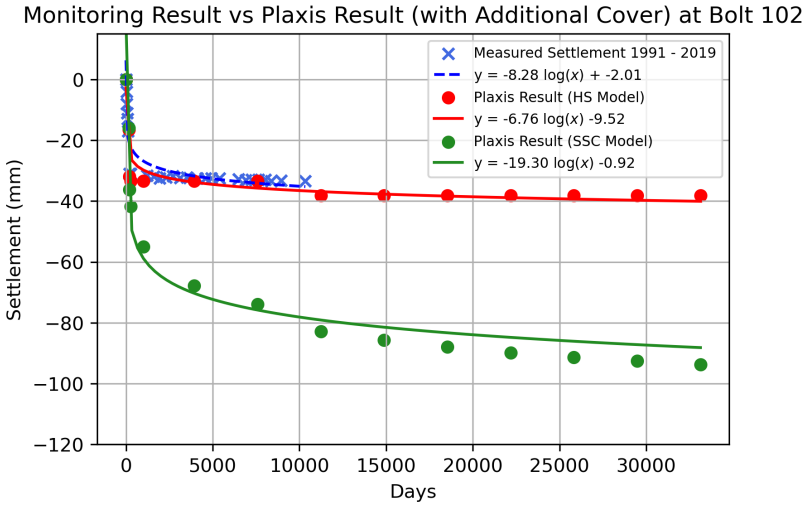

(a) Immersion Joint 1

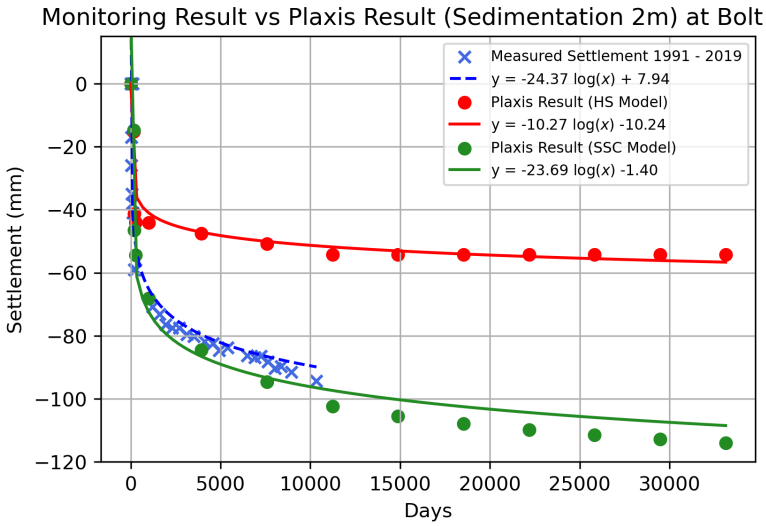

(b) Immersion Joint 2

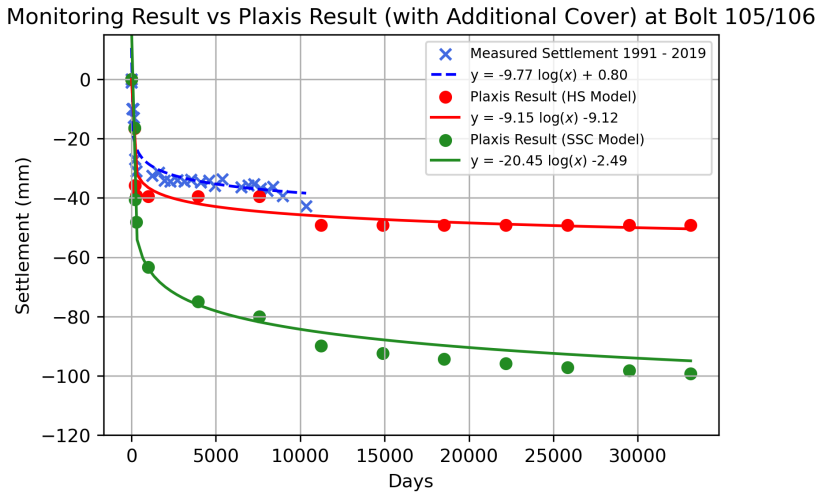

(c) Immersion Joint 3

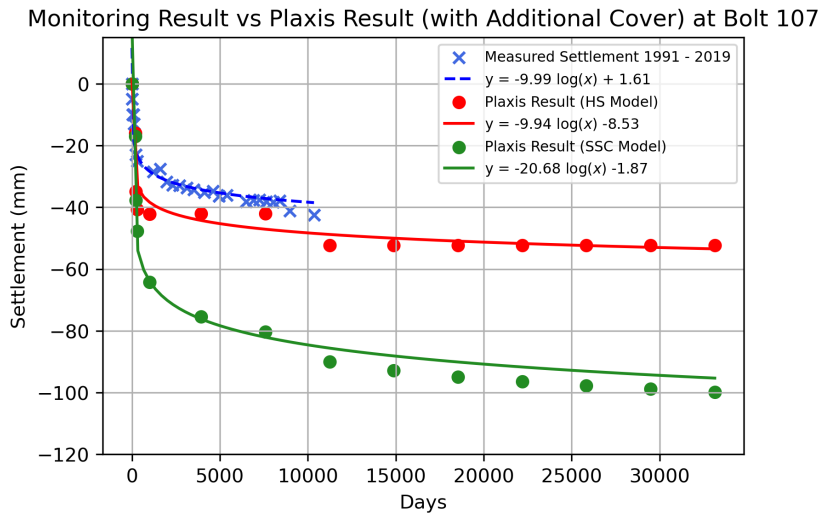

(d) Immersion Joint 4

Figure 5.20: The settlement results after adding sedimentation and additional cover into the simulation

5.5 SENSITIVITY ANALYSIS

The sensitivity analysis examines the effect of various soil parameter values on the magnitude of settlement. This analysis's two objectives are to determine which soil parameters have the most significant impact on settlement and how much the settlement would deviate from its initial result. The analysis begins by identifying the soil layer that contributes most to the settlement. Since some laboratory test data were missing, some geotechnical parameters are derived from the correlation method or empirical formula, as explained in Chapter 4. Thus, two approaches were taken in the sensitivity analysis. The first approach is carried out by changing the soil parameters within 10 % of its initial values to see which parameters influence settlement the most. The second approach is to modify the soil stiffness by using statistical methods. This approach begins by calculating the standard deviation of the soil's stiffness parameter. The confidence interval (5^{th} and 95^{th} percentiles) of the data was selected to determine how much the settlement would deviate from its initial results due to stiffness variability in the field.

5.5.1 Concise Method

As previously described in Chapter 4, some laboratory test data were missing and the soil properties used for the simulation were derived from the correlation method, empirical formula, and average value of Robertson (2010) SBT chart. Thus, to investigate which parameters influence the most to settlement, the soil properties of the most compressible soil in each immersion joint are set as 10% higher and 10% lower than the initial value of the model in Chapter 5.

As explained in Section 5.6, four of the five models, immersion joints 1, 3, 4, and 5, have settlement tendencies consistent with the Hardening Soil model—meanwhile, only immersion joint two exhibits a settlement tendency as the Soft Soil Creep model predicted. Thus, in this research, the sensitivity analysis for immersion joints 1, 3, 4, and 5 was conducted using HS Model, while only immersion joint 2 used SSC Model. The sensitivity analysis begins by identifying the soil layer that contributes the most to settlement. The simulation results in Chapter 5 indicate that sand 38b has the most significant impact on the settlement in immersion joints 1, 3, and 4. Conversely, clay 38 exhibits the highest compressibility among other layers in immersion joints 2 and 5. Thus, the soil parameters of sand 38b and clay 38 are modified as part of the sensitivity analysis.

Figure 5.21 depicts the result of Sand 38b's sensitivity analysis at immersion joints 1, 3, and 4. It can be observed that the unloading-reloading stiffness (E_{ur}) is the most sensitive parameter for Sand 38b. Applying the upper and lower limits of the E_{ur} value at immersion joints 1, 3, and 4 will increase and decrease settlement by approximately 1, 6, and 1.5 millimeters, respectively. Moreover, it is interesting that the sand's weight could also significantly impact the settlement compared to the other parameters at immersion joints 3 and 4. Although the settlement impact is not as high as E_{ur}, increasing or decreasing the sand's weight at those two locations will alter the initial result by 0.8 and 0.9 mm, respectively. However, at immersion joint 1, the friction angle is more sensitive than the sand's weight. Changing the friction angle (ϕ) value by 10% higher or lower will deviate the initial result by around 1 mm.

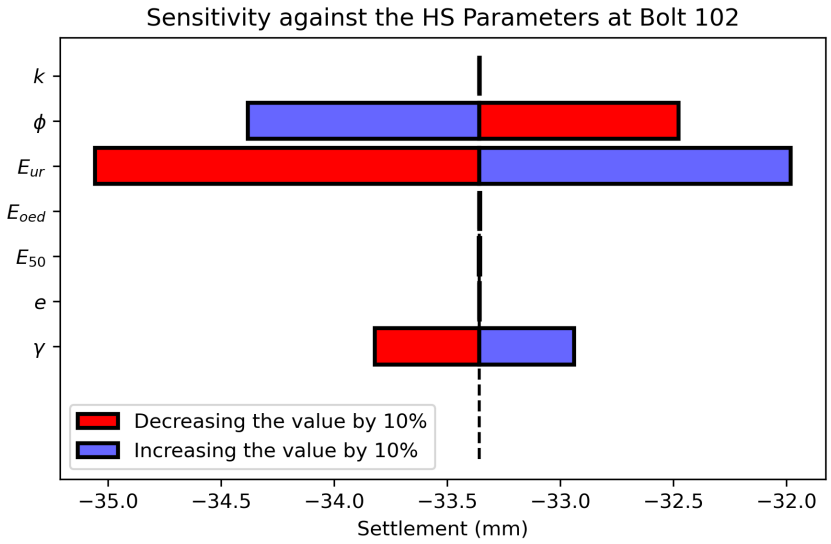

(a) The sensitivity analysis result for sand 38b at Immersion Joint 1

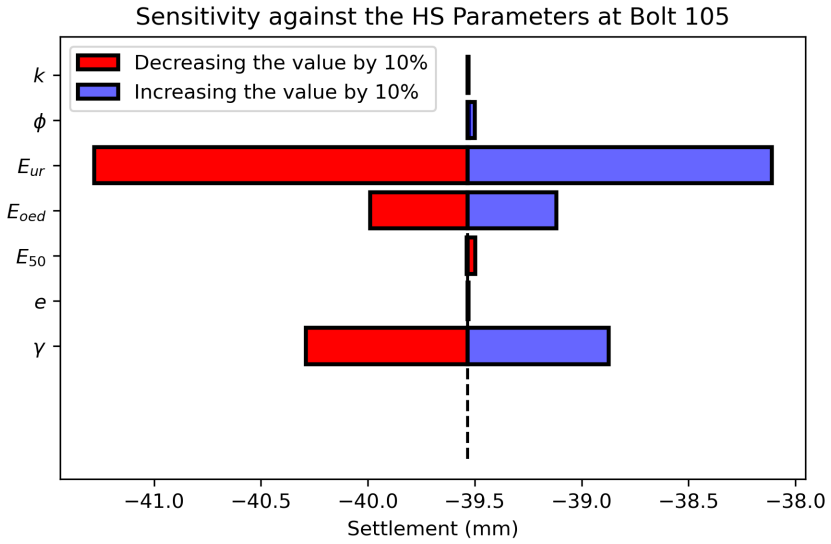

(b) The sensitivity analysis result for sand 38b at Immersion Joint 3

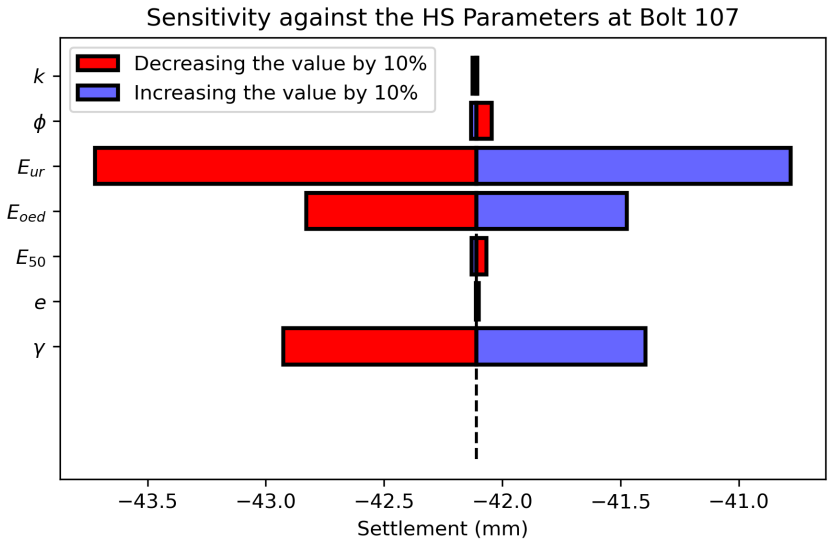

(c) The sensitivity analysis result for sand 38b at Immersion Joint 4

Figure 5.21: The tornado plot for all soil parameters of Sand 38b at immersion joint 1, 3, and 4

As previously mentioned, clay 38 is the most compressible layer at immersion joints 2 and 5. Figure 5.22 shows the sensitivity result for clay 38 at immersion joint five, where the sensitivity analysis is conducted in HS Model. It can be seen that E_{oed} is the most sensitive parameter in this location, as altering its value could cause a 2 mm change in settlement. This result is expected because, at this location, the combined weight of soil improvement, tunnel, and backfill is heavier than the soil removed. Thus, the maximum stress history is exceeded, resulting in primary compression of the subsoil.

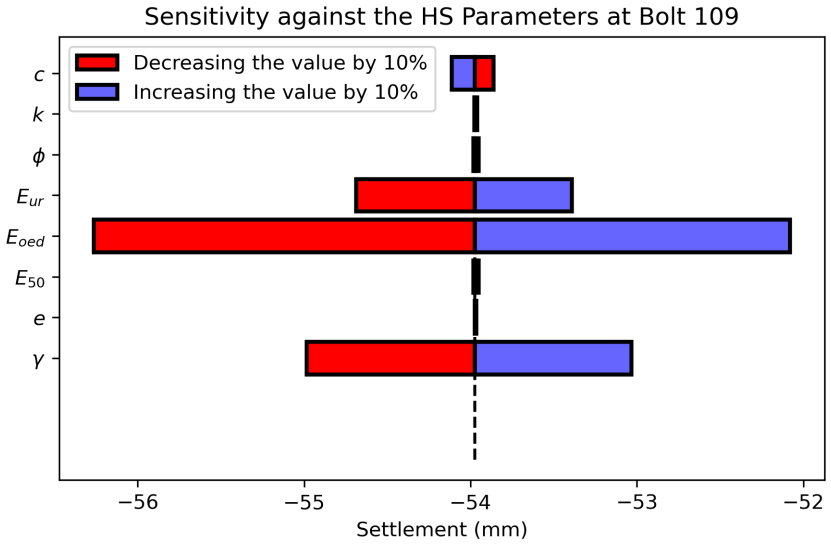

Figure 5.22: The tornado plot of sensitivity result for Clay 38 at immersion joint 5

In addition, at immersion joint 2, clay 38 is simulated in SSC Model. Figure 5.23 depicts the result of the sensitivity analysis, where the modified creep index is the most sensitive parameter. Increasing or decreasing the value by 10% will change the settlement result by around 4 mm.

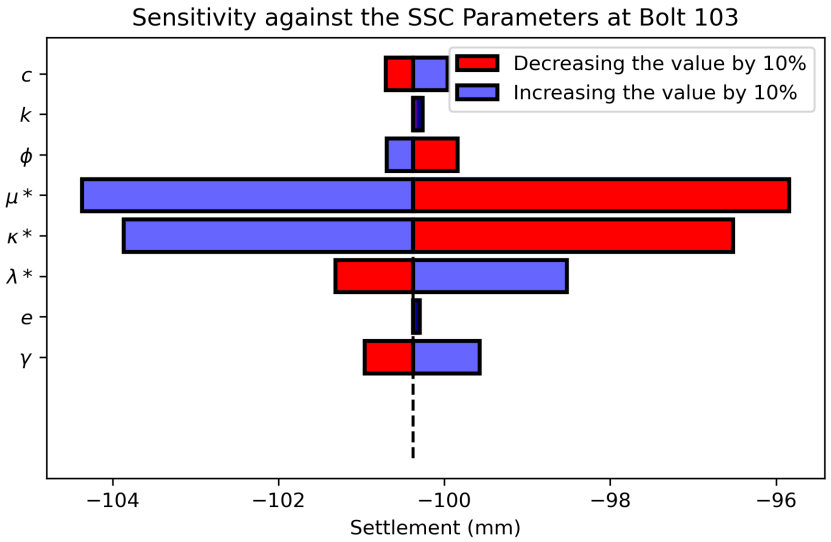

Figure 5.23: The tornado plot of sensitivity result for Clay 38 at immersion joint 2

In summary, the unloading-reloading stiffness of sand 38b is the most sensitive parameter at immersion joints 1, 3, and 4. However, at immersion joint 5, the clay 38 is the most com-

pressible layer, which E_{oed} is the most sensitive soil parameter. This is significant evidence that the removed soil weighs less than the combined weight of the soil improvement, tunnel, and backfill. This weight exceeds the location's maximal stress history, resulting in primary consolidation. Lastly, at immersion joint 2, the modified creep index (μ^*) of clay 38 is the most sensitive parameter.

5.5.2 Statistical Method

The statistical approach aims to assess the extent of deviation of settlement between the simulation results and their initial values when considering the variability of soil stiffness in the field. In this research, the absence of laboratory data for soil stiffness required deriving those parameters solely from CPT and Table 2b correlation. The CPT data revealed varying tip resistance values for one soil type in one to another location. Additionally, it should be noted that the CPT and NEN Table 2b correlation of coarse-grained soil is also determined by the weight of soil on top of it, which varies across different locations. Consequently, the CPT and NEN Table 2b correlation indicate that soil stiffness varies along the tunnel's longitudinal direction. In this statistical approach, the stiffness parameter values are tried to be set by using Python to randomize a set of parameter values based on the normal distribution model. The mean ($\bar{x}$) and standard deviation (σ) of the parameters are calculated by the following formula.

$$\bar{x} = \frac{\sum_{i=1}^{n} x}{n} \tag{5.1}$$

$$\sigma = \sqrt{\frac{\sum_{(} x_i - \bar{x})^2}{n-1}} \tag{5.2}$$

where, x is the value in the data distribution; $\bar{x}$ is the sample mean; s is the standard deviation of the data;and n is the total number of sample.

The stiffness values obtained from Chapter 4 are set as reference values. The data's mean and standard deviation are computed using equation (5.1) and (5.2), before proceeding with the randomization procedure. After that, the confidence interval (percentile 5 and 95) is established from the normal distribution. It should be noted that the value of p_5 and p_{95} of each parameter could be lower or higher than the upper and lower boundary from Subsection 5.5.1. Furthermore, similar to the previous subsection, the sensitivity analysis for immersion joints 1, 3, 4, and 5 uses the Hardening Soil model, whereas immersion joint 2 employs the Soft Soil Creep model.

Table 5.9 and Figure 5.24 show the statistical result and the probability density function for sand 38b, respectively. It can be observed that for sand 38b, the standard deviation for E_{50}, E_{oed}, and e is relatively small compared to E_{ur}. This is because those parameter values fall within a relatively narrow distribution range. In contrast, the E_{ur} standard deviation is more significant because the initial model assumes that the E_{ur} value in the reference values is three times higher than E_{50}.

Table 5.9: The quantified parameters obtained from the normal distribution for 38b

Parameters	Unit	Mean	Standard Deviation	p5	p95
E_{50}	MPa	17.40	0.65	16.34	18.46
E_{oed}	MPa	17.40	0.65	16.32	18.47
E_{ur}	MPa	52.19	1.95	49.00	55.35
e	-	0.61	0.0056	0.60	0.62

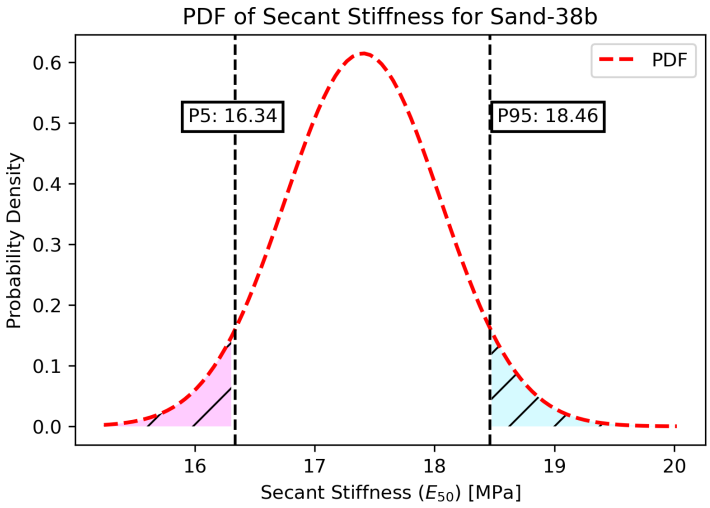

(a) PDF of E_{50} for Sand-38b

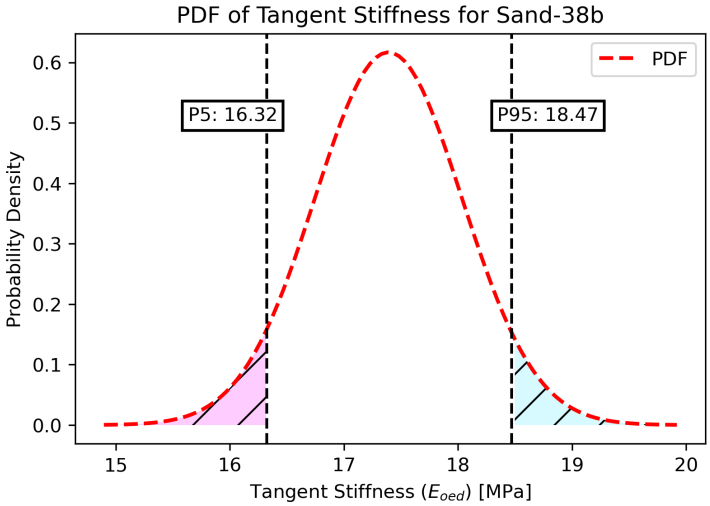

(b) PDF of E_{oed} for Sand-38b

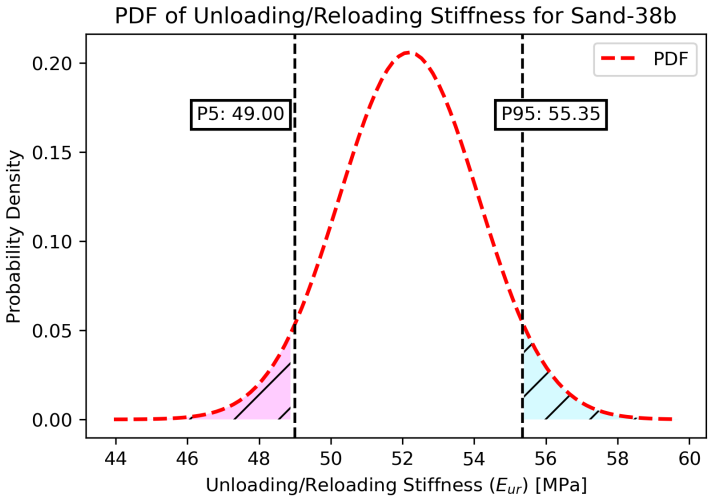

(c) PDF of E_{ur} for Sand-38b

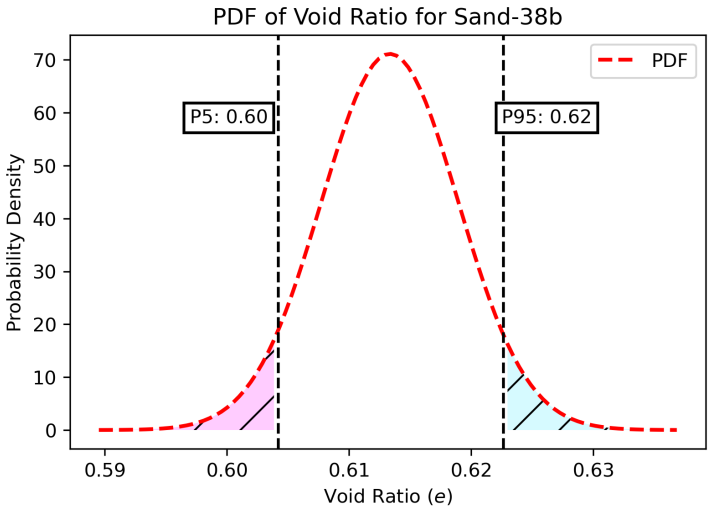

(d) PDF of e for Sand-38b

Figure 5.24: The probability density function of sand 38b stiffness and void ratio (continued)

In addition, the modified compression index, swelling index, and creep index are set as the reference values for clay 38. The statistical results are shown in Table 5.10 and Figure 5.25. Similar to sand 38b, the standard deviation of the clay soil's parameters is insignificant due to the narrow distributed range.

Table 5.10: The quantified parameters obtained from the normal distribution for clay 38

Parameters	Unit	Mean	Standard Deviation	p5	p95
λ^*	-	$3.22x10^{-2}$	$1.5x10^{-3}$	$2.97x10^{-2}$	$3.48x10^{-2}$
μ^*	-	$8.63x10^{-4}$	$4.92x10^{-5}$	$7.8x10^{-4}$	$9.4x10^{-4}$
κ^*	-	$2.15x10^{-2}$	$1.04x10^{-3}$	$1.98x10^{-2}$	$2.32x10^{-2}$

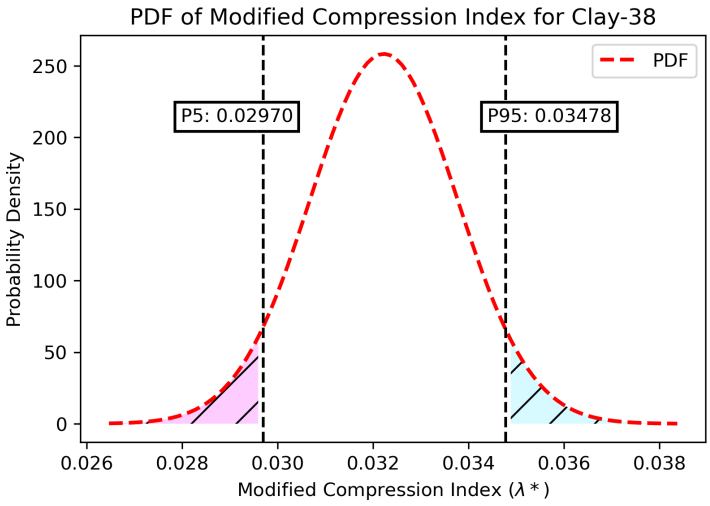

(a) PDF of λ_* for Clay-38

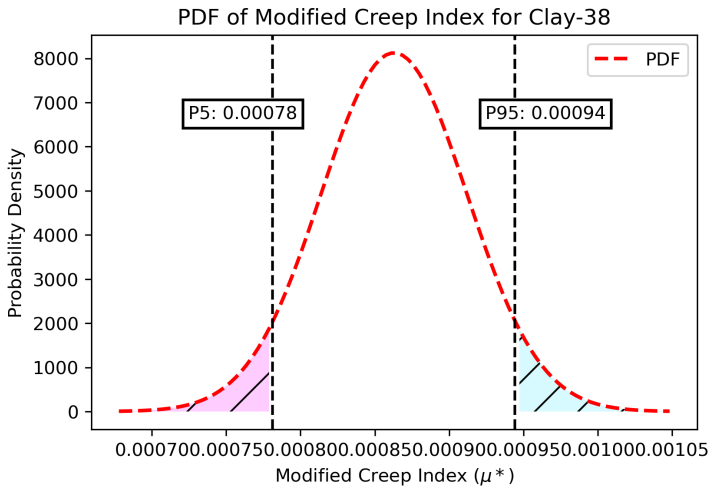

(b) PDF of μ_* for Clay-38

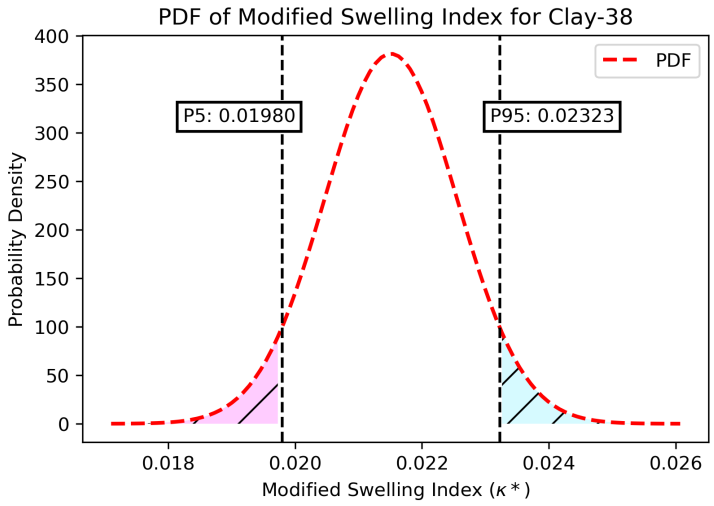

(c) PDF of κ_* for Clay-38

Figure 5.25: The probability density function of Clay-38 stiffness (continued)

After establishing the normal distribution of those parameters, the fifth percentile (p_5) and the ninety-fifth (p_{95}) are set as the lower and upper boundary of the sensitivity analysis, as ninety percent of the reference values lie within those ranges. The sensitivity analysis examines the deviation in settlement from its initial results after 30 years of tunnel operation. Figure 5.26 shows the sensitivity results for sand 38b at immersion joints 1, 3, 4, and 5, respectively. The stiffness in unloading and reloading is the most sensitive parameter at immersion joints 1, 3, and 4. It demonstrates that the subsoil is very sensitive to the unloading-reloading procedure during tunnel construction in those particular areas. However, only at immersion joint 5, unloading-reloading and Oedometer stiffness are the most sensitive parameters due to the soil improvement conducted in those areas.

Looking at the details, Figure 5.26a indicates that the unloading-reloading stiffness (E_{ur}) is the most sensitive parameter, whereas the other parameters produce settlement differences close to zero. It is strong evidence for the impact of the unloading-reloading procedure when the weight of the soil removed is much greater than the total weight of the tunnel and backfill. Additionally, the simulation result with E_{ur} at p_{95} will result in a 2 mm lesser settlement than the original result. In contrast, using E_{ur} at p_5 will result in a settlement value that is roughly

0.3 mm greater. The difference in settlement magnitude is more significant when using p_{95} than p_5 because the initial value of E_{ur} lies near the lower boundary of the data distribution.

Similar to immersion joint 1, the parameter that exhibits the most sensitivity in immersion joints 3 and 4 is the unloading-reloading stiffness E_{ur}, as illustrated in Figures 5.26b and 5.26c. Adjusting the E_{ur} value to the fifth percentile and the ninety-fifth percentile would lead to a settlement increase of approximately 1.31 mm and a decrease of 0.61 mm in immersion joint 3. In addition, by adjusting the E_{ur} value to p_5 and p_{95}, it is observed that the settlement at immersion joint four experiences an increase of 1.22 mm and a decrease of 0.55 mm, respectively. It is important to note that while modifying the E_{oed} value at immersion joints 3 and 4 may impact the overall settlement by either increasing or decreasing it, the magnitude of this change could be considered negligible since it falls within a range of 1 mm. Furthermore, Figure 5.26d reveals that the most sensitive parameters at immersion joint 5 are E_{oed} and E_{ur}. This is because, in this location, the removed soil is significantly lighter than the combined weight of the soil improvement, tunnel, and backfill, resulting in primary consolidation in the subsoil. Additionally, lowering the E_{oed} and E_{ur} to p_5 will increase the settlement to 1.3 and 1.5 mm, respectively. On the other hand, increasing the parameters value to p_{95} only reduced the settlement by 0.2 and 0.3, respectively. This phenomenon shows that the initial value of E_{oed} and E_{ur} falls near the upper boundary of the data distribution.

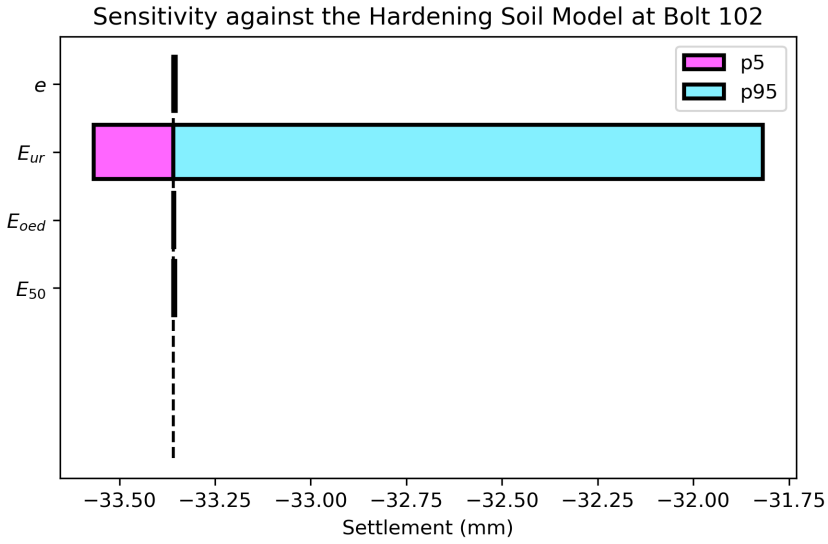

(a) The sensitivity analysis result for sand 38b at Immersion Joint 1

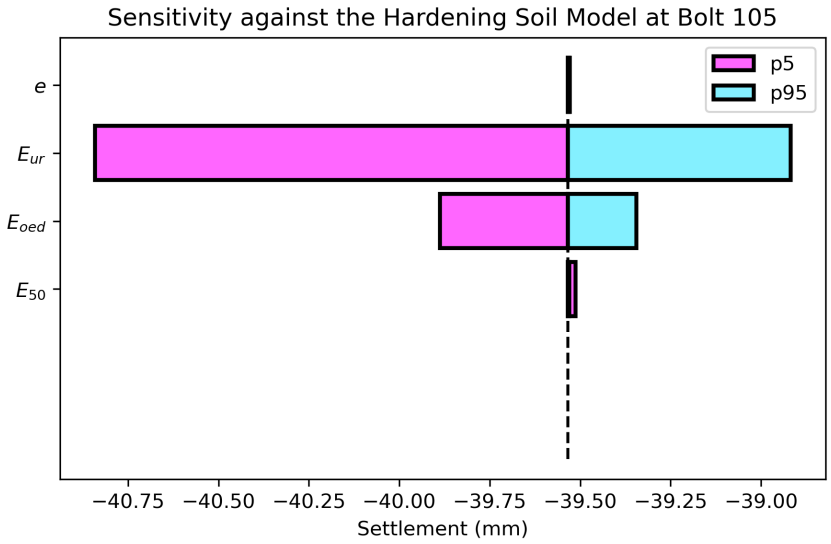

(b) The sensitivity analysis result for sand 38b at Immersion Joint 3

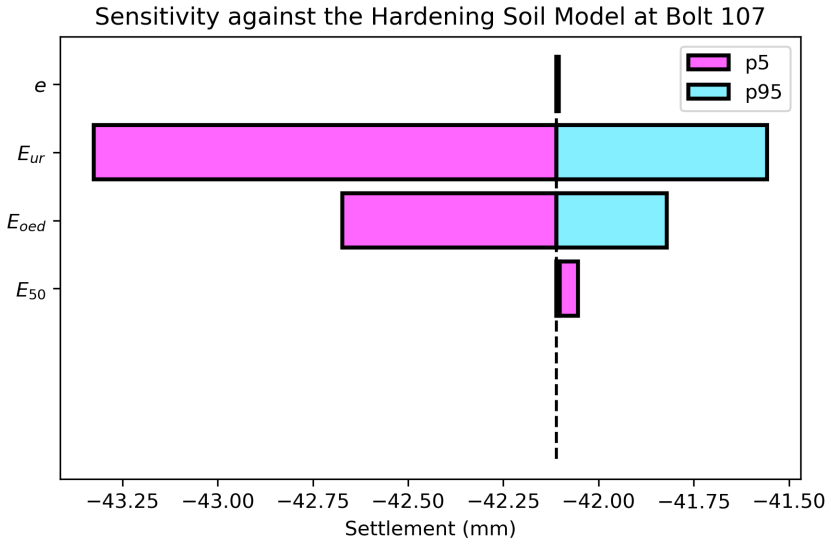

(c) The sensitivity analysis result for sand 38b at Immersion Joint 4

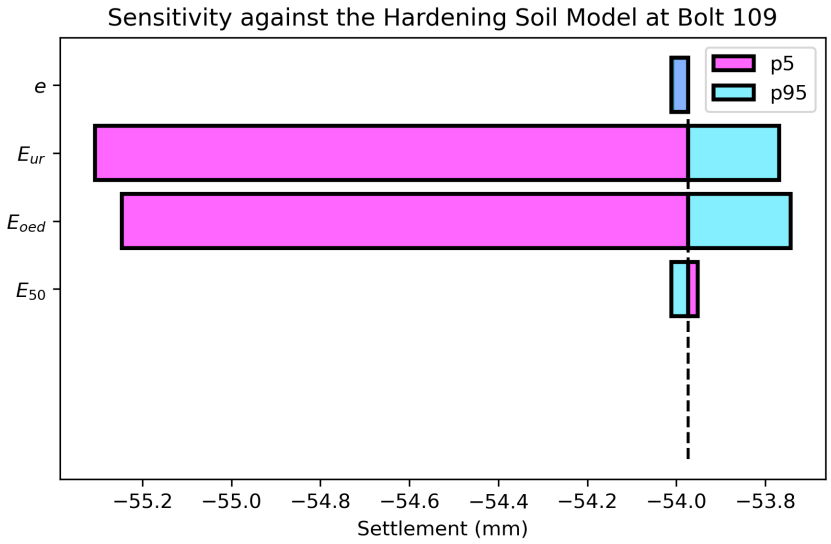

(d) The sensitivity analysis result for sand 38b at Immersion Joint 5

Figure 5.26: The tornado plot of sensitivity result for Sand 38b at immersion joint 1, 3, 4, and 5

Figure 5.27 shows the sensitivity analysis results for clay 38 at the second immersion joint, where the modified creep index (μ^*) contributes the most to the settlement magnitude. In addition, it can be seen that the modified swelling index (κ^*) and creep index (μ^*) are positively correlated to settlement. Decreasing the κ^* and μ^* value to p_5 will reduce the settlement up to 4.3 to 5.5 mm, respectively. When the values are increased to p_{95}, the settlement will increase by 1.5 and 1.9 mm, respectively. In contrast, the modified compression index (λ^*) is negatively correlated to the settlement magnitude, meaning decreasing the value will lead to a more significant settlement.

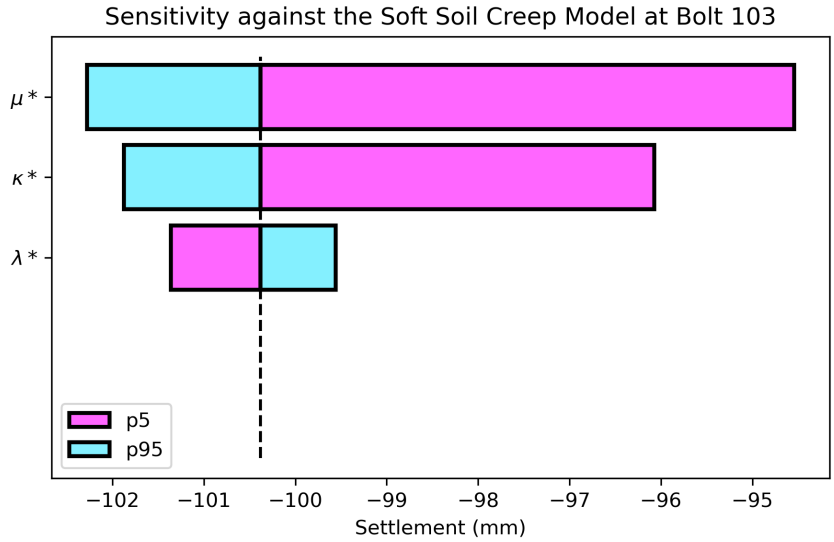

Figure 5.27: The tornado plot of sensitivity result for Clay 38 at immersion joint 2

5.6 SETTLEMENT PREDICTION

The forthcoming settlement of the Noordtunnel is estimated by identifying the settlement tendency that closely matches the monitoring data. Looking at the simulation result, model 1, which is developed based on the as-built drawing, could produce a similar tendency to the monitoring data. In model 1, the subsoil is subjected to the load generated by the weight of the tunnel and the soil backfill. However, when the traffic load introduces in model 2, the simulation gives an overestimated result as explained in Subsection 5.3.2. It is because the traffic load is represented as a static distribution load. Moreover, higher settlement is also expected after the maintenance was conducted in 2022. This activity indeed caused an increase in effective stress to the subsoil, but how much the impact is not yet known since no settlement monitoring has been conducted after maintenance. In addition, the settlement increment for the second immersion joint is slightly different due to sedimentation in the first 30 years.

In this research, the latest simulation scenario is chosen to predict the settlement magnitude in the Noordtunnel, as it is obvious that adding soil cover will lead to increasing subsoil settlement. The upcoming settlement at immersion joint two is predicted using SSC Model, while the HS Model is employed for the remaining immersion joints. According to the modeling results, the settlement tends to flatten once the waterway maintenance is done. This suggests that the pore water pressure can dissipate in a relatively short time period after the gravel is placed over the tunnel. Additionally, only the second immersion joint shows a slightly larger settlement rate for the upcoming years due to the creep effect caused by soft soil in the subsoil.

The simulation result indicates that soft soil beneath immersion joint two will lead to a settlement of approximately 15.13 mm over the remaining lifespan of the tunnel. On the other hand, at the other immersion joints, settlement in the range of 4 to 5 mm is predicted to occur within the next 67 years. The settlement prediction in the upcoming years at all immersion joints is shown in Table 5.11, and visualized in Figure 5.28.

Table 5.11: The Settlement Prediction at All Immersion Joints

Settlement (mm)					
Years	**IJ 1**	**IJ 2**	**IJ 3**	**IJ 4**	**IJ 5**
2024	-37.20	-98.39	-46.58	-49.23	54.19
2027	-37.44	-99.26	-46.92	-49.59	-54.54
2030	-37.67	-100.06	-47.23	-49.93	-54.87
2040	-38.33	-102.36	-48.11	-50.89	-55.81
2050	-38.86	-104.23	-48.84	-51.68	-56.57
2060	-39.32	-105.82	-49.45	-52.34	-57.22
2090	-40.36	-109.49	-50.87	-53.88	-58.72

*) Note: IJ: Immersion Joint

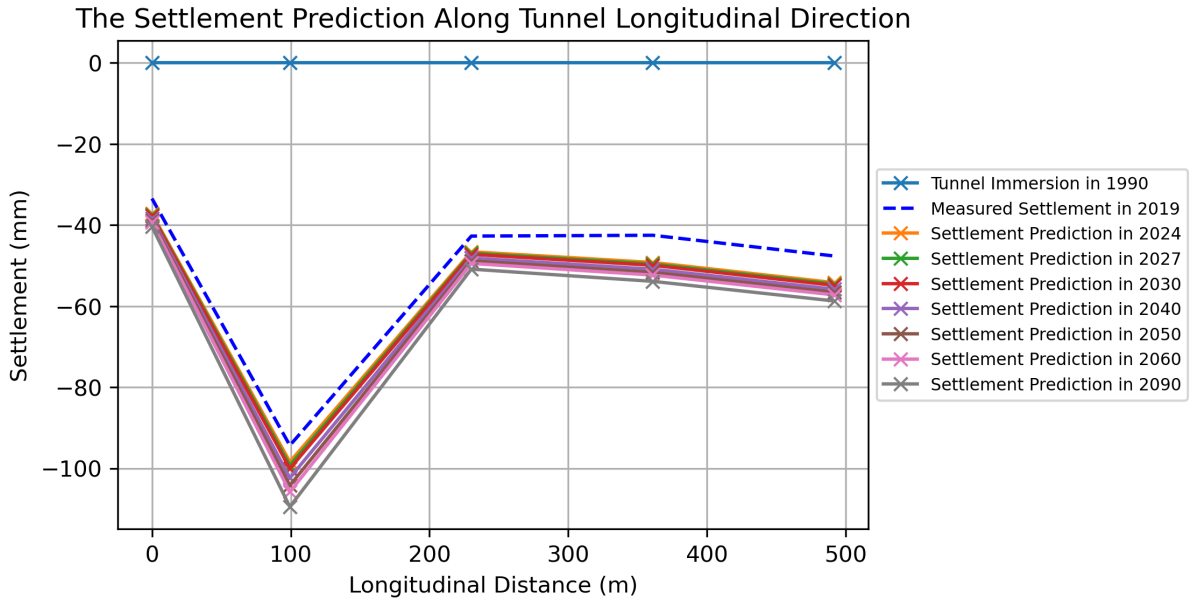

Figure 5.28: The Final Settlement Prediction Along Tunnel Longitudinal Direction

5.7 DISCUSSIONS

In this chapter, three types of models have been developed to depict the settlement behaviour of the Noordtunnel, namely: (1) model 1, which is based on the as-built drawing; (2) model 2, which considers the traffic load, and (3) model 3, which consider sedimentation and waterway maintenance. Two constitutive laws are selected to depict the settlement behaviour of those models: the hardening soil model and the soft soil creep model. What distinguishes these two constitutive laws is that there is no significant long-term settlement increment in the HS Model if no additional load is applied to the soil. This is because there is no change in the effective stress, and the remaining triggering factor of settlement is the dissipation of excess pore water pressure in the fine-grained soil. When all excess pore water pressure is already dissipated, the settlement no longer occurs. On the other hand, the SSC Model shows a time-dependent

behaviour where the settlement is kept going over time but at a lower rate, which illustrates the creep effect. Thus, the SSC Model gives a higher settlement rate than the HS Model.

Looking at the simulation results, all immersion joints, except for the second, show a lower settlement rate after 206 days of the immersion phase. It means that the primary compression at all immersion joints is finished after seven months. The following settlement that occurs afterward is relatively small and most likely occurs to the dissipation of excess pore water pressure. Thus, the four immersion joints' settlement tendency follows the HS Model. On the other hand, the second immersion joint has a similar settlement tendency to SSC Model. The presence of localized peat and clay beneath the tunnel is the main cause of excessive settlement in this particular area. Soft soil generally has a significant degree of compressibility, making it susceptible to volume reduction and settling under a constant applied load. As a result, creep behaviour becomes more pronounced in the second immersion joint, leading to a higher ongoing settlement after the primary compression stage. According to the simulation result, the soft soil underneath immersion joint 2 is responsible for at least 20 mm of settlement. Additionally, the natural sedimentation on top of the tunnel elements contributes to increasing effective stress on the subsoil, leading to settlement. The sedimentation causes at least 8 mm of settlement within 30 years of tunnel operation. Assuming the sedimentation rate is linear, this phenomenon could cause a 0.27 mm settlement per year at the second immersion joint. Therefore, the combination of localized soft soil and sedimentation at immersion joint two is highly likely the main factor of the higher settlement observed in the second immersion joint.

A sensitivity analysis is performed to examine the parameter that has the greatest impact on settlement and to determine the extent to which simulation outcomes may diverge when accounting for soil variability in the field. In the initial analysis approach, it becomes evident that the unloading-reloading stiffness (E_{ur}) of sand 38b is the most sensitive parameter at immersion joints 1, 3, and 4. However, for immersion joint 5, the significance shifts to both E_{ur} and the Oedometer stiffness (E_{oed}). This is expected since, at this location, soil improvement is conducted during the construction process. Thus, the cumulative weight of soil improvement, tunnel weight, and soil cover is heavier than the soil replaced, resulting in the subsoil reaching the pre-consolidation stress. In addition, the modified creep index (μ^*) of clay 38 emerges as the most sensitive parameter at immersion joint 2.

The sensitivity analysis reveals that the E_{oed} and E_{ur} are negatively correlated to settlement, meaning that increasing the value will result in a decrease in settlement. In contrast, $\mu*$ is positively correlated to settlement, meaning that increasing the value will result in an increase in settlement. However, it is important to note that considering the narrow spread of reference values in the field, adjusting E_{ur} within ninety percent of its distribution in the simulation will only result in deviations ranging from 0.3 to 2 mm at immersion joints 1, 3, and 4. For immersion joint 5, as the initial values of E_{oed} and E_{ur} fall near the p_{95}, adjusting the value to the upper boundary will only reduce the settlement by 0.2 and 0.3 mm, respectively. However, when applying p_5, the settlement is projected to increase by 1.3 to 1.5 mm. Furthermore, adjusting the μ^* value at immersion joint 2 to the upper and lower bounds of the reference values distribution will increase and decrease settlement by 1.9 and 5.55 mm. Additionally, both approaches also validate the model, as altering parameter values using p_5/p_{95} and $\pm 10\%$ yields similar settlement tendencies in the results. Lastly, the sensitivity analysis also shows that the model is robust enough since after adjusting the most sensitive parameter, the simulation results only deviate by a maximum of 4% at immersion joints 1, 3, 4, and 5 and 5.48% at immersion joint 2. Therefore, the model is expected to generate reasonable future settlement predictions.

Furthermore, model 3 has been selected to predict the upcoming settlement in the Noordtunnel, as it is apparent that waterway maintenance by dumping gravel on top of the tunnel will enhance the effective stress on the subsoil, inducing settlement. It is predicted that settlement within a range of 4 to 5 mm is anticipated at immersion joints 1, 3, 4, and 5 over the remaining tunnel's operational lifetime. However, due to the presence of soft soil, an expected settlement of 15.13 mm is projected at immersion joint two until 2090.

5.8 CONCLUSIONS

The following points highlight the most important findings of this chapter, which also could be used to answer the sub-research questions formulated in Chapter 1:

- The simulation results reveal that the monitored settlements at all immersion joints show a similar tendency with the HS Model, except for the second immersion joint which followed the SSC Model.
- The simulation outcomes indicate that the excessive settlement observed at the second immersion joint is most likely attributed to the presence of localized soft soil. According to the simulation, the soft soil layer is responsible for a significant 20 mm settlement. Additionally, sedimentation above this immersion joint contributes an additional 8 mm, making the excessive settlement more pronounced.
- Despite the absence of the current settlement measurement data, it is predicted that the waterway maintenance conducted in 2022 will increase the effective stress of the subsoil, resulting in additional settlement. Thus, model 3 is chosen to predict the future settlement of the Noordtunnel.
- The sensitivity analysis of the most compressible layer shows that E_{ur} of sand is the most sensitive parameter for immersion joints 1, 3, and 4. However, at immersion joint 5, E_{oed} and E_{ur} are the most sensitive parameters due to the impact of soil improvement in the area. Additionally, μ^* of clay is the most sensitive parameter at immersion joint 2.
- The two sensitivity analysis approaches presented in section 5.5 yield similar settlement tendencies, and it becomes evident that the PLAXIS model is valid. Moreover, considering the variability in the field, adjusting the value of the most sensitive parameter will not change the settlement much due to the narrow spread of the reference values. Modifying the most sensitive parameter at immersion joints 1, 3, 4, and 5 will change the settlement by 0.3 to 2 mm (maximum deviation of 4% from the initial model). Furthermore, adjusting the μ^* value at immersion joint 2 will deviate the settlement by 1.9 to 5.5 mm (maximum deviation of 5.48% from the initial model). These results show that the model is robust enough and is expected to generate reasonable future settlement predictions.
- It is predicted that uneven settlement will occur in the Noordtunnel within its remaining design lifetime. Since soft soil has a time-dependent behaviour under constant load, 15.13 mm of settlement is expected to occur at the second immersion joint. In contrast, 'only' 4 to 5 mm of additional settlement is anticipated at the other immersion joints within the next 67 years.

6 EFFECTS OF ONGOING SETTLEMENT ON STRUCTURAL SAFETY AND PROPOSED OPTIMIZED MONITORING PROCEDURE

As the last step of the research approach mentioned in Section 1.4, this chapter aims to examine two topics: the effect of the continuing settlement on tunnel structural safety and the proposed monitoring procedure of the Noordtunnel. The chapter begins by describing structural problems that have occurred in the Noordtunnel. Next, potential structural issues that arise due to, including but not limited to, the differential settlement will also be elaborated. Finally, an optimized monitoring plan is proposed for the Noordtunnel for future safety assurance.

6.1 STRUCTURAL PROBLEMS IN THE NOORDTUNNEL

Several problems have occurred in the Noordtunnel during its operational life. The reconstructed settlement history of the Noordtunnel (see Fig. 3.6) shows that differential settlement occurred in the Noordtunnel, with the second immersion joint showing prominent excessive settlement compared to other immersion joints. Moreover, the SWECO (2020) report highlighted the occurrence of leakages in the Noordtunnel, as shown in Figure 6.1. Among the detected leakages, four out of five leakage were located at the segment joints on the tunnel's roof (indicated by numbers 1 to 4). Meanwhile, the remaining leakage was observed at the immersion joint on the tunnel's floor.

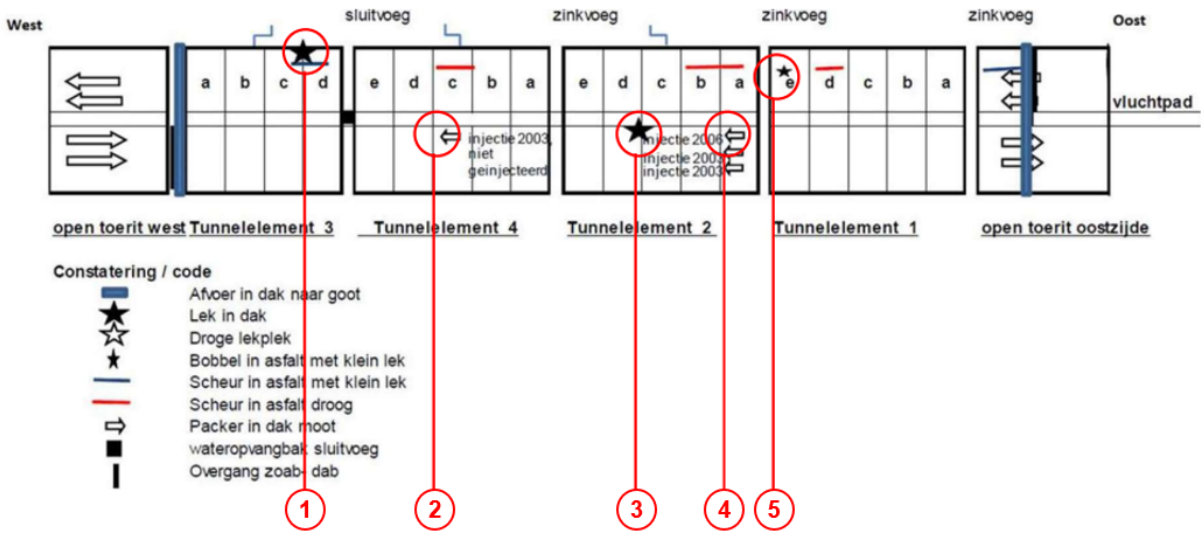

Figure 6.1: The damages and leakages occurred in the Noordtunnel (SWECO, 2020)

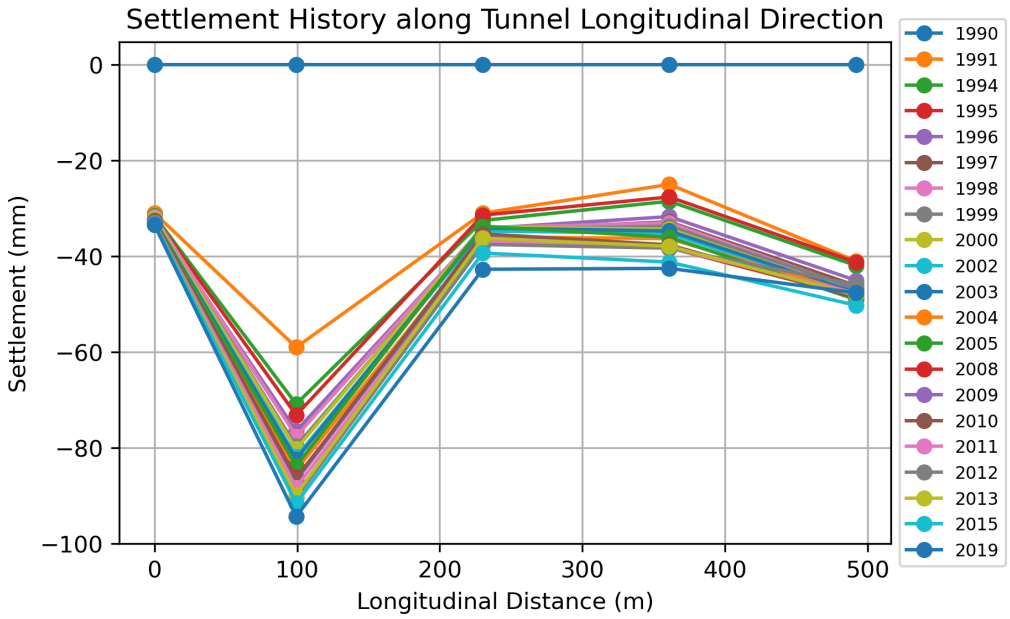

Figure 6.2: The monitored settlement of the Noordtunnel at immersion joints

In addition, differential settlement is recorded during the tunnel operation, as depicted in Figure 6.2. According to the simulation results described in Chapter 5, the excessive settlement at the second immersion joint occurred highly likely due to localized soft soil underneath the tunnel and the natural sedimentation. The soft soil is compressible and tends to settle under a constant load from the tunnel and backfill weight, resulting in a creep effect. Additionally, the surcharge from the natural sedimentation causes an additional load on the subsoil. The sediment on top of the tunnel acts like a distributed load on the subsoil, leading to a higher settlement in the subsoil. Moreover, this ongoing uneven settlement has the potential to induce tilting of the tunnel elements along their vertical plane, leading to either compression or decompression at the immersion joints.

6.2 POTENTIAL STRUCTURAL ISSUES IN FUTURE TUNNEL OPERATION

Chapter 5 reveals that uneven settlement will still be occurring in the Noordtunnel. The simulation predicted that an additional settlement of 15.13 mm would occur in the second immersion joint. In contrast, a smaller additional settlement, ranging from 4 to 5 mm, is anticipated for the other immersion joints within the next 67 years. The additional settlement can increase the uneven settlement between the tunnel elements and cause structural problems, such as leakage. Thus, this section examines the potential structural problems during the remaining tunnel's operation time.

6.2.1 Tunnel Deformation Due to Differential Settlement

The Noordtunnel's structure, which is a segmented tunnel element, can experience deformation in three directions: longitudinal (movement in the y-axis), vertical (movement in the z-axis), and transverse displacement (movement in the x-axis), as depicted in Figure 6.3. However, in this research, the tunnel element is assumed to behave as a rigid body due to the limited measured settlement at segment joints. Thus, only the effect of deformation at the immersion joint is examined.

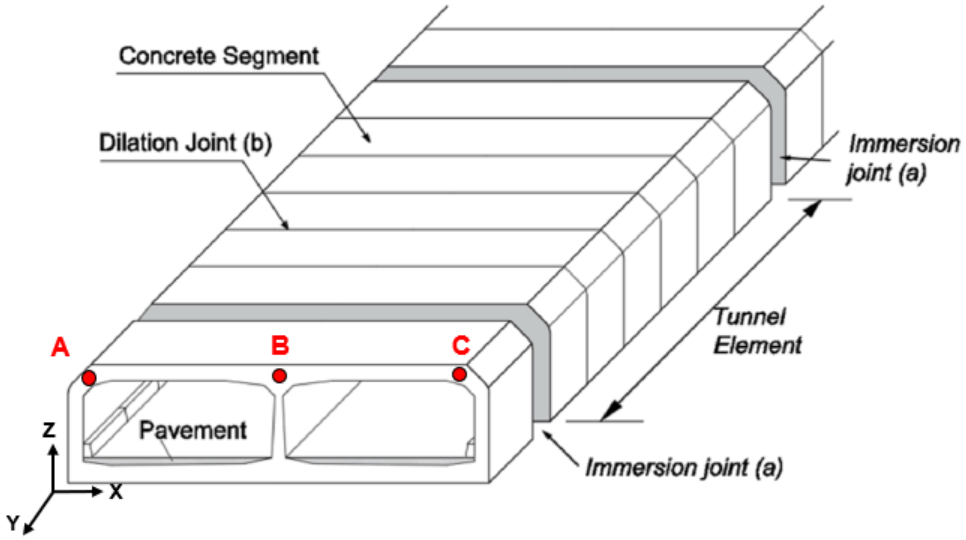

Figure 6.3: The visualization of segmented tunnel elements based on Zhang and Broere (2023b)

The immersion joint, located between two adjacent tunnel elements, consists of two components: the GINA gasket and the omega profile, as depicted in Figure 6.4. This joint is designed to allow limited deformation and provide watertightness to the tunnel element. Consequently, the immersion joint must withstand external loads resulting from displacement.

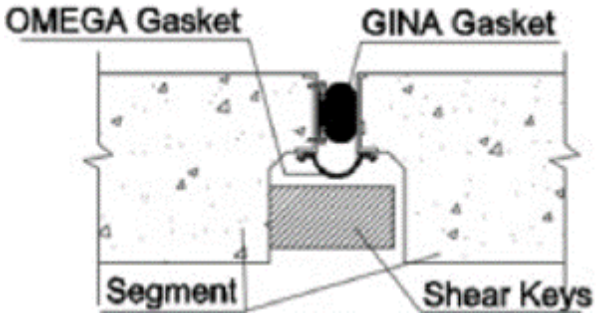

Figure 6.4: The components of the immersion joint (Zhang and Broere, 2023b)

The vertical deformation of an immersed tunnel is mainly caused by uneven settlement. The differential settlement may occur in both tunnel's longitudinal and transverse directions. In the longitudinal direction, a differential settlement could lead to tunnel movement in the y and z-axis. Differential settlement in the z-axis between two adjacent tunnel elements will cause a vertically concentrated shear deformation for the immersion joint in the tunnel, as illustrated in Figure 6.5. This deformation mode can alter the tunnel alignment and deform the rubber gasket. Leeuw (2008) has observed that this uneven settlement could also lead to the failure of the shear connection, as evidenced by local concrete cracking at the dilation joint, typically localized at the roof and floor concrete collars, and shear key cracking at the immersion joint. Furthermore, the combination of differential settlement in the longitudinal and transverse directions could cause torsion and rotation in the tunnel body.

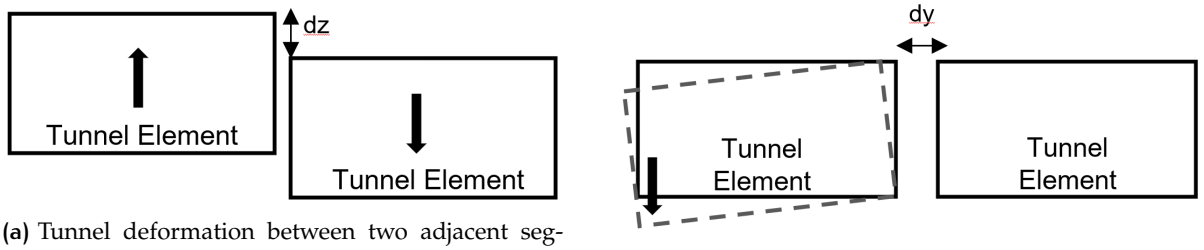

(a) Tunnel deformation between two adjacent segments

(b) Tunnel deformation within a segment

Figure 6.5: Visualization of tunnel deformation mode in vertical direction

The simulation results (see Figure 5.28) predict that settlements at all the Noordtunnel's immersion joints show a flattening trend, except at immersion joint 2. Additional settlement of 15.13 mm is predicted to occur at immersion joint 2 within the tunnel's remaining lifetime. In contrast, a 4 to 5 mm settlement is anticipated at the other immersion joints in the next 67 years. The uneven settlement in the Noordtunnel longitudinal direction could cause unequal joint opening/closure at the upper and lower tunnel transverse direction. Taking Kiltunnel as an example, this deformation mode has been considered the main factor for joint opening resulting in leakage (Leeuw, 2008).

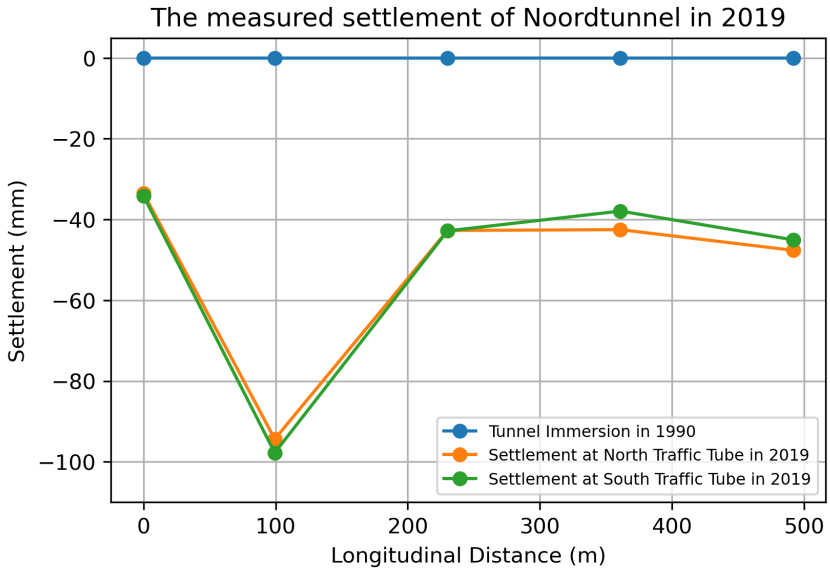

Figure 6.6: The monitored settlement at north and south traffic tube of the Noordtunnel at 2019

Moreover, when the north and south tubes of the tunnel move differently (illustrated as points A and C in Figure 6.3 move differently in vertical direction), segment rotation occurs. The force generated by this rotation is ideally absorbed by the collar construction in the roof or floor, depending on the direction of displacement. However, the sealing profile will experience vertical shearing if the collar collapses. This rotation effect also could lead to tunnel misalignment, joint gap opening/closure, deformation of rubber gasket, and leakage. Figure 6.6 shows that a slightly different settlement magnitude of approximately 2 to 4.5 mm is recorded on the north and south side of the tunnel, indicating that the tunnel is tilting in the transverse direction. However, it is important to note that the accuracy of this transverse tilting cannot be entirely relied upon, as it falls within the margin of error of observational leveling. Additionally, predicting the extent of future tilting in the transverse direction is also constrained due to the limitations of the data. Furthermore, the monitoring and simulation results indicate

that the tunnel moves in three distinct directions (points A, B, and C in Figure 6.3 all move in different directions). The simulation result indicates that the tunnel settles unevenly along its longitudinal axis, while the monitoring results show a slightly uneven settlement in its transverse direction. If, in the future, a more pronounced uneven settlement arises in the tunnel's transverse direction, for example due to irregular sedimentation, this might lead to a scenario where the combination of uneven settlement in both transverse and longitudinal directions could trigger rotation of the tunnel structure.

6.2.2 Joints Opening/Closure Due to Uneven Settlement

As depicted in Figure 6.5b, the non-uniform settlement has the potential to induce longitudinal tilting of tunnel elements, resulting in unequal compression or decompression of the immersion joints. The illustration presented in Figure 6.7 depicts the inclination of tunnel elements resulting from the differential settlements, indicated in red dashed lines. The tilting center of the tunnel elements is set to be at the tunnel floor of each tunnel element with less settlement. The positive sign indicates compression, while the negative sign represents decompression in immersion joints. It can be observed that decompression occurs at the roof of immersion joints 1, 3, 5 and at the floor of immersion joints 2 and 4. Meanwhile, the compression occurs at the roof of immersion joints 2 and 4. Decompression at the immersion joint causes a joint opening, affecting the rubber sealing performance and raising a water tightness issue. Meanwhile, joint compression causes a joint closure that could lead to overcompression of the joint (Zhang and Broere, 2023b).

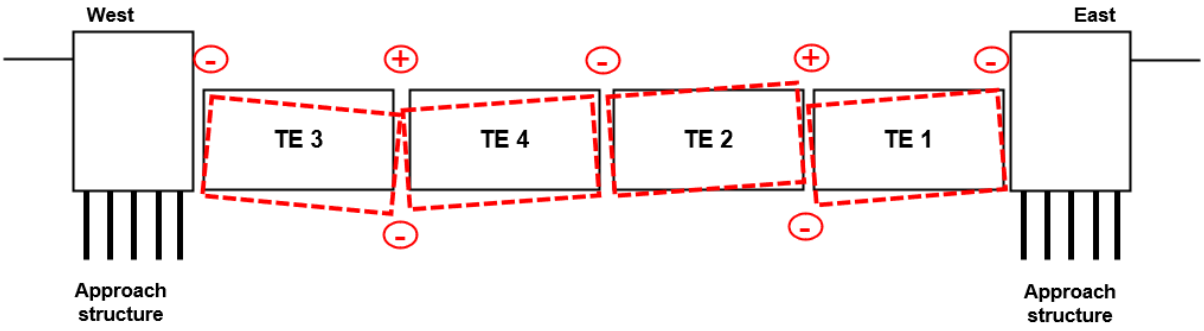

Figure 6.7: Longitudinal compression and decompression at immersion joints of the Noordtunnel (not to scale)

In this research, the impact of uneven settlement on leakage at immersion joints is investigated. Nonetheless, it is important to note that leakage could also potentially occur at dilation joints. According to Leeuw (2018), leakage through dilation joints is the most frequent in an immersed tunnel. However, this research's scope does not encompass the analysis of joint opening or closure at dilation joints due to the limited availability of monitoring data.

The occurrence of leakage at the immersion joint may be attributed to the failure of the GINA and Omega seals (van Montfort, 2018). However, usually, the Omega seal has much higher properties than the GINA gasket. Thus, considering the worst scenario, the primary objective of this subsection is to investigate the impact of rubber gasket compression and decompression on the risk of leaking. The total joint opening or closure is calculated using Formula 6.1.

$$y = \sum \Delta y_i \tag{6.1}$$

where, y is the longitudinal deformation of the immersion joints, and Δy_i is the measured joint opening or closure of the two adjacent segments at the end of the tunnel element. The

calculated joint opening and closure at each immersion joint is presented in Table 6.1. However, it should be noted that the second immersion joint is a closure joint where a rigid joint is used at that particular location instead of a flexible joint. Therefore, immersion joint 2 is not considered in the calculation.

Table 6.1: The measured and predicted joint opening/closure

Years	Description	IJ 1	IJ 2	IJ 3	IJ 4	IJ 5
2019	y (mm) at roof	-6.07	-	-1.94	1.89	-1.91
	y (mm) at floor	0.00	-	-0.40	-0.15	0.00
2040	y (mm) at roof	-6.52	-	-1.74	1.92	-2.20
	y (mm) at floor	0.00	-	0.00	-0.13	0.00
2090	y (mm) at roof	-6.99	-	-1.96	2.01	-2.31
	y (mm) at floor	0.00	-	0.00	-0.13	0.00
Note:		IJ: Immersion Joint IJ 2: Closure joint Compression (+) Decompression (-)				

In order to examine the potential risk of leakage at the immersion joints, it is necessary to determine the initial compression of the GINA gasket. During construction, the tunnel element is immersed and linked to other finished ones on the riverbed or the approach structure. The GINA gasket, positioned on one end of the element, undergoes compression due to the water pressure. The extent of compression depends on the depth of the element immersed in water. The initial compression of the GINA gasket is determined from the force-compression curve of the GINA type used. In the Noordtunnel, GINA-type ETS-130-160 is used at all immersion joints. Figure 6.8 shows the force-compression curve of GINA type ETS-130-160.

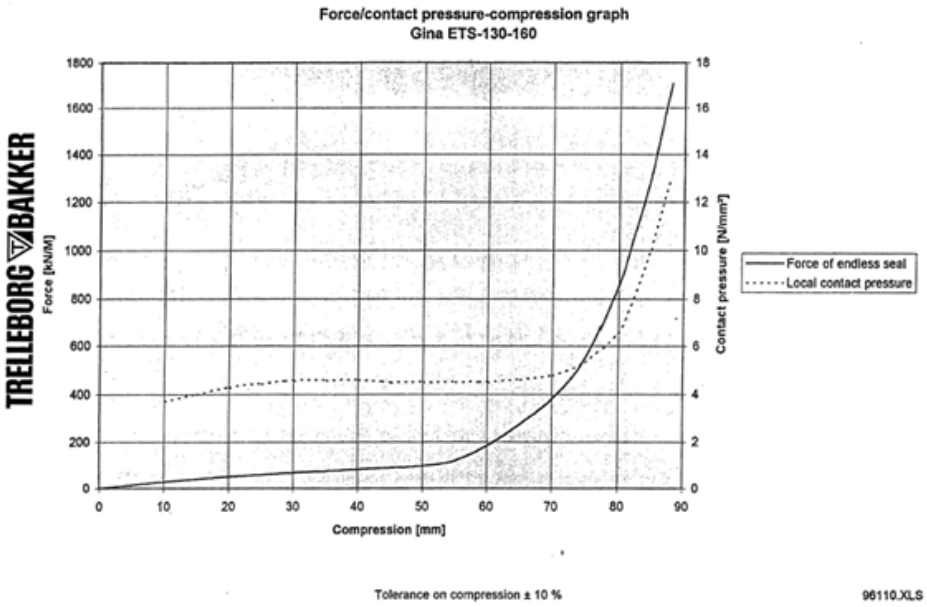

Figure 6.8: Force against compression curve of the GINA type ETS-130-160

Furthermore, Table 6.2 presents the calculated hydrostatic pressure and the initial compression of the GINA gasket at each specific joint. The initial compression of the GINA is set as the

baseline and the remaining compression on each investigated year is calculated by adding the opening/closure magnitude in Table 6.1 to the baseline.

Table 6.2: The GINA compression status at each immersion joint

Description	IJ 1	IJ 2	IJ 3	IJ 4	IJ 5
Depth (section-middle, m)	10.241	-	10.241	12.306	11.074
Hydrostatic force (kN)	25800	-	25800	30760	27801
GINA gasket length (m)	75.23	-	75.23	75.23	75.23
Force per meter (kN/m)	342.97	-	342.97	408.90	369.56
Initial compression (mm)	69	-	69	72	70.5
Compression at roof in 2019 (mm)	62.93	-	67.06	73.89	68.59
Compression at floor in 2019 (mm)	69.0	-	68.60	71.85	70.5
Compression at roof in 2040 (mm)	62.48	-	67.26	73.92	68.30
Compression at floor in 2040 (mm)	69.0	-	69	71.87	70.5
Compression at roof in 2090 (mm)	62.01	-	67.04	74.01	68.19
Compression at floor in 2090 (mm)	69.0	-	69	71.87	70.5
*)Note:	IJ: Immersion Joint IJ2: Closure Joint				

Figure 6.9 depicts the variations in GINA compression status over time. It can be seen that immersion joint 4 has the highest initial compression of 72 mm, due to the greater depth of the secondary end of tunnel element 2. Additionally, the initial compression at immersion joints 1 and 3 is 69 mm, which is the lowest value among the other immersion joints. This is because the hydrostatic force calculation is based on the closure joint elevation, which is shallower compared to the other immersion joints. Furthermore, as depicted in Figure 6.9, it is evident that joint openings on the roof of immersion joints 1, 3, and 5 lead to a minor reduction in GINA compression. Conversely, joint closure results in an increase in compression at immersion joint 4.

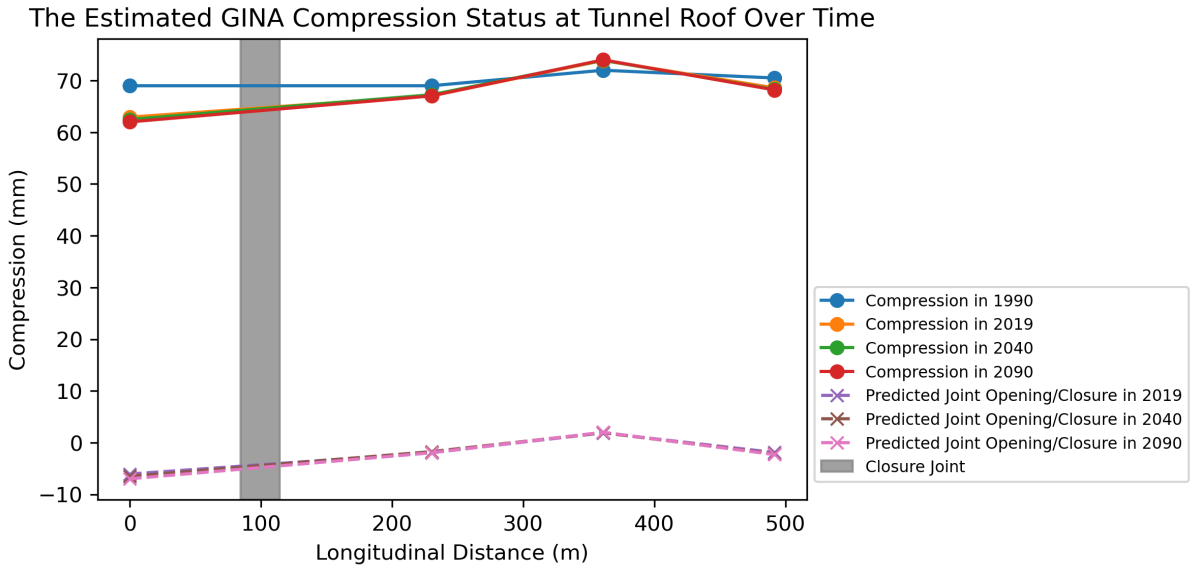

Figure 6.9: The estimated GINA compression status over time

The water tightness of the immersion joints can be examined by considering the equilibrium between the friction of the rubber gasket and the external load applied to the GINA (van

Montfort, 2018), as illustrated in Figure 6.10. It was assumed that leakage could occur if the applied water and soil load were much higher than the friction force of the GINA.

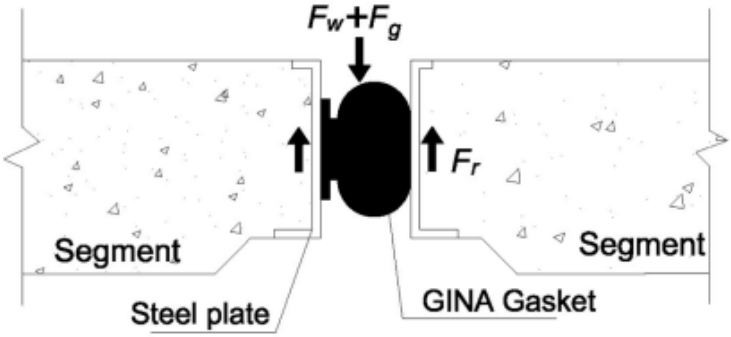

Figure 6.10: Leakage risk due to joint decompression (Zhang and Broere, 2023b)

The frictional force F_r value can be calculated by multiplying the compression force with the friction coefficient between rubber and steel plates. In this particular case, a friction coefficient of 0.6 is selected based on the work of van Montfort (2018).

$$F_r \geq F_w + F_g \tag{6.2}$$

where F_r represents the friction force of the rubber gasket to the two sides of steel plates, while F_w and F_g are the upstream water pressure force and soil cover force, respectively. Nevertheless, it is important to acknowledge that this equilibrium represents a worst-case scenario in which the bolt fixture's resistance is eliminated due to the full corrosion of the bolt.

According to van Montfort (2018), the GINA gasket shows a time-dependent relaxation behaviour, causing a decrease in its friction force. The remaining force percentage can be estimated using the subsequent formula.

$$R = 1 - 0.01 \cdot r \cdot log(t \cdot 365 \cdot 24 \cdot 60) \tag{6.3}$$

where r is the relaxation coefficient per decade (here 0.5 is taken according to van Montfort (2018)), and t is the time duration in years counted after the immersion is completed.

Moreover, determining the external force applied to the rubber gasket involves an initial calculation of the joint width, which represents the rubber gasket's surface area subjected to the external force. The joint width can be calculated by subtracting the compression value induced by differential settlement from the uncompressed height of the GINA gasket.

$$S_{jwp} = h_G - c_G \tag{6.4}$$

where h_G is the uncompressed height of the GINA gasket, with a specific value of 166 mm according to the manufacturer data, and c_G is the calculated compression width obtained from Table 6.2. For the external force calculation, the soil's unit weight follows the properties presented in Table 5.1 with an initial thickness of 0.5 m and then extended to 1 m following the completion of maintenance work in 2022. Table 6.3 presents the friction force that has been estimated for the purpose of evaluating the water tightness of the Noordtunnel throughout its design life.

Table 6.3: The watertightness evaluation of immersion joints in 2019

Joint	IJ 1	IJ 2	IJ 3	IJ 4	IJ 5
Year 2019					
Depth (section-top, m)	2.36	6.73	8.80	7.56	3.06
Force per meter of GINA (kN/m)	225	-	300	490	370
Friction force of GINA, F_r (kN/m)	135	-	180	294	222
Remaining force after relaxation, R	0.64	-	0.64	0.64	0.64
Remaining friction force of GINA, F_r (kN/m)	86.51	-	115.35	188.41	142.27
Joint width at roof (mm)	103.07	-	98.94	92.11	97.41
F_w (kN)	2.46	-	8.70	6.97	2.98
F_g (kN)	0.47	-	0.45	0.41	0.44
Total external force (kN)	2.89	-	9.15	7.38	3.41
Total friction force (kN)	83.62	-	106.20	181.03	138.85
Year 2040					
Remaining friction force of GINA, F_r (kN/m)	77.37	-	117.00	186.82	135.87
Joint width at roof (mm)	103.52	-	98.74	92.08	97.70
Total external force (kN)	3.37	-	9.57	7.79	3.86
Total friction force (kN)	74.00	-	107.42	179.02	132.00
Year 2090					
Remaining friction force of GINA, F_r (kN/m)	71.83	-	110.51	184.19	130.78
Joint width at roof (mm)	103.99	-	98.96	91.99	97.81
Total external force (kN)	3.38	-	9.59	7.79	3.87
Total friction force (kN)	68.45	-	100.92	176.40	126.91

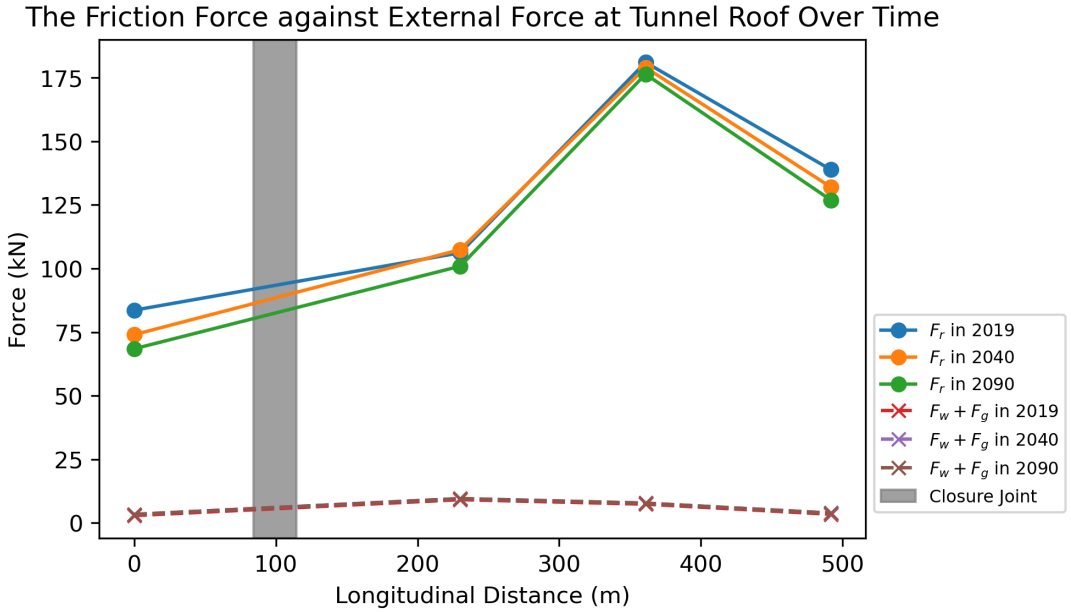

Figure 6.11: The friction force against external force at the tunnel roof over time

It can be observed from Figure 6.11 that the external pressures applied on the GINA gasket, illustrated with dashed lines, are significantly lower in magnitude compared to the total friction force. It shows that the impact of uneven settlement on the water tightness of immersion joints is generally minimal.

6.3 PROPOSED OPTIMIZED MONITORING PLAN

In this thesis, the monitored settlement is used to validate the simulation results. Although the analysis of reconstructed historic settlements in Chapter 3 generated a reasonable settlement trendline from monitoring data, certain points still exhibit an inconsistent trend with the settlement curve shown as an uplift (though infrequently and with minor magnitudes). These inconsistencies could potentially introduce deviations and biases, which might have an indirect impact on the validity of the simulation results. Therefore, this section aims to give the manager an option of an optimized monitoring procedure to eliminate any shortcomings associated with the current monitoring procedure.

6.3.1 The Current Monitoring Procedure

The settlement of the Noordtunnel is monitored during two-time frames: the first ten months after immersion and the regular settlement measurements. The initial measurement is conducted by monitoring the settlement at immersion joints after the immersion process is completed. Meanwhile, the regular settlement measurements in the Noordtunnel began on 17 September 1993, which was approximately 30 months after the last element was immersed. The settlement is monitored using manual leveling, with baseline measuring bolts installed at each traffic tube on top of the road barrier, as depicted in Figure 6.12. The monitoring is conducted annually with an accuracy of around 3 mm.

Figure 6.12: The measuring bolts (number 101 and 102) for regular measurement at immersion joint 1 (SWECO, 2020)

In 2013, the monitoring bolts were installed at each segment joint at both traffic tubes, illustrated as red dots in Figure 3.2. However, only settlement in 2015 and 2019 is measured at segment joints. Thus, due to the limited data collected at the segment joints, the historical settlement of the Noordtunnel can only be constructed by using the settlement measurement at immersion joints.

For the monitoring procedure, the ideal scenario would involve measuring deformation across the entire tunnel length. However, this approach is considered impractical and inefficient. The current strategy of situating monitoring points near immersion and dilation joints is a

good and effective approach for monitoring the settlement in the tunnel's longitudinal and transverse directions Still, the current monitoring procedure has several drawbacks.

Firstly, as described in Chapter 3, the stability of the initial reference point is questionable due to its susceptibility to temperature fluctuations. Additionally, although implementing a 'corrected' reference point offers improved settlement tendencies, some points still exhibit occasional inconsistent trends, even though with minimal frequency and magnitude. Secondly, the current monitoring instrument cannot capture the 'real-time' behaviour of the Noordtunnel due to tidal influence or seasonal temperature changes, which may harm the structural safety of the tunnel. Moreover, the accuracy and the high probability of observational error of the current reference point have also become an issue from the current monitoring procedure. Therefore, the proposed monitoring plan objective is to overcome the limitations of the current monitoring procedure in the Noordtunnel.

6.3.2 Parameters to be Monitored

In this research, the focus of improved monitoring procedure lie on the three most critical factors that pose potential threats. These include excessive settlements, joint opening/closure, and the occurrence of leakage. The presence of excessive settlement within the Noordtunnel can have wide-ranging consequences. Such excessive settlement can induce variations in the tunnel's alignment, causing movements in the immersion and dilation joints, and leading to the potential damage of shear keys and the development of concrete cracks. These cumulative effects could compromise the water tightness and overall structural safety of the Noordtunnel.

Furthermore, the uneven opening and closing of joints, driven by uneven settlement patterns and temperature fluctuations, can be a gateway for leakage. If the joint opening exceeds its allowable limit, then leakage could occur inside the tunnel. This has the potential to pave the way for both water and possibly soil infiltration, consequently amplifying the settlement effects and creating visual disturbances for the tunnel users. Notably, in scenarios where leakage occurs during winter, the freeze-thaw cycle can transform the road surface into a hazardous terrain for the tunnel users.

Given the potentially far-reaching implications of the ongoing settlement and the limitations of the current monitoring procedure, this research proposes three parameters to be monitored: vertical displacement (settlement), transverse displacement, and joint opening/closure. The monitoring of these parameters could serve as an invaluable early warning system, allowing for the detection of emerging structural issues within the Noordtunnel. By utilizing accurate and up-to-date data obtained from these monitored parameters, any remediation actions can be executed in a timely manner, thus reducing the probability of substantial damage occurring within the tunnel's structure. This approach could contribute to the tunnel's long-term structural and operational safety.

6.3.3 Proposed Monitoring Instruments

Conventionally, the joint opening/closure could be measured using an extensometer. Alternatively, the extensometer can be mounted at each edge of two adjacent segments, spanning the joint gap. A conventional point extensometer typically requires a connection cable (electrical or fiber optics) plugged into a datalogger at the other end, as depicted in Figure 6.13. This instrument mostly works by directly measuring the strain variation (of the two mounting feet) and further interprets the relative displacement at the joint between two adjacent segments. When the joints open and close, as a response to the occurring settlement or another trigger-

ing factor, the sensors measure the change in joint width. Using extensometers for measuring opening deformation at a joint might be deemed adequate. However, since the Noordtunnel consists of 5 immersion joints and 15 dilation joints in total, applying this monitoring instrument for large monitoring points requires multiple connection cables, thus not highly practical.

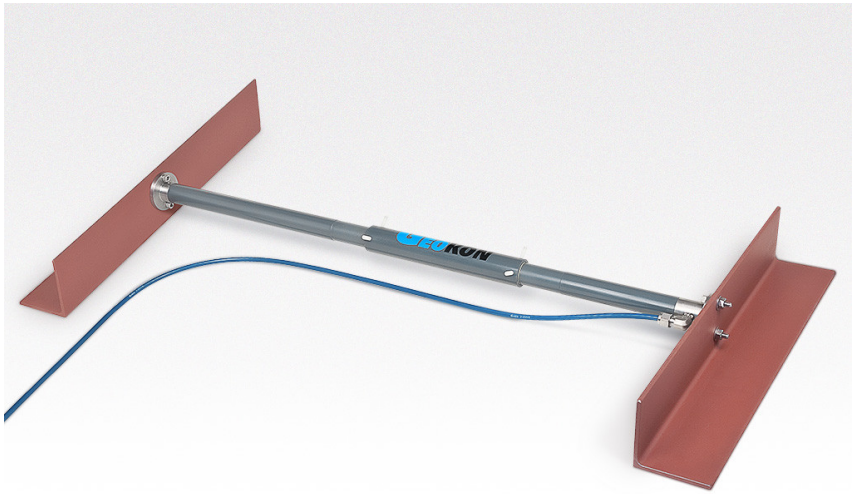

Figure 6.13: The example of an extensometer with optical fiber (Geokon, 2019)

A proposed optimized monitoring instrument necessitates careful consideration of two crucial factors: the precision and reliability of the instrument's data and the practical installation. Ideally, the deformation along the entire tunnel is measured. However, this approach is considered impractical and inefficient. Instead, the behaviour of the Noordtunnel can be observed by measuring and examining joint deformation. Furthermore, closing a busy traffic connection such as the Noorctunnel to measure its deformation is undesirable. Thus, considering the two main factors mentioned above, DOFS system can be installed at each immersion and dilation joint to measure the vertical and transverse displacement, and the joint opening/closure with minimal traffic hindrance.

Based on the work of Zhang and Broere (2022), DOFS system for tunnel monitoring comprises an optical fiber for sensing purposes and a terminal signal interrogator (with data-taking software), as depicted in Figure 6.14. The optical fiber serves as both a sensing component and a channel for signal transmission. Therefore, the optical fiber can be extended and connected to the structure near the immersion and dilation joints. While the fiber end is inserted into the interrogator for signal stimulation and processing.

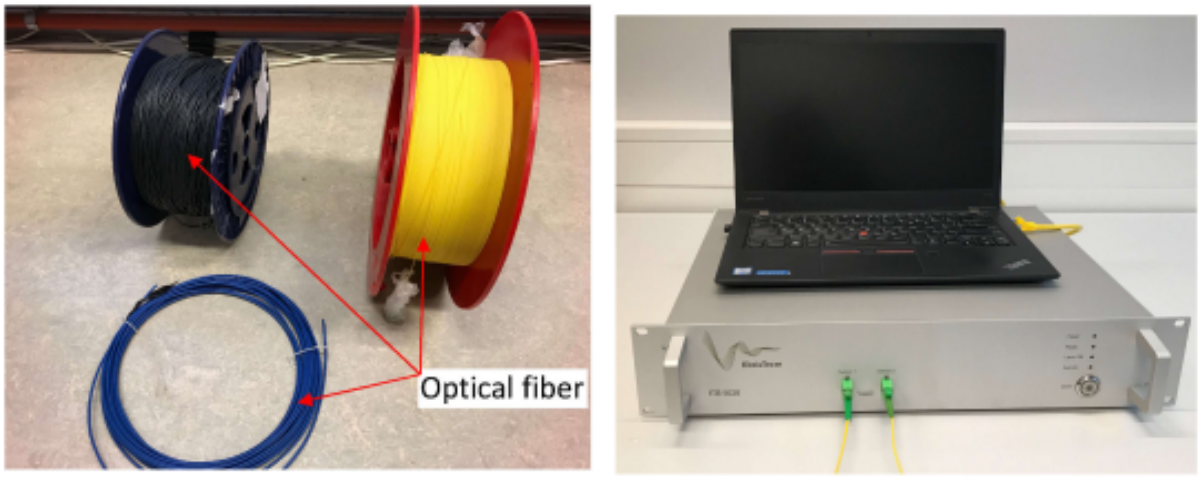

(a) The optical fiber sensor **(b)** The terminal signal interrogator

Figure 6.14: The required components of DOFS system (Zhang, 2022)

One of the biggest advantages of DOFS lies in its remarkable capability for extended sensing distances (Zhang and Broere, 2022). This attribute presents an opportunity to apply the sensor across the entire length of the Noordtunnel, with specialized arrangements at each individual joint to capture the deformation, as depicted in Figure 6.15. Installing DOFS at the entire joints inside the tunnel also presents several benefits. Firstly, the sensor's capability to measure deformations daily (and even hourly) with submillimeter accuracy (Zhang and Broere, 2023a). Secondly, having a year-long dataset for all immersion and dilation joints can also reveal the impact of temperature fluctuations on the immersed tunnel's deformation.

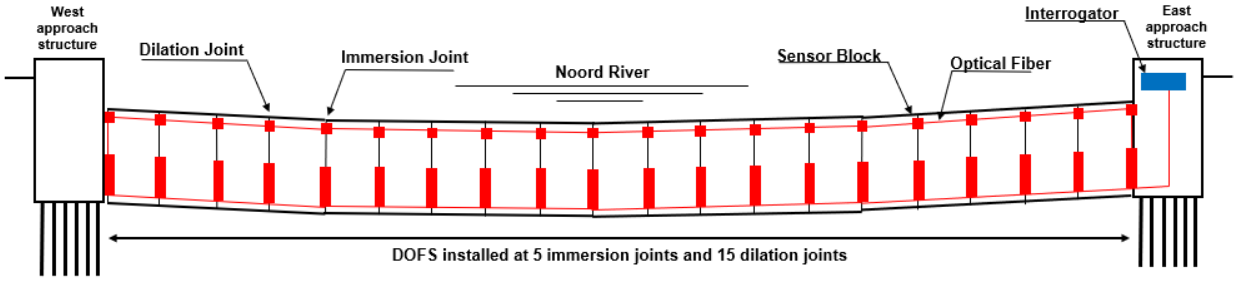

Figure 6.15: The propose configuration of DOFS monitoring system

In order to ensure the instrument's ability to measure the intended parameters (relative displacement and joint opening/closure), the sensors should be installed at the proposed layout, as depicted in Figure 6.16. As mentioned before, the behaviour of the Noordtunnel can be observed by measuring and examining joint deformation, a short-length optical fiber can be installed and fixed at two points of the adjacent segments. The interval fiber section between (gauge length) works as an extensometer and relative displacement (of the two fixture points) can be measured. It is important to acknowledge that before installation, the fiber must undergo pre-tensioning in order to enable the detection of both contraction and extension.

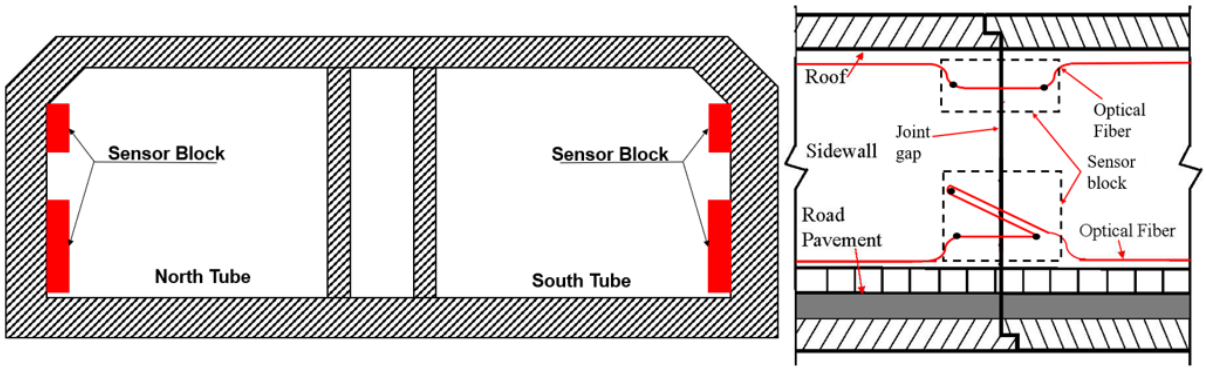

Figure 6.16: The proposed typical DOFS sensor layout based on Zhang (2022) with additional sensor on the tunnel roof

It is suggested that one side sensor block should cover the bottom and upper part of the tunnel. This configuration will measure vertical settlement and joint opening width at the floor and roof of the tunnel more precisely. The sensor blocks consist of three short sections of the optical fiber lines. These five lines are fixed at five specific points (P1 to P5) at each joint of the Noordtunnel, as illustrated in Figure 6.17. Fiber lines 1 and 2 (FL 1 and FL 2), situated above the road barrier, aim to measure joint opening/closure at the tunnel floor ($y - axis$) and the relative displacement ($z - axis$) between two adjacent segments. Additionally, FL3, positioned near the tunnel roof, is designed to detect the opening/closure of joints along the tunnel roof, specifically in its longitudinal directions.

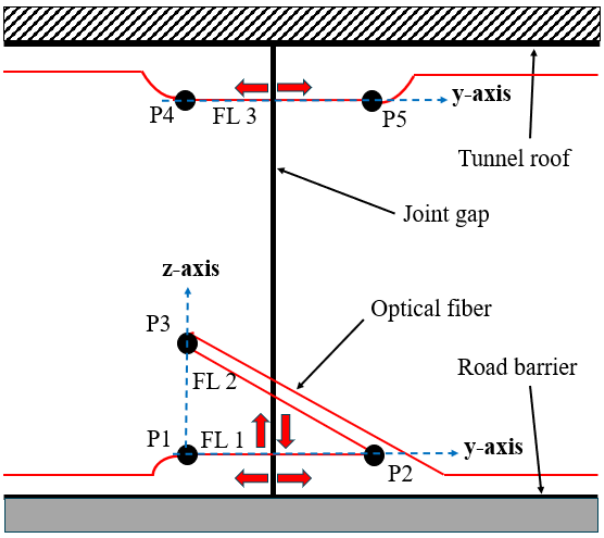

Figure 6.17: The proposed sensor block configuration based on Zhang (2022) with additional sensor on the tunnel roof

Furthermore, the uneven settlement in the Noordtunnel has the potential to generate concrete cracks in the tunnel structure. Usually, concrete fissures are visually inspected periodically. If a concrete crack is detected later in the future, Vibrating Wire Strain Gauges (VWSG) can be used to monitor the development of the concrete crack inside the tunnel. These instruments can be welded across the concrete cracks or bonded with the DOFS at the wall surface. These cost-effective sensors are suited for remote, long-term monitoring of crack width development. Moreover, VWSG monitoring instrument also has a high accuracy with an error of ± 0.1 to $\pm 0.5\%$ (Jacob, 2023).

6.4 DISCUSSIONS

In this chapter, the effect of the ongoing settlement on the immersion joint of the Noordtunnel is examined. The uneven settlement in the Noordtunnel can cause vertical deformation, cracking in the dilation joint, shear key cracking at immersion joints, unequal joint opening and closure, and rotation to the tunnel body. The vertical movement between two adjacent segments will cause a vertical shear deformation that can alter the tunnel alignment and deform the rubber gasket. This situation can lead to shear connection failure and shear key cracking at the immersion joint in extreme conditions. Moreover, the combination of differential settlement in tunnel transverse and longitudinal directions may lead to rotation of the tunnel structure.

The uneven settlement in the longitudinal direction causes tilting of the tunnel element, resulting in unequal compression or decompression of the immersion joints. Compression at the immersion joint occurs when two adjacent tunnel elements move closer to each other, resulting in joint closure. In contrast, decompression occurs when two adjacent tunnel elements move away from each other, leading to a joint opening. The decompression at the immersion joint could affect the rubber sealing performance and compromise the water tightness. The occurrence of leakage at the immersion joint may be attributed to the failure of the GINA and Omega profiles. However, this research assesses the risk of leakage by considering the worst-case scenario where only the GINA gasket provides watertightness for the tunnel.

The risk of leakage is examined by comparing the friction force of the GINA gasket to the external force applied to the rubber gasket. The result, visualized in Figure 6.9, shows that the initial compression of GINA gasket depends on the depth of the other end of the tunnel element. A greater depth will result in greater initial compression. Figure 6.9 also shows that the joint opening/closure is increasing as the uneven settlement keeps occurring. The increasing joint opening causes a decrease in rubber gasket compression. Consequently, the width of the rubber gasket is also increased. This rising joint opening leads to a subsequent escalation in the external load subjected to the rubber gasket. However, the result shown in Figure 6.11, reveals that even after considering the relaxation of the GINA gasket, the applied external force remained considerably lower than the friction force of the gasket. Taking immersion joint 1 as an example, it is predicted that although the uneven settlement causes the widest joint opening in the particular area, the total external force is still significantly lower than the total friction force. Consequently, it can be inferred that a single factor of uneven settlement has a minimal effect on the water tightness of the immersion joints. Nevertheless, it is important to point out that the analysis conducted in section 6.2 excluded the longitudinal deformation of the tunnel due to seasonal joint expansion. In certain instances, such as in the Heinenoordtunnel, the fluctuation in seasonal temperatures can result in a cumulative longitudinal expansion and contraction of 41.5 mm (Zhang and Broere, 2023b). The potential joint decompression resulting from the combined effects of seasonal temperature fluctuations and the differential settlement may surpass the minimal capacity of joint compression at immersion or dilation joints. Consequently, the tunnel manager must be aware of the risk of joint decompression.

Furthermore, as the extent of the usefulness of the simulation results depends on the measured settlement, an improved monitoring procedure is also proposed in this chapter. The existing monitoring procedure by manual leveling is recognized to possess certain limitations, i.e., it is less accurate and has a high probability of observational error. In order to mitigate these concerns, a DOFS monitoring system is proposed with a specific sensor layout as depicted in Figure 6.17. The arrangement of DOFS installation is tailored to enable the sensor to

work as an extensometer to measure tunnel deformation in three directions. FL1 is designed to measure the joint opening/closure at the tunnel floor, while FL3 aims to measure the joint opening at the tunnel roof. In addition, FL2 is designed to measure the relative displacement between two adjacent segments. This arrangement enables the measurement of uneven settlement and the differentiation of each joint's tilting or rotation center in the Noordtunnel within its longitudinal directions.

While the issue of excessive settlement of the Noordtunnel only occurs at the second immersion joint, a strategy could involve the installation of DOFS at each segment of tunnel elements 3 and 4, primarily addressing the monitoring of excessive settlement for that specific location. Still, a more comprehensive approach is recommended by installing the DOFS along the entire tunnel joints (both for immersion and dilation joints). Such extensive coverage not only enhances the detection of localized issues but also offers holistic monitoring data within the entire Noordtunnel facilitated by a single monitoring instrument, reinforcing the effectiveness of the monitoring system. Moreover, to measure the displacement in the Noordtunnel's transverse direction ($x - axis$), installing the DOFS system at both of the tunnel traffic tubes is recommended. However, if this approach is considered too labor-intensive, an alternative suggestion is to install the DOFS at each immersion and dilation joint only in one tunnel tube. Simultaneously, on the other tube, DOFS can be mounted only at the immersion joints. This configuration of monitoring instruments will provide the tunnel manager with comprehensive data regarding tunnel deformation in three dimensions, encompassing longitudinal displacement ($y - axis$), vertical displacement ($z - axis$), and transverse displacement ($x - axis$). By adopting this monitoring procedure, the tunnel manager can access real-time data on tunnel deformation in all dimensions with submillimeter accuracy.

6.5 CONCLUSIONS

The following points give the key takeaways of this chapter, which also could be used to answer the sub-research questions given in Chapter 1:

- The uneven settlement in tunnel longitudinal directions triggered tunnel elements to tilt in $y - axis$, leading to compression and decompression at the immersion joints. While compression will lead to joint closure, decompression will lead to joint opening.
- The GINA compression status, presented in Figure 6.9, shows a decreasing compression at immersion joints 1, 3, and 5 due to joint opening. In contrast, joint closure causes an increase in GINA compression at immersion joint 4.
- Considering the relaxation of the GINA gasket and the anticipated ongoing settlement over the next 67 years, the overall external load subjected to the GINA gasket remains notably lower than the friction force between the GINA gasket and the steel plate. Thus, it is predicted that differential settlement is unlikely to cause a leakage in in the immersion joints of the Noordtunnel.
- The current monitoring procedure has some shortcomings, a DOFS system could be an option for optimizing the monitoring procedure.
- DOFS can work as an extensometer to measure the strain between two adjacent segments. Installing DOFS on the entire tunnel joints will enable the tunnel manager to monitor the joint opening/closure and the relative displacement in the Noordtunnel's longitudinal and transverse directions with submillimeter accuracy.

7 CONCLUSIONS AND RECOMMENDATIONS

This thesis has systematically examined several crucial aspects concerning the settlement of the Noordtunnel. The thesis begins by reconstructing the measured settlement of the Noordtunnel. Then, soil profile and geotechnical parameters are determined for simulation purposes. The 2D Finite Element Method (FEM) simulations were carried out in PLAXIS while considering the effect of load variations to uncover the underlying reasons for the excessive settlement observed in the Noordtunnel and predict its future settlement. Based on the simulation results, this thesis also examined the impact of the ongoing settlement on the potential risk of leakage. In the final chapter, an optimized monitoring procedure is proposed as an alternative to address the limitations of the current monitoring approach.

7.1 CONCLUSIONS

This section provides the answers to sub-questions and the main research questions formulated in Chapter 1. The answers are derived from the findings of the analysis and simulation results described in Chapters 3 to 6.

How to interpret the historic settlement of the Noordtunnel?
The reconstructed historical settlement of the Noordtunnel shows logarithmic trendlines, with a maximum estimated settlement of about 94.36 mm occurring at immersion joint 2 during the thirty years of service. The logarithmic trendlines indicate that the settlement that occurred in the Noordtunnel is mainly derived by a geotechnical mechanism. The historical settlement data indicates that the consolidation process mainly occurs in the first seven months after immersion. Subsequently, a creep is observed with immersion joint 2 being the most pronounced. Considering the equivalent effective stress subjected to the subsoil, the uneven settlement along the tunnel's longitudinal direction is likely to occur due to the geological conditions in the field.

What are the accountable reasons that induced the local excessive settlement observed in the Noordtunnel?
The simulation results indicate that the excessive settlement observed in the Noordtunnel is most likely attributed to the localized presence of soft soil underneath immersion joint 2. The soft soil has a time-dependent behaviour, which makes the soil keep settling under a constant load. The simulation results reveal that the soft soil under the tunnel is responsible for at least 20 mm of settlement. In addition, the sedimentation at immersion joint two causes at least 8 mm of settlement, making the excessive settlement more pronounced.

Which geotechnical parameter has the most dominant influence on the settlement of the Noordtunnel?
The simulation results show that the bottomost sand layer is the most compressible layer at immersion joints 1, 3, and 4, while clay is the most compressible layer at immersion joints 2 and 5. The sensitivity analysis shows that the unloading-reloading stiffness (E_{ur}) is the most

sensitive parameter at immersion joints 1,3, and 4. Moreover, at immersion joint 5, the E_{ur} and the oedometer stifffness (E_{oed}) is the most sensitive parameter due to the impact of soil improvement in that area. At immersion joint 2, the modified creep index (μ^*) is the most sensitive parameter since the soft soil has a dominant influence on settlement in that area. However, due to the narrow distribution of the reference values, adjusting the most sensitive parameter will lead to a maximum deviation of 5.48% at immersion joint 2 and 4% at the other immersion joints.

How does the ongoing settlement impact the tunnel structural safety? And what measures can be conducted to optimize the present monitoring work and mitigate the structure deterioration?
The differential settlement that occurs in the Noordtunnel triggered the tunnel elements to tilt in their longitudinal directions, leading to compression and decompression at the immersion joints. While compression will lead to joint closure, decompression will lead to joint opening. The potential risk of leakage is examined by taking into account the effect of uneven settlement on the extension of joint opening at the immersion joints in the worst-case scenario where only the GINA gasket works to prevent leakage. The results show that even after considering the relaxation of the GINA gasket and the expected ongoing settlement over the next 67 years, the overall external load applied subjected to the GINA gasket remains significantly lower than the friction force of the GINA gasket.

Regarding the proposed optimization of the monitoring procedure, the Distributed Optical Fiber Sensor (DOFS) can work as extensometer and can be an option for monitoring the deformation of the Noordtunnel. A specific sensor layout consisting of three fiber lines (FL 1, 2, and 3) could measure the joint opening/closure as well as the relative displacement between two adjacent segments. FL 1 and 2, located near the tunnel floor could be used to measure joint opening/closure at the tunnel floor (in y-axis) and the relative displacement (in z-axis). In addition, FL 3 is designed to measure the joint opening/closure near the tunnel roof. By adopting DOFS on the entire tunnel joints of both tubes will enable the tunnel manager to monitor the joint opening/closure and the relative displacement in the Noordtunnel's longitudinal and transverse directions with submillimeter accuracy.

Finally, the main research question below could be answered:

"How to reasonably predict the future settlement of the Noordtunnel and assess its impact on structural safety?"
The future settlement of the Noordtunnel can be predicted by conducting a simulation in the FEM program. As soil profile and geotechnical are needed for creating the model, CPT and NEN Table 2b correlation are employed to estimate the soil properties in the field. In the simulation, the variations of load subjected to the subsoil are taken into account by introducing the traffic load and additional soil cover on top of the tunnel. Furthermore, two types of soil constitutive law were employed in the simulation: Hardening Soil Model (HS Model) and Soft Soil Creep Model (SSC Model). The HS Model is used as the soil is subjected to loading-unloading behaviour during the construction stages, while the SSC Model is utilized to capture the time-dependent behaviour, particularly in areas where the soft soil significantly influences the settlement behaviour. The accuracy and reliability of the simulation outcomes were then evaluated by aligning the simulation results with the reconstructed monitoring data. This process served as the foundation for identifying excessive settlement and predicting future settlement tendencies.

The results of this thesis show how the localized soft soil underneath the tunnel and the additional soil cover on top of the tunnel significantly influence the settlement of the Noordtunnel. Furthermore, the simulation outcomes presented in this thesis offer the capability to anticipate forthcoming settlement patterns over the Noordtunnel's intended operational lifetime. Based on the simulation results, it is predicted that uneven settlement will occur in the Noordtunnel within its remaining design lifetime. An additional settlement of 15.13 mm of settlement is expected to occur at immersion joint 2, while 'only' 4 to 5 mm of additional settlement is anticipated at the other immersion joints within the next 67 years.

Although the uneven settlement is expected to continue occurring at a lower rate in the future, the water tightness evaluation shows that the external loads subjected to the GINA gasket remain considerably lower than the GINA gasket-steel plate friction force. Thus, it is predicted that a single factor of uneven settlement imposes quite a limited risk of any leakage problem at the immersion joints within the Noordtunnel's remaining designed lifetime.

7.2 RECOMMENDATIONS

The following recommendations encompass proposals for further research and practical measures the tunnel owner might undertake:

1. Although simulating settlement using 2D FEM can provide pretty satisfying results, it still remains incapable of depicting the settlement distribution in all directions along the tunnel element, even if the tunnel is modeled longitudinally. Therefore, the utilisation of 3D simulations may serve as a viable solution for addressing these limitations.
2. As it is evident that the localised soft soil significantly impacts the Noordtunnel's settlement, it is recommended to conduct further site investigations to discover the extent of localised soft soil underneath the tunnel.
3. In this research, the impact of uneven settlement is examined by analysing the tunnel potential of leakage at the immersion joints. Further research on tunnel structural safety due to long-term settlement behavior, tidal and seasonal temperature changes may provide valuable knowledge in predicting the occurrence of any damage to the tunnel. Thus, remediation measures can be taken before any severe damage, and the serviceability of the tunnel can be maintained during its service life.
4. In this research, the historical settlement at dilation joints cannot be reconstructed due to the limited measurement data. Moreover, it is also found that the current monitoring procedure has some shortcomings. Therefore, to be able to discover the entire tunnel settlement's behaviour and overcome such existing limitations, the tunnel owner may consider installing Distributed Optical Fiber Sensor (DOFS) with a specific sensor layout, as previously explained in Chapter 6, as an alternative to measuring the Noordtunnel's deformation.

REFERENCES

Brinkgreve, R. B. (2022). Lecture notes of behaviour of soils and rocks. *TU Delft*.

Celik, S. (2017). Comparison of mohr-coulomb and hardening soil models' numerical estimation of ground surface settlement caused by tunneling. *Iğdır Univ. J. Inst. Sci. Tech.*, 7(4):95–102.

de Vries and van de Wiel (2022). Afleverdossier: Vtw-083 dekking tunnel a15 de noord. *de Vries, and van de Wiel*.

DINOloket (2023). https://www.dinoloket.nl/en. Retrieved on 16 June 2023.

Eurocode (1991). *Eurocode 1: Actions on structures - Part 2: Traffic loads on bridges. EN 1991-2:2003*. European Committee For Standardization.

Gavin, K., Broere, W., Kovacevic, M., and de Haas, K. (2019). Investigation of the remaining life of an immersed tube tunnel in The Netherlands. *Proceedings And Monographs In Engineering, Water And Earth Sciences*, pages 4831–4838.

Geokon (2019). *Intruction Manual Model 4435 VW Extensometer*. GEOKON, 48 Spencer Street, NH 03766 USA.

Glerum, A. (1988). Immersed tunnels: why, when, and where. *Tunneling and underground space technology*, 3:347–351.

Grantz, W. C. (2001). Immersed tunnel settlements part 1: Nature of settlements. *Tunneling and Underground Space Technology*, 16:195–201.

GrondmechanicaDelft (1984). *Noordtunnel Stabiliteit Bouwput West. CO-244450/114*. Laboratorium voor Grondmechanica Delft.

GrondmechanicaDelft (1986). *Tunnel Onder De Noord. CO-244451/112*. Laboratorium voor Grondmechanica Delft.

Jacob, J. (2023). *Optimization of Design and Monitoring of Immersed Tunnels*. Master's thesis. Delft University of Technology.

Leeuw, L. (2008). Lekkage in tunnels-dilatatievoegen en beton. *Technical report. RWS Bouwdienst*.

Leeuw, L. (2018). *Lekkage in tunnels II*. COB.

Liu, R., Zhang, G., Li, S., Feng, S., and Xin, J. (2022). Application of impact imaging method on nondestructive detection of void defects in sandwich-structured immersed tunnel. *Mathematical Problems in Engineering*, 2022.

Lunnis, R. and Baber, J. (2013). *Immersed Tunnel*. CRC Press.

Luttikholt, A., Doorduyn, A., de Wit, H., and Li, Y. (2022). Consideration of concrete and steel sandwich tunnel elements. *Tunneling and Underground Space Technology incorporating Trenchless Technology Research*, 121.

Nagel, G. W. (2011). Dynamic behaviour of tunnel elements during the immersion process - A study to the influence of swell waves and wind waves on the immersion systems. *TU Delft Repository*.

NEN (2017). *NEN9997-1+C2:2017, Geotechnical Design of Structures - Part 1: General rules.* Stichting Koninklijk Nederlands Nomalisatie Instituut.

Olsen, T., T., K., and de Wit, J. (2022). Immersed tunnel in soft soil conditions experience from the last 20 years. *Tunneling and Underground Space Technology*, 121.

PLAXIS (2020). *PLAXIS Material Models Connect Edition V20.02*. PLAXIS B.V.

PLAXIS (2021). *PLAXIS 3D TUNNEL Material Models Manual version 2*. PLAXIS B.V.

Puzrin, A. M., Alonso, E. E., and Pinyol, N. M. (2010). *Geomechanics of Failure*. Springer.

Reinders, K. (2019). Lecture notes of bored and immersed tunnels. *TU Delft*.

Robertson, P. (2010). Soil behaviour type from the CPT: an update. *Proc. 2nd International Symposium on Cone Penetration Testing, CPT'10, Huntington Beach, CA, USA*.

Robertson, P. (2015). Soil behavior type using the DMT. *Gregg Drilling Testing Inc., Signal Hill, CA, USA*.

Robertson, P. K. (2013). Cone penetration testing interpretation of soil parameters - coarse-grained soils.

Schanz, T., Vermeer, P., and Bonnier, P. (2019). The hardening soil model: Formulation and verification. *Beyond 2000 in Computational Geotechnics*, 16:281–296.

SWECO (2020). *North Tunnel risk analysis*. SWECO Netherlands BV, Bilt.

TEC (1992). De noordtunnel referentie meting hoogteligging tunnel. 1000n/cb/lg/b92512.

van Montfort, R. (2018). *Insufficiency of immersion joints in existing immersed tunnels. Case study on functioning of Gina-seal and Omega-seal in the Kil Tunnel*. Master's thesis. Delft University of Technology.

Wang, S., Zhang, X., and Bai, Y. (2020). Comparative study on foundation treatment methods of immersed tunnels in china. *Frontiers of Structural and Civil Engineering*, 14:82–93.

Wei, G., Qui, H., and Wei, X. (2012). Analysis of settlement reasons and mechanism in immersed tunnel. *Applied Mechanics and Materials*, 238:803–807.

Zhang, X. (2022). *Monitoring the deformation behavior of an immersed tunnel with Distributed Optical Fiber Sensor (DOFS)*. Doctoral thesis. Delft University of Technology.

Zhang, X. and Broere, W. (2019). Settlements of immersed tunnel on soft ground: A case study. *Tunnels and Underground Cities: Engineering and Innovation meet Archaeology, Architecture and Art*, pages 1234–1241.

Zhang, X. and Broere, W. (2022). Sensing fiber selection for point displacement measuring with distributed optic fiber sensor. *Measurement*, 197.

Zhang, X. and Broere, W. (2023a). Design of a distributed optical fiber sensor system for measuring immersed tunnel joint deformations. *Tunnelling and Underground Space Technology*, 131.

Zhang, X. and Broere, W. (2023b). Monitoring seasonal deformation behavior of an immersed tunnel with distributed optical fiber sensors. *Measurement*, 219.

A | APPENDIX A

This appendix is a supplementary section, providing additional data and information supporting the findings and analyses presented in Chapter 3.

The graph below depicts the settlement measurements at all immersion joints during the initial ten months after the tunnel immersion. In the graph, the solid line corresponds to the primary end of the tunnel, which is connected to the previous structures. On the other hand, the dashed line represents the secondary end, which is yet connected to any structures during the immersion process.

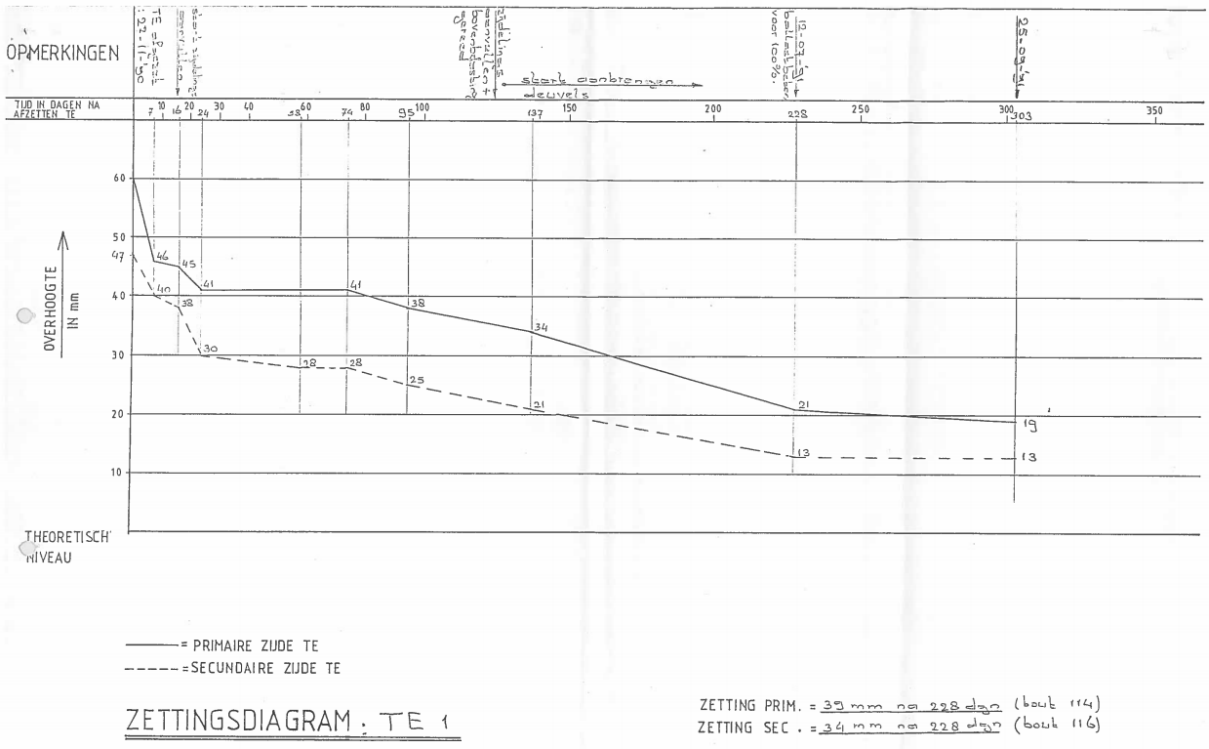

Figure A.1: The measured settlement on the first ten months at tunnel element 1

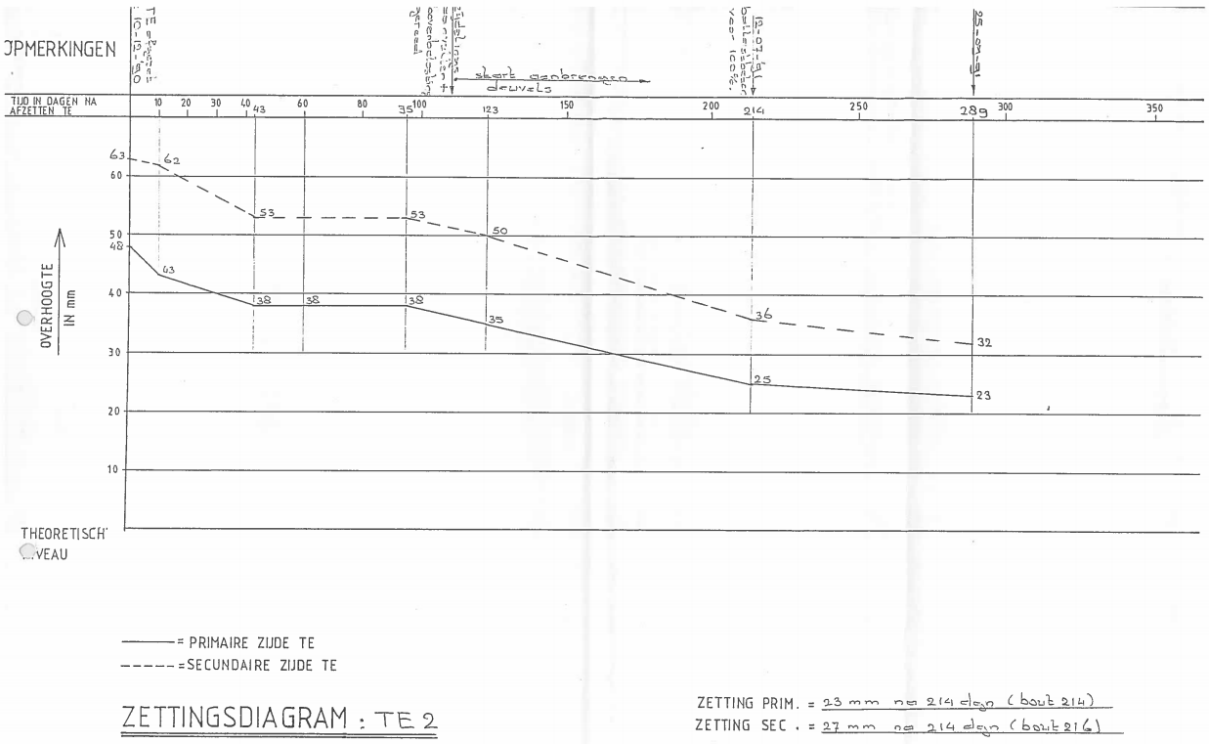

Figure A.2: The measured settlement on the first ten months at tunnel element 2

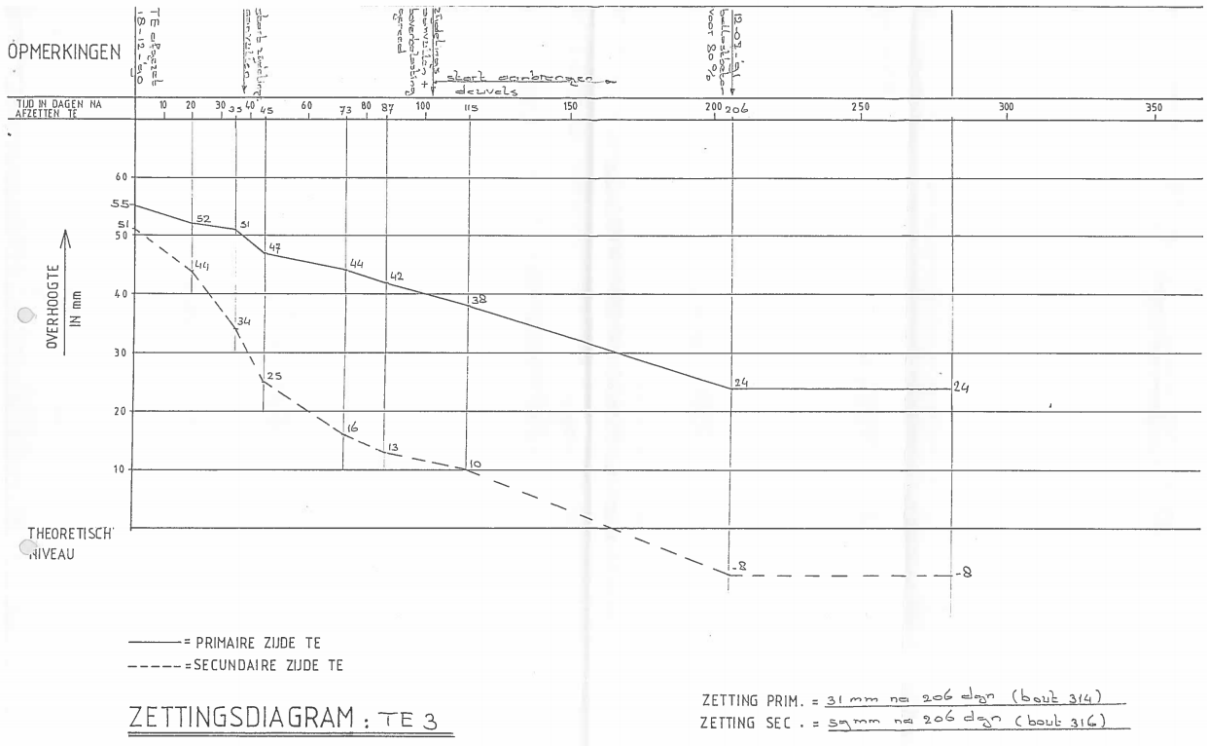

Figure A.3: The measured settlement on the first ten months at tunnel element 3

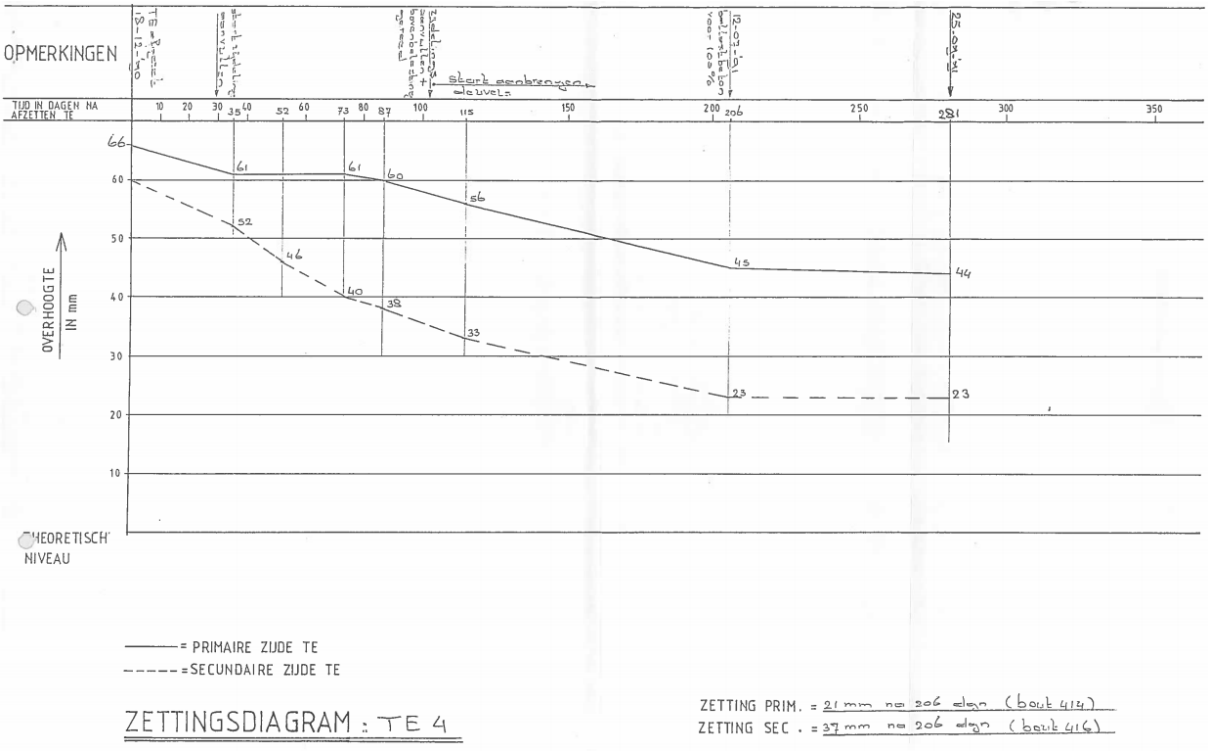

Figure A.4: The measured settlement on the first ten months at tunnel element 4

The following pictures depict the settlement tendency of all measuring points toward the possible new reference point. These settlement trends are plotted based on the regular measurements conducted from 1993 to 2019.

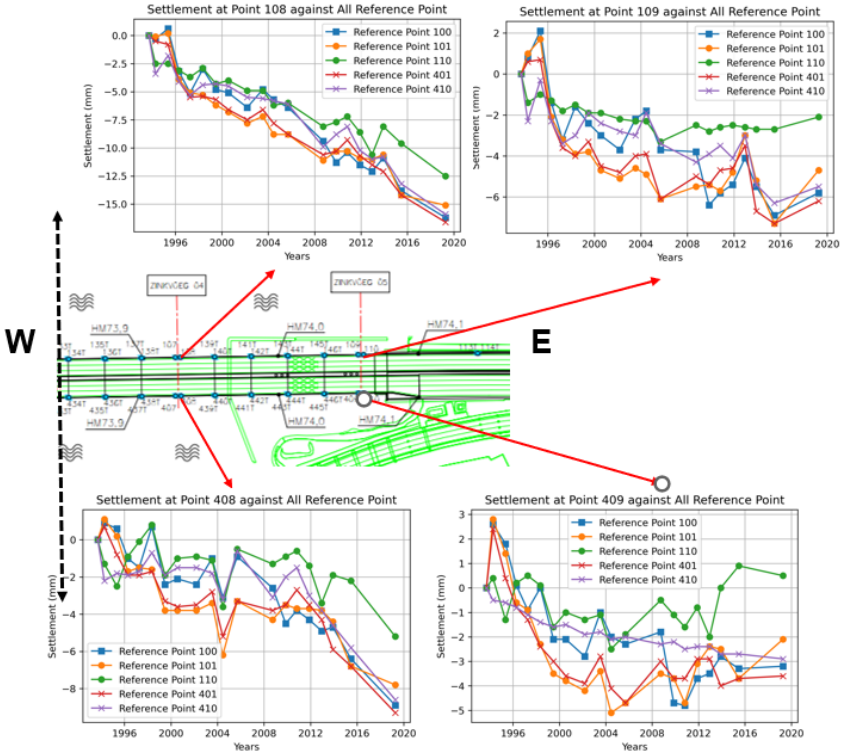

Figure A.5: The settlement trendline of regular measurement at tunnel element one

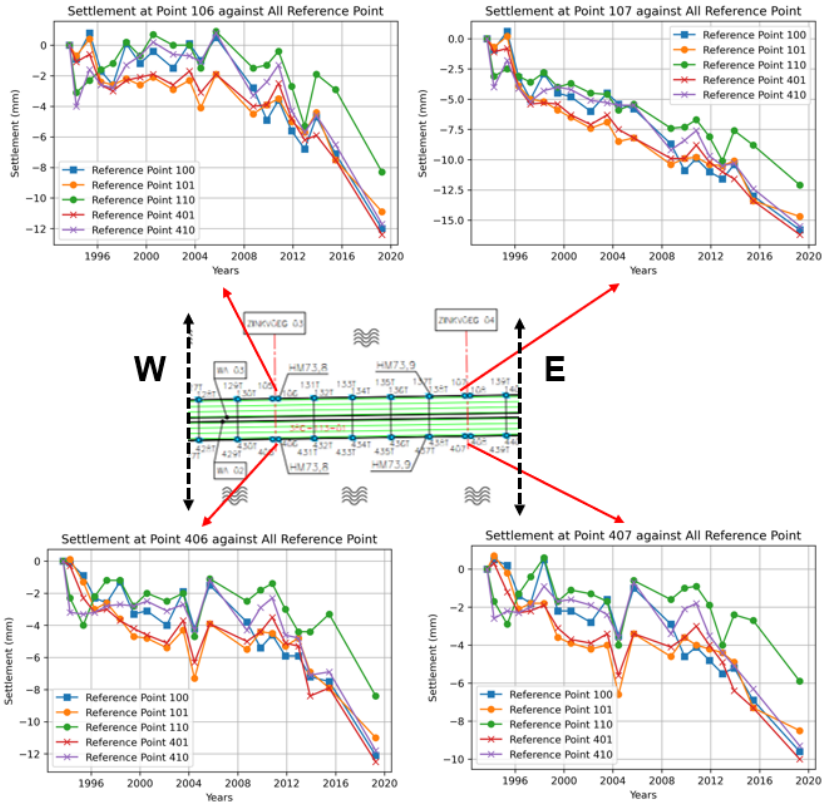

Figure A.6: The settlement trendline of regular measurement at tunnel element two

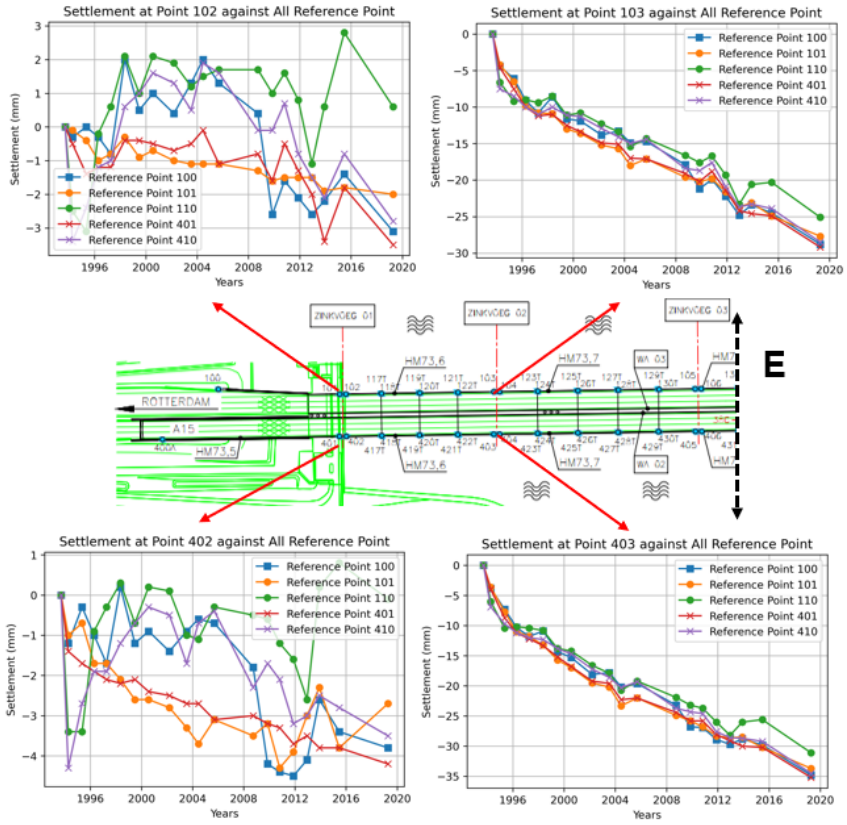

Figure A.7: The settlement trendline of regular measurement at tunnel element three

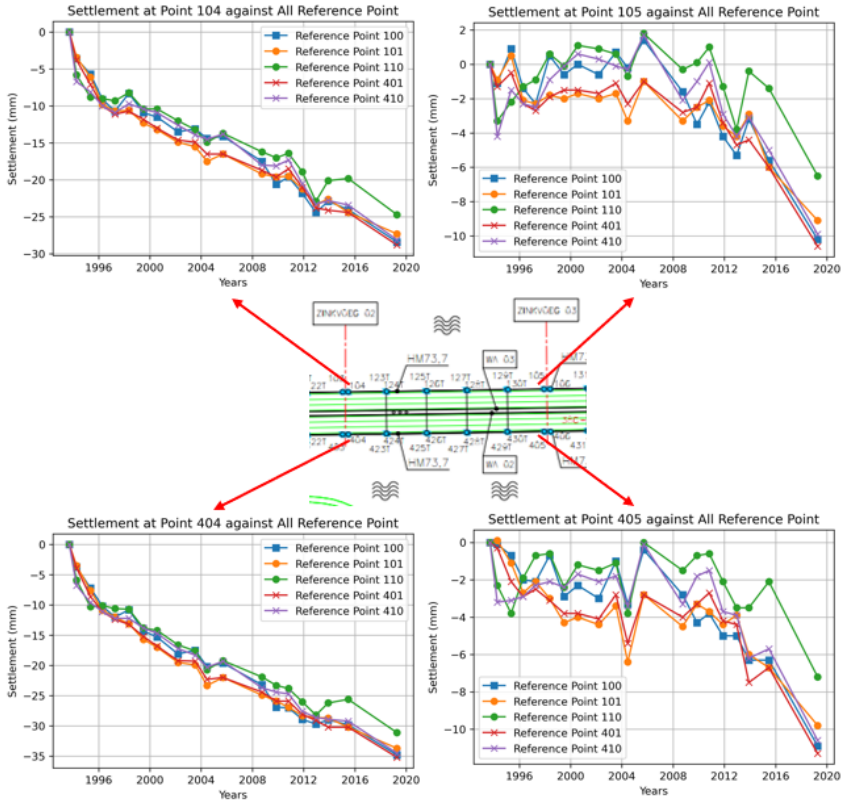

Figure A.8: The settlement trendline of regular measurement at tunnel element four

The following figures depict the historical settlement of Noordtunnel at all immersion joints.

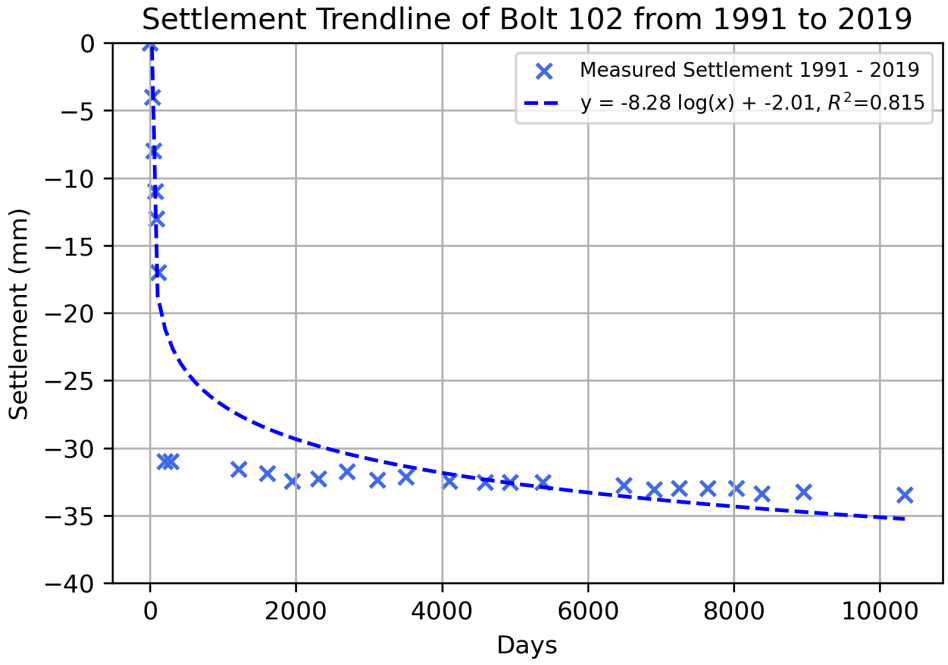

(a) The settlement history of immersion joint 1

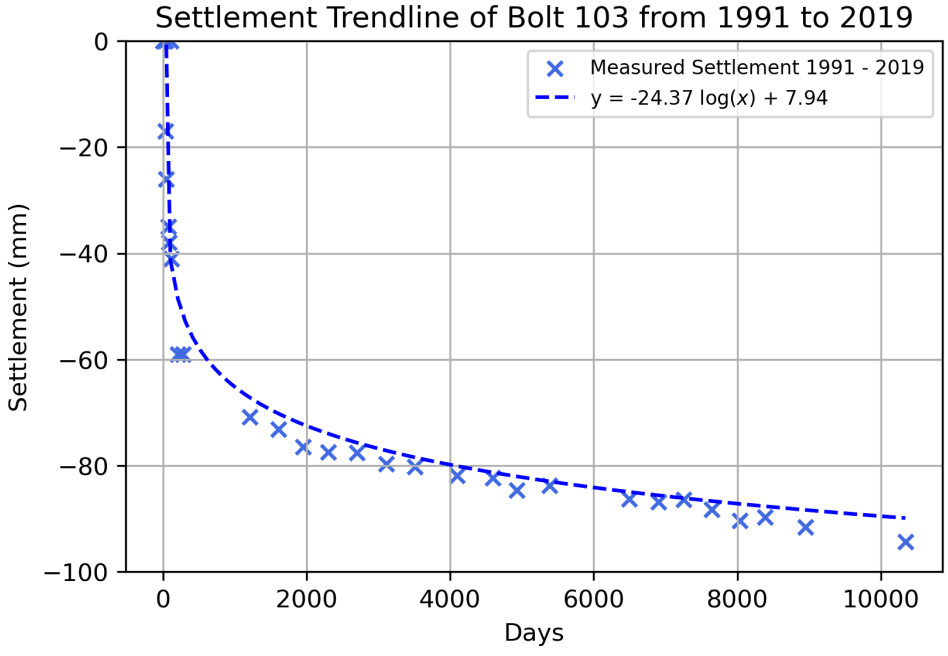

(b) The settlement history of immersion joint 2

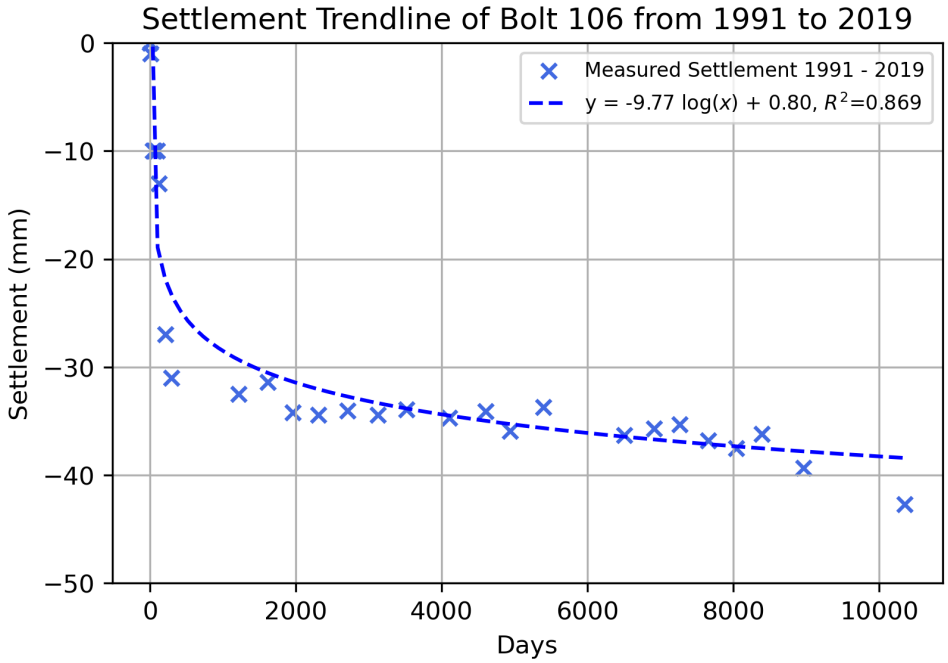

(c) The settlement history of immersion joint 3

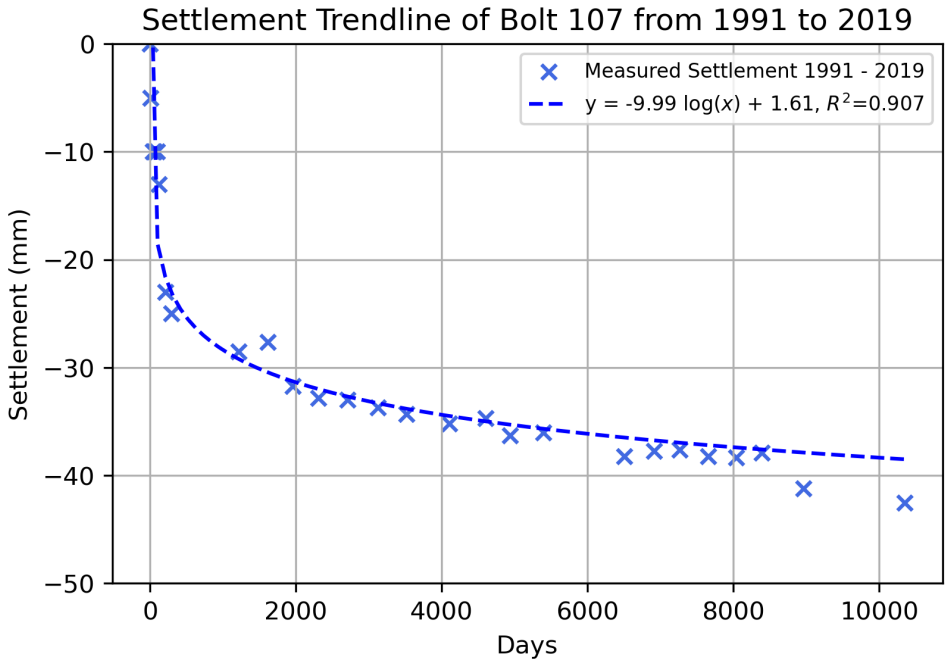

(d) The settlement history of immersion joint 4

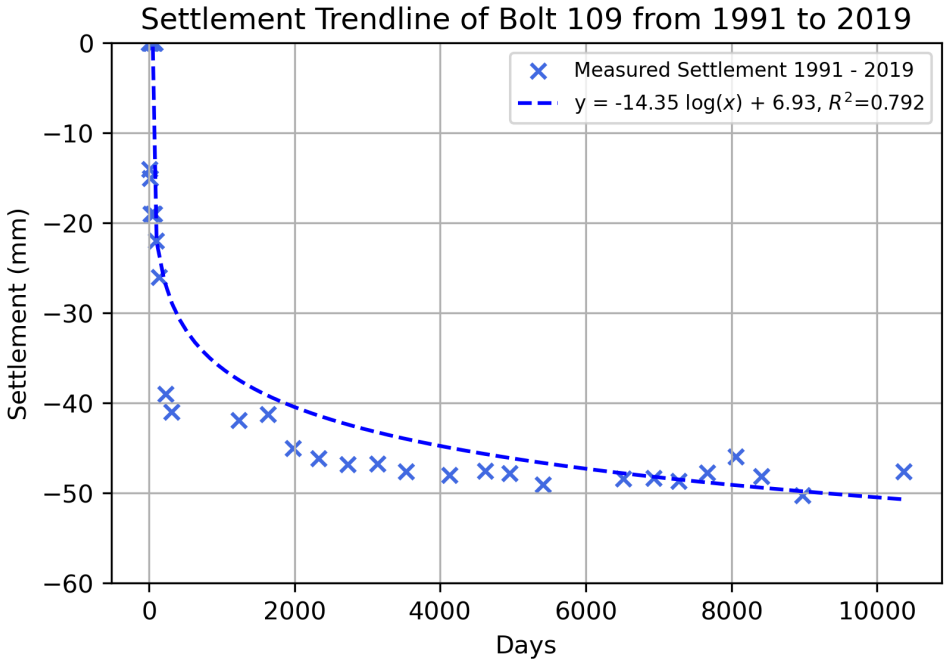

(e) The settlement history of immersion joint 5

Figure A.9: The historical settlement of the Noordtunnel at all immersion joints

B APPENDIX B

This appendix is a supplementary section, providing additional data and information on Chapter 4.

The figure below depicts the site map of the Noordtunnel's longitudinal direction. The figure also indicates the location of CPT that used to determine geotechnical parameters for the simulation.

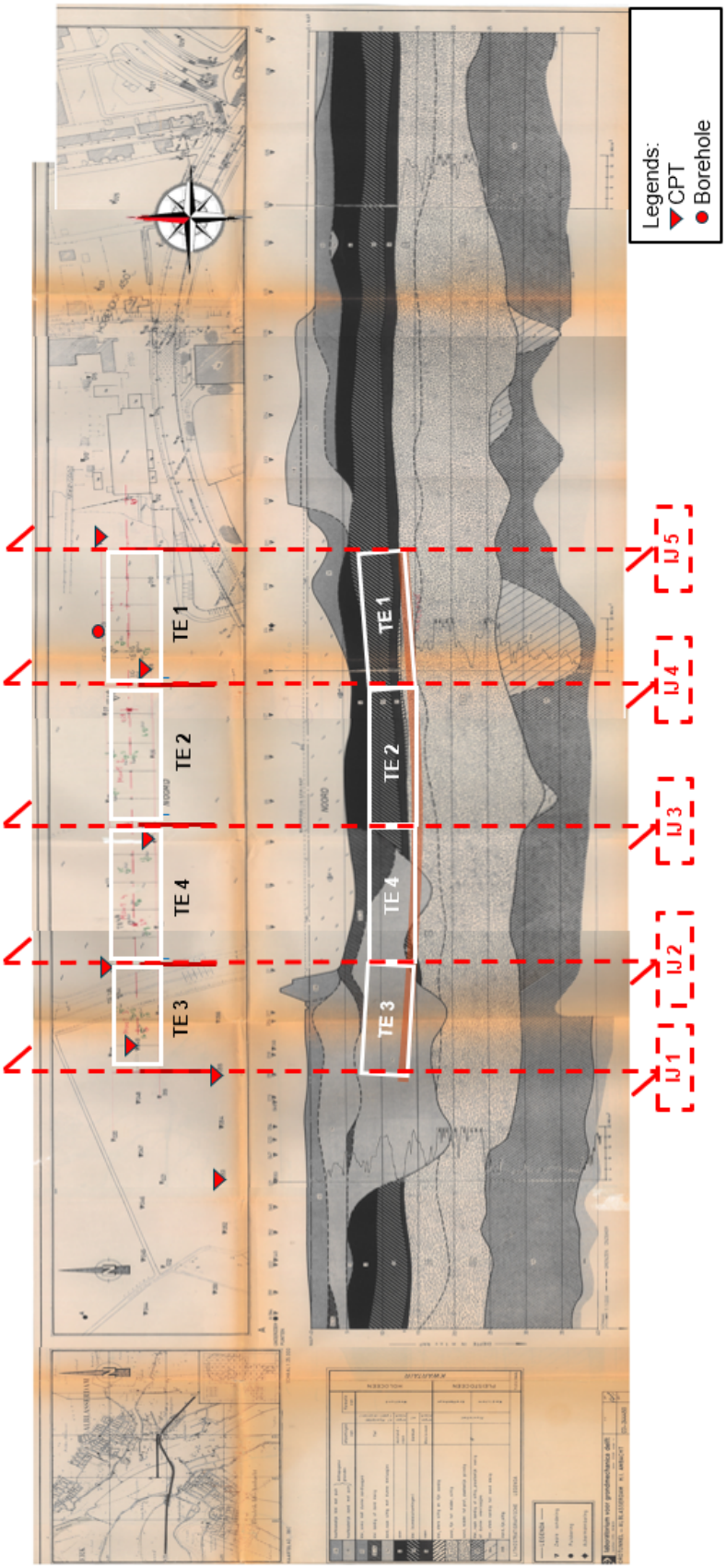

Figure B.1: The site map depicts the soil profile along the Noordtunnel's longitudinal direction

C | APPENDIX C

This appendix is a supplementary section, providing Python code snippet to create Python-PLAXIS interface used for the simulation presented in Chapter 5.

The following is the Python code to make a python-PLAXIS interface to automate the input implemented in this research.

```
#Create Python-PLAXIS Connection
import numpy as np
from math import pi
import math
import os
import sys
import shutil
import subprocess
import time
import pandas as pd
from math import acos, degrees
import imp
import matplotlib.pyplot as plt
from plxscripting.easy import*
s_i, g_i = new_server('localhost', port=10000, password=write your PLAXIS password here)
s_o, g_o = new_server('localhost', port=10001, password=write your PLAXIS password here)
```

Listing C.1: Python code snippet to create Python-Plaxis connection

```
#Create New Project
s_i.new()
# Set model and element properties
g_i.setproperties("Title", "Name of The Project",
                  "UnitForce", "kN",
                  "UnitLength","m")
#Set Model's Boundaries
xmax = 125
xmin = -xmax
ymax = 5
ymin = -75
g_i.SoilContour.initializerectangular(xmin, ymin, xmax, ymax)
#Define types of constitutive laws for soil
softsoil_model = "HS" #Choose "HS" or "SSC"
#Define types of constitutive laws for concrete structure
concrete_model = "LE" #"LE" or "concrete"

#Set the geometry of the tunnel
tunnel_length = 492.7
tunnel_x_loc = 0
tunnel_y_loc = -14.251
tunnel_x_bot = 15.975
tunnel_height = 8.020
tunnel_foot_y = 1.050
tunnel_foot_x = 1.000
tunnel_outerwall_y = 5.665
tunnel_outerwall_x = 13.725
#edge of tunnel
a_edge = 1.250 #x edge
b_edge = 1.305 #y edge
c_edge = np.sqrt(a_edge**2 + b_edge**2)
angle_edge = math.degrees(math.atan2(a_edge, b_edge))
#Tunnel geometry (subsection)
tunnel_slabbot_start = 1.175
tunnel_slabbot_y = 1.4 #m, tunnel bottom slab thickness
tunnel_wall_thick = 1.0 #m, tunnel wall thickness
tunnel_center_wall = 0.5 #m
tunnel_innerwall_y = 5.113
```

```
a_inner_edge = 0.677 #x edge
b_inner_edge = 0.707 #y edge
c_inner_edge = np.sqrt(a_inner_edge**2 + b_inner_edge**2)
angle_inner_edge = math.degrees(math.atan2(a_inner_edge, b_inner_edge))
tunnel_centertube = 1.350
#Tunnel plate (at the middle of the slab and wall)
plate_wall_y = 5.914
plate_roof_x = 13.512
plate_a_edge = 0.963 #x edge
plate_b_edge = 1.006 #y edge
plate_c_edge = np.sqrt(plate_a_edge**2 + plate_b_edge**2)
plate_angle_edge = math.degrees(math.atan2(plate_a_edge, plate_b_edge))

#Set properties of concrete
concrete_stiffness = 30 * 1000000 #kPa (30 GPa)
concrete_unitweight = 25 #kN/m3
b_tunnel = 1 #m, dimension of the tunnel in out of plane direction, i.e.
    perpendicular to the screen
d_bottom = tunnel_slabbot_y #m, thickness at the bottom of tunnel
d_wall = tunnel_wall_thick #m, thickness at the outer wall
d_foot = tunnel_foot_y #m, thickness at the tunnelfoot
d_innerwall = tunnel_center_wall #m, thickness at the inner wall
ballast_concrete_unitweight = 24 #kN/m3
asphalt_unitweight = 22 #kN/m3

#Create the soil geometry
water_level = 0.5 #m, NAP
soil1_topelevation = -4.5 #m
soil1_bottomelevation = -7 #m
soil2_thickness = 7  #thickness soil layer 2
soil3_thickness = 0.5  #thickness soil layer 3
soil4_thickness = 1 #thickness soil layer 4
soil5_thickness = 2.5  #thickness soil layer 5
soil6_thickness = 10  #thickness soil layer 6
soil7_thickness = 10  #thickness soil layer 7
soil8_thickness = 37  #thickness soil layer 8

trench_slope = 4 #trench slope = 1:4
sandfloor_thickness = 0.5
sandflow_thickness = 0.5
y_edge_sandflow = 1.05
soilcover_thickness = 0.5

# Create borehole and define the thickness of each soil layer
borehole1 = g_i.borehole(0)
borehole1.Head = 0.5 # water level
g_i.soillayer(0) #1st layer from top
g_i.soillayer_1.Zones[0].Top = soil1_topelevation
g_i.soillayer_1.Zones[0].Bottom = soil1_bottomelevation #1st layer
g_i.soillayer(soil2_thickness) #2nd layer
g_i.soillayer(soil3_thickness) #3rd layer
g_i.soillayer(soil4_thickness) #4th layer
g_i.soillayer(soil5_thickness) #5th layer
g_i.soillayer(soil6_thickness) #6th layer
g_i.soillayer(soil7_thickness) #7th layer
g_i.soillayer(soil8_thickness) #8th layer
```

Listing C.2: Python code snippet to create new project and set model properties

```
#Example to Define The Soil Properties
g_i.gotosoil()
g_i.gotosoil()
```

```
clay_sandy = g_i.soilmat() #clay (clay sandy or sandy clay), code: 12-14
if softsoil_model == "HS":  #select the soil constitutive law
    #Clay with sand or sandy clay (code: 12-14) properties:
    #General
    clay_sandy.setproperties(("MaterialName", "clay_sandy"), ("SoilModel", 3), ("DrainageType","Undrained (A)")) #HS
    g_i.clay_sandy.gammaUnsat = 16  #gamma Unsat
    g_i.clay_sandy.gammaSat = clay_sandy_gammasat  #gamma sat
    #Parameters
    E_clay_sandy = 2 * 1000 #kPa (E100 in kPa)
    g_i.clay_sandy.E50ref = E_clay_sandy  #E_50_ref
    g_i.clay_sandy.EoedRef = 0.5 * E_clay_sandy    #E_oed_ref
    g_i.clay_sandy.EurRef = 3 * E_clay_sandy #Eur_ref
    g_i.clay_sandy.powerm = 0.8  #power m
    g_i.clay_sandy.cref = 5.4    #cohession
    g_i.clay_sandy.phi = 21.6    #phi, friction angle
    g_i.clay_sandy.nu = 0.2   #nu, Poisson's ratio
    #Groundwater
    g_i.clay_sandy.SoilTypeFlow = "Medium Fine" #groundwater soil type flow
    g_i.clay_sandy.perm_primary_horizontal_axis = 0.00432
    g_i.clay_sandy.perm_vertical_axis = 0.00432
    #Interfaces
    g_i.clay_sandy.InterfaceStrength = "Manual" #Interfaces Strength
    g_i.clay_sandy.Rinter = 0.7 #Rinter

else: #model = Soft Soil Creep
    #Clay with sand or sandy clay (code: 12-14) properties:
    #General
    clay_sandy.setproperties(("MaterialName", "clay_sandy"), ("SoilModel", 6), ("DrainageType","Undrained (A)")) #HS
    g_i.clay_sandy.gammaUnsat = 16  #gamma Unsat
    g_i.clay_sandy.gammaSat = clay_sandy_gammasat  #gamma sat
    #Parameters
    g_i.clay_sandy.lambdaModified = 0.0667  #lambda*
    g_i.clay_sandy.kappaModified = 0.0444  #kappa*
    g_i.clay_sandy.MuModified = 0.0018  #nu*
    g_i.clay_sandy.cref = 5.4    #cohession
    g_i.clay_sandy.phi = 21.6    #phi, friction angle
    #g_i.clay_sandy.psi = g_i.clay_sandy_SSC.phi - 30   #psi, dilatation angle
    g_i.clay_sandy.nu = 0.2   #nu, Poisson's ratio
    #Groundwater
    g_i.clay_sandy.SoilTypeFlow = "Medium Fine" #groundwater soil type flow
    g_i.clay_sandy.perm_primary_horizontal_axis = 0.00432
    g_i.clay_sandy.perm_vertical_axis = 0.00432
    #Interfaces
    g_i.clay_sandy.InterfaceStrength = "Manual" #Interfaces Strength
    g_i.clay_sandy.Rinter = 0.7 #Rinter

#Define the concrete porperties:
#General
if concrete_model == "LE":
    concrete.setproperties(("MaterialName", "concrete"), ("SoilModel", 1), ("DrainageType","Non-porous")) #Concrete
    g_i.concrete.gammaUnsat = concrete_unitweight #gamma Unsat
    g_i.concrete.einit = 0.03  #gamma Unsat
    #Parameters
    E_concrete = concrete_stiffness #kPa (E in kPa)
    nu_concrete = 0.2
    g_i.concrete.Eref = E_concrete  #E28
    g_i.concrete.nu = nu_concrete   #nu, Poisson's ratio
    #g_i.concrete.Gref = E_concrete / (2*(1+nu_concrete))
```

```
    #g.i.concrete.Eoed = E'concrete * (1-nu'concrete) / ((1+nu'concrete) * (1-2*
    nu'concrete))
    #g.i.concrete.Vs = 2215
    #g.i.concrete.Vp = 3617

    ballast'concrete.setproperties(("MaterialName", "ballast'concrete"), ("
    SoilModel", 1), ("DrainageType","Non-porous")) #Concrete
    g.i.ballast'concrete.gammaUnsat = ballast'concrete'unitweight #gamma Unsat
    g.i.ballast'concrete.einit = 0.03  #gamma Unsat
    #Parameters
    E'concrete = concrete'stiffness #kPa (E in kPa)
    nu'concrete = 0.2
    g.i.ballast'concrete.Eref = E'concrete  #E28
    g.i.ballast'concrete.nu = nu'concrete   #nu, Poisson's ratio
    #g.i.concrete.Gref = E'concrete / (2*(1+nu'concrete))
    #g.i.concrete.Eoed = E'concrete * (1-nu'concrete) / ((1+nu'concrete) * (1-2*
    nu'concrete))
    #g.i.concrete.Vs = 2215
    #g.i.concrete.Vp = 3617

else: #concrete model = concrete
    concrete.setproperties(("MaterialName", "concrete"), ("SoilModel", 13), ("
    DrainageType","Non-porous")) #Concrete
    g.i.concrete.gammaUnsat = concrete'unitweight  #gamma Unsat
    g.i.concrete.einit = 0.03  #gamma Unsat
    #Parameters
    E'concrete = 30000 * 1000 #kPa (E100 in kPa)
    g.i.concrete.ppE28 = E'concrete  #E28
    g.i.concrete.nu = 0.2   #nu, Poisson's ratio
    g.i.concrete.phimax = 90   #phi

#Assign soil properties to the soil layers
g.i.setmaterial((g.i.Soillayers[0]), clay'sandy)
g.i.setmaterial((g.i.Soillayers[1]), sand'silty)
g.i.setmaterial((g.i.Soillayers[2]), clay'withplant)
g.i.setmaterial((g.i.Soillayers[3]), peat'base)
g.i.setmaterial((g.i.Soillayers[4]), sand'32)
g.i.setmaterial((g.i.Soillayers[5]), sand'32A)
g.i.setmaterial((g.i.Soillayers[6]), clay'38)
g.i.setmaterial((g.i.Soillayers[7]), sand'38b)
```

Listing C.3: Python code snippet to define soil and concrete properties

```
# Create tunnel outer wall
g.i.gotostructures()
outerwall = g.i.line((tunnel'x'loc, tunnel'y'loc), (tunnel'x'bot, tunnel'y'loc), (
    tunnel'x'bot, tunnel'y'loc+tunnel'foot'y), (tunnel'x'bot-tunnel'foot'x,
    tunnel'y'loc+tunnel'foot'y), (tunnel'x'bot-tunnel'foot'x, tunnel'y'loc+
    tunnel'foot'y+tunnel'outerwall'y), (tunnel'x'bot-tunnel'foot'x-a'edge,
    tunnel'y'loc+tunnel'height), (tunnel'x'loc, tunnel'y'loc+tunnel'height), "
        (-tunnel'x'loc, tunnel'y'loc), (-tunnel'x'bot, tunnel'y'loc), (-
    tunnel'x'bot, tunnel'y'loc+tunnel'foot'y), (-tunnel'x'bot+tunnel'foot'x,
    tunnel'y'loc+tunnel'foot'y), (-tunnel'x'bot+tunnel'foot'x, tunnel'y'loc+
    tunnel'foot'y+tunnel'outerwall'y), (-tunnel'x'bot+tunnel'foot'x+a'edge,
    tunnel'y'loc+tunnel'height), (-tunnel'x'loc, tunnel'y'loc+tunnel'height))
g.i.delete(g.i.line'7)

#Create the hollow space using line
#Center tube
center'tube = g.i.line((-tunnel'centertube/2, tunnel'y'loc+tunnel'slabbot'y), (
    tunnel'centertube/2, tunnel'y'loc+tunnel'slabbot'y), (tunnel'centertube/2,
    tunnel'y'loc + tunnel'height - tunnel'wall'thick), (-tunnel'centertube/2,
```

```
    tunnel.y.loc + tunnel.height - tunnel.wall.thick), (-tunnel.centertube/2,
    tunnel.y.loc+tunnel.slabbot.y))
#Left tube
left.tube = g.i.line((-tunnel.slabbot.start, tunnel.y.loc+tunnel.slabbot.y), (-
    tunnel.x.bot + tunnel.foot.x + tunnel.wall.thick, tunnel.y.loc+
    tunnel.slabbot.y), (-tunnel.x.bot + tunnel.foot.x + tunnel.wall.thick,
    tunnel.y.loc+tunnel.innerwall.y+tunnel.slabbot.y), (-tunnel.x.bot +
    tunnel.foot.x + tunnel.wall.thick + a.inner.edge, tunnel.y.loc+tunnel.height -
     tunnel.wall.thick), (-tunnel.slabbot.start, tunnel.y.loc+tunnel.height -
    tunnel.wall.thick), (-tunnel.slabbot.start, tunnel.y.loc+tunnel.slabbot.y))
#Left tube
right.tube = g.i.line((tunnel.slabbot.start, tunnel.y.loc+tunnel.slabbot.y), (
    tunnel.x.bot - tunnel.foot.x - tunnel.wall.thick, tunnel.y.loc+
    tunnel.slabbot.y), (tunnel.x.bot - tunnel.foot.x - tunnel.wall.thick,
    tunnel.y.loc+tunnel.innerwall.y+tunnel.slabbot.y), (tunnel.x.bot -
    tunnel.foot.x - tunnel.wall.thick - a.inner.edge, tunnel.y.loc+tunnel.height -
     tunnel.wall.thick), (tunnel.slabbot.start, tunnel.y.loc+tunnel.height -
    tunnel.wall.thick), (tunnel.slabbot.start, tunnel.y.loc+tunnel.slabbot.y))

#Adding Plate to the tunnel
Plate.1 = g.i.plate((-tunnel.x.bot  + tunnel.foot.x + tunnel.wall.thick/2,
    tunnel.y.loc+tunnel.slabbot.y/2), (tunnel.x.bot- tunnel.foot.x -
    tunnel.wall.thick/2, tunnel.y.loc+tunnel.slabbot.y/2)) # at the bottom
Plate.2 = g.i.plate((-tunnel.x.bot+ tunnel.foot.x + tunnel.wall.thick/2,
    tunnel.y.loc+tunnel.slabbot.y/2), (-tunnel.x.bot+ tunnel.foot.x +
    tunnel.wall.thick/2, tunnel.y.loc+tunnel.slabbot.y/2+plate.wall.y), (-
    tunnel.x.bot+ tunnel.foot.x + tunnel.wall.thick/2+plate.a.edge, tunnel.y.loc+
    tunnel.slabbot.y/2+plate.wall.y+plate.b.edge)) #left outer wall
Plate.3 = g.i.plate((-tunnel.x.bot+ tunnel.foot.x + tunnel.wall.thick/2+
    plate.a.edge, tunnel.y.loc+tunnel.slabbot.y/2+plate.wall.y+plate.b.edge), (
    tunnel.x.bot- tunnel.foot.x - tunnel.wall.thick/2-plate.a.edge, tunnel.y.loc+
    tunnel.slabbot.y/2+plate.wall.y+plate.b.edge)) # at the roof
Plate.4 = g.i.plate((tunnel.x.bot- tunnel.foot.x - tunnel.wall.thick/2,
    tunnel.y.loc+tunnel.slabbot.y/2), (tunnel.x.bot- tunnel.foot.x -
    tunnel.wall.thick/2, tunnel.y.loc+tunnel.slabbot.y/2+plate.wall.y), (
    tunnel.x.bot- tunnel.foot.x - tunnel.wall.thick/2-plate.a.edge, tunnel.y.loc+
    tunnel.slabbot.y/2+plate.wall.y+plate.b.edge)) #right outer wall

# Add plate at the foot
Plate.5 = g.i.plate((tunnel.x.bot - tunnel.foot.x - tunnel.wall.thick/2,
    tunnel.y.loc+tunnel.slabbot.y/2), (tunnel.x.bot, tunnel.y.loc+tunnel.slabbot.y
    /2))
Plate.6 = g.i.plate((-tunnel.x.bot + tunnel.foot.x + tunnel.wall.thick/2,
    tunnel.y.loc+tunnel.slabbot.y/2), (-tunnel.x.bot, tunnel.y.loc+
    tunnel.slabbot.y/2))
# Add plate at the center tube
Plate.7 = g.i.plate((tunnel.slabbot.start-tunnel.center.wall/2, tunnel.y.loc+
    tunnel.slabbot.y/2), (tunnel.slabbot.start-tunnel.center.wall/2, tunnel.y.loc+
    tunnel.height-tunnel.wall.thick/2))
Plate.8 = g.i.plate((-tunnel.slabbot.start+tunnel.center.wall/2, tunnel.y.loc+
    tunnel.slabbot.y/2), (-tunnel.slabbot.start+tunnel.center.wall/2, tunnel.y.loc
    +tunnel.height-tunnel.wall.thick/2))

#%% Define a material for the tunnel
# Plate for the outer wall
mat.lining.1 = g.i.platemat()
mat.lining.1.setproperties(("MaterialName", "Lining.1"), ("Elasticity", 1), ("
    IsIsotropic", True)) # material is set to elastic which means it assumed that
    failure in the structure is not occurred
g.i.Lining.1.EA = concrete.stiffness/1000 * b.tunnel * d.bottom
g.i.Lining.1.EI = concrete.stiffness/1000 * b.tunnel * (d.bottom**3) / 12
g.i.Lining.1.nu = 0.15  #obtained from Plaxis manual book
```

```
g.i.Lining.1.PreventPunching = False

# Plate for the outer wall
mat_lining_2 = g.i.platemat()
mat_lining_2.setproperties(("MaterialName", "Lining.2"), ("Elasticity", 1), ("IsIsotropic", True)) # material is set to elastic which means it assumed that failure in the structure is not occurred
g.i.Lining.2.EA = concrete_stiffness/1000 * b_tunnel * d_wall
g.i.Lining.2.EI = concrete_stiffness/1000 * b_tunnel * (d_wall**3) / 12
g.i.Lining.2.nu = 0.15  #obtained from Plaxis manual book
g.i.Lining.2.PreventPunching = False

#Plate for the tunnel foot
mat_lining_3 = g.i.platemat()
mat_lining_3.setproperties(("MaterialName", "Lining.3"), ("Elasticity", 1), ("IsIsotropic", True)) # material is set to elastic which means it assumed that failure in the structure is not occured
g.i.Lining.3.EA = concrete_stiffness/1000 * b_tunnel * d_foot
g.i.Lining.3.EI = concrete_stiffness/1000 * b_tunnel * (d_foot**3) / 12
g.i.Lining.3.nu = 0.15  #obtained from Plaxis manual book
g.i.Lining.3.PreventPunching = False

#Plate for the center tube
mat_lining_4 = g.i.platemat()
mat_lining_4.setproperties(("MaterialName", "Lining.4"), ("Elasticity", 1), ("IsIsotropic", True)) # material is set to elastic which means it assumed that failure in the structure is not occured
g.i.Lining.4.EA = concrete_stiffness/1000 * b_tunnel * d_innerwall
g.i.Lining.4.EI = concrete_stiffness/1000 * b_tunnel * (d_innerwall**3) / 12
g.i.Lining.4.nu = 0.15  #obtained from Plaxis manual book
g.i.Lining.4.PreventPunching = False

# Assign material for each segments
g.i.setmaterial((g.i.Plate.1), mat_lining_1)
g.i.setmaterial((g.i.Plate.2, g.i.Plate.3, g.i.Plate.4, g.i.Plate.5, g.i.Plate.6), mat_lining_2)
g.i.setmaterial((g.i.Plate.7, g.i.Plate.8), mat_lining_3)
g.i.setmaterial((g.i.Plate.9, g.i.Plate.10), mat_lining_4)
#Create negative interface
g.i.neginterface(g.i.Line.27, g.i.Line.28, g.i.Line.29, g.i.Line.30, g.i.Line.31, g.i.Line.32, g.i.Line.33, g.i.Line.34, g.i.Line.35, g.i.Line.36)
```

Listing C.4: Python code snippet to create tunnel geometry

```
g.i.gotostructures()
# Geometry of the slope
x_sidesand = 5 #side-wide / offset distance of the sand flow below the tunnel (exclude the tunnel wide)
y_slope = np.abs(tunnel_y_loc - 1 - g.i.Soillayer.1.Zones[0].Top)
x_slope = trench_slope * y_slope #because the slope is 1:4
l_slope = np.sqrt(x_slope*x_slope + y_slope*y_slope)

#Geometry of the sand flow foundation
x_edge_sandflow = trench_slope * sandflow_thickness
#trench line
trench_line   = g.i.line((-tunnel_x_bot+tunnel_foot_x-x_sidesand-x_slope, g.i.Soillayer.1.Zones[0].Top), (-tunnel_x_bot+tunnel_foot_x-x_sidesand, tunnel_y_loc-1), (+tunnel_x_bot-tunnel_foot_x+x_sidesand, tunnel_y_loc-1), (+tunnel_x_bot-tunnel_foot_x+x_sidesand+x_slope, g.i.Soillayer.1.Zones[0].Top))
trench_line_2 = g.i.line((-tunnel_x_bot+tunnel_foot_x-x_sidesand, tunnel_y_loc-1), (-tunnel_x_bot+tunnel_foot_x-x_sidesand, soil5_thickness+soil6_thickness+soil7_thickness+soil8_thickness-75))
```

```
trench_line_3 = g_i.line((+tunnel_x_bot-tunnel_foot_x+x_sidesand, soil5_thickness+soil6_thickness+soil7_thickness+soil8_thickness-75), (+tunnel_x_bot-tunnel_foot_x+x_sidesand, tunnel_y_loc-1))
#sandflow line
sandflow_line = g_i.line((-tunnel_x_bot+tunnel_foot_x-x_sidesand-x_edge_sandfloor-x_edge_sandflow, tunnel_y_loc), (+tunnel_x_bot-tunnel_foot_x+x_sidesand+x_edge_sandfloor+x_edge_sandflow, tunnel_y_loc))
#soil cover
x_edge_soilcover = (tunnel_height+soilcover_thickness)*4
x_edge_soilcover2 = (tunnel_height)*4
soilcover_line = g_i.line((-tunnel_x_bot+tunnel_foot_x-x_sidesand-x_edge_sandfloor-x_edge_sandflow - x_edge_soilcover, tunnel_y_loc+tunnel_height+soilcover_thickness), (+tunnel_x_bot-tunnel_foot_x+x_sidesand+x_edge_sandfloor+x_edge_sandflow+x_edge_soilcover, tunnel_y_loc+tunnel_height+soilcover_thickness))
soilcover_line2 = g_i.line((-tunnel_x_bot+tunnel_foot_x-x_sidesand-x_edge_sandfloor-x_edge_sandflow - x_edge_soilcover2, tunnel_y_loc+tunnel_height), (+tunnel_x_bot-tunnel_foot_x+x_sidesand+x_edge_sandfloor+x_edge_sandflow+x_edge_soilcover2, tunnel_y_loc+tunnel_height))
```

Listing C.5: Python code snippet to create trench slope and sand foundation

```
#Concrete volweight
concrete_vol_bot = ((tunnel_x_bot - tunnel_foot_x - tunnel_wall_thick) * tunnel_slabbot_y) * 2
concrete_vol_foot = (tunnel_foot_x * tunnel_foot_y) * 2
concrete_vol_outerwall = (tunnel_wall_thick * (tunnel_height - tunnel_slabbot_y - tunnel_wall_thick)) * 2
concrete_vol_innerwall = (tunnel_center_wall * tunnel_innerwall_y) * 2
concrete_vol_roof = ((tunnel_x_bot - tunnel_foot_x - tunnel_wall_thick) * tunnel_wall_thick) * 2
total_concrete_vol = concrete_vol_bot + concrete_vol_foot + concrete_vol_outerwall + concrete_vol_innerwall + concrete_vol_roof
volweight_concrete = total_concrete_vol * concrete_gammaUnsat
total_volweight_applied = volweight_sandfloor + volweight_sandflow + volweight_concrete

#Buoyancy effect
#Hollow space area
hollow_space_center = (tunnel_centertube * (tunnel_height - tunnel_slabbot_y - tunnel_wall_thick))
hollow_space_side = (((tunnel_x_bot - tunnel_centertube/2 - tunnel_center_wall - tunnel_foot_x - tunnel_wall_thick) * tunnel_innerwall_y) + ((tunnel_x_bot - tunnel_centertube/2 - tunnel_center_wall - tunnel_foot_x - tunnel_wall_thick - a_inner_edge) * b_inner_edge) + (a_inner_edge * b_inner_edge/2)) * 2
hollow_space = hollow_space_center + hollow_space_side

#Ballast beton weight
width_ballastconcrete = np.abs(tunnel_x_bot -tunnel_centertube/2 - tunnel_center_wall - tunnel_foot_x - tunnel_wall_thick)
height_ballastconcrete = 0.649 #m
vol_ballastconcrete = width_ballastconcrete * height_ballastconcrete
weight_ballastconcrete = width_ballastconcrete * height_ballastconcrete * ballast_concrete_unitweight

#Hollow space during operational
hollow_space_operational = (tunnel_centertube * tunnel_innerwall_y) + ((tunnel_x_bot - tunnel_foot_x - tunnel_wall_thick - tunnel_slabbot_start) * (tunnel_innerwall_y - height_ballastconcrete)) * 2

#Asphalt Weight
```

```
width_asphalt = np.abs(tunnel_x_bot -tunnel_centertube/2 - tunnel_center_wall - tunnel_foot_x - tunnel_wall_thick)
height_asphalt = 0.07 #m
vol_asphalt = width_asphalt * height_asphalt
weight_asphalt = width_asphalt * height_asphalt * asphalt_unitweight

#Soil above the foot tunnel
h_soil_abovefoot = tunnel_height - tunnel_foot_y
weight_soilabovefoot = h_soil_abovefoot * tunnel_foot_x * (soil_cover_gammasat - gammawater)

#Volume above the tunnel roof
t_8 = np.abs(tunnel_y_loc) - np.abs(tunnel_height) - np.abs(soil1_topelevation)
a_8 = tunnel_outerwall_x*2
weight_roof_backfill = a_8 * t_8 * (soil_cover_gammasat - gammawater)

#Buoyancy effect
SF_immersion = 1.05
ballast_water_immersion = ((SF_immersion * (hollow_space + total_concrete_vol) * gammawater) - volweight_concrete) / 2 / (tunnel_x_bot -tunnel_centertube/2 - tunnel_center_wall - tunnel_foot_x - tunnel_wall_thick)
udl_ballast_concrete = weight_ballastconcrete / (width_ballastconcrete * 1)
udl_asphalt = weight_asphalt / (width_asphalt * 1)

SF_operational = 1.1
R_uplift = ((hollow_space + total_concrete_vol) * gammawater)
R_down = volweight_concrete + weight_ballastconcrete*2 + weight_asphalt*2

delta_R = R_down - R_uplift
SF_operation = R_down/R_uplift

deadload_operational = ((SF_operational * R_uplift) - R_down)
delta_dl_operation = 100 - deadload_operational
DL_operation = (deadload_operational+delta_dl_operation) / 2 / (tunnel_x_bot - tunnel_centertube/2 - tunnel_center_wall - tunnel_foot_x - tunnel_wall_thick)
udl_operation = udl_ballast_concrete + udl_asphalt + DL_operation

#Adding the line load to represents the water tank during immersion
LineLoad_1 = g_i.lineload((tunnel_slabbot_start), (tunnel_y_loc+tunnel_slabbot_y), (tunnel_x_bot - tunnel_foot_x - tunnel_wall_thick), tunnel_y_loc+tunnel_slabbot_y)
LineLoad_2 = g_i.lineload((-tunnel_slabbot_start), (tunnel_y_loc+tunnel_slabbot_y), (-tunnel_x_bot + tunnel_foot_x + tunnel_wall_thick), tunnel_y_loc+tunnel_slabbot_y)
g_i.LineLoad_1.qy_start = -(ballast_water_immersion) #in the right tube
g_i.LineLoad_2.qy_start = -(ballast_water_immersion) #in the left tube
```

Listing C.6: Python code snippet to calculate the load and safety factor

```
g_i.gotomesh()
msize = 0.03
g_i.mesh(msize, True)
```

Listing C.7: Python code snippet to generate mesh

```
# Staged Construction
g_i.gotostages()
g_i.InitialPhase.Identification = "Initial"
g_i.InitialPhase.DeformCalcType = "k0 procedure"
g_i.InitialPhase.PorePresCalcType = "Phreatic"

```

```
g.i.activate((g.i.GWFlowBaseBC.116, g.i.GWFlowBaseBC.114, g.i.GWFlowBaseBC.111, g.i.GWFlowBaseBC.108, g.i.GWFlowBaseBC.105, g.i.GWFlowBaseBC.95, g.i.GWFlowBaseBC.81, g.i.GWFlowBaseBC.52, g.i.GWFlowBaseBC.7, "
            g.i.GWFlowBaseBC.115, g.i.GWFlowBaseBC.112, g.i.GWFlowBaseBC.109, g.i.GWFlowBaseBC.106, g.i.GWFlowBaseBC.96, g.i.GWFlowBaseBC.82, g.i.GWFlowBaseBC.55, g.i.GWFlowBaseBC.8), g.i.InitialPhase)
g.i.GWFlowBaseBC.116.Behaviour[g.i.InitialPhase]= "Closed"
g.i.GroundwaterFlow.BoundaryYMin[g.i.InitialPhase]= "Closed"

# 1st Phase (Trench Excavation)
phase1 = g.i.phase(g.i.InitialPhase)
phase1.Identification = "Trench Excavation"
phase1.DeformCalcType = "Plastic"
phase1.PorePresCalcType = "Phreatic"
phase1.TimeInterval = time.phase.1
phase1.Deform.IgnoreUndrainedBehaviour = True
phase1.Deform.ResetDisplacementsToZero = True
g.i.deactivate((g.i.Soil.1.1, g.i.Soil.1.4, g.i.Soil.1.6, g.i.Soil.1.5, g.i.Soil.1.8, g.i.Soil.1.7, "
              g.i.Soil.2.1, g.i.Soil.2.9, g.i.Soil.2.7, g.i.Soil.2.4, g.i.Soil.2.3, g.i.Soil.2.6, g.i.Soil.2.8, g.i.Soil.2.5, g.i.Soil.2.10, g.i.Soil.2.2, g.i.Soil.2.13, "
              g.i.Soil.3.1, g.i.Soil.3.3, g.i.Soil.3.2, g.i.Soil.3.6, "
              g.i.Soil.4.1), phase1)
g.i.GroundwaterFlow.BoundaryYMin[g.i.Phase.1]= "Closed"

# 2nd Phase
phase2 = g.i.phase(phase1)
phase2.Identification = "Sandflow Foundation"
phase2.DeformCalcType = "Plastic"
phase2.PorePresCalcType = "Phreatic"
phase2.TimeInterval = time.phase.2
phase2.Deform.IgnoreUndrainedBehaviour = True
phase2.Deform.ResetDisplacementsToZero = False
g.i.activate((g.i.Soil.4.1, g.i.Soil.3.6,), phase2)
g.i.Soil.4.1.setmaterial(phase2, sandflow.foundation)
g.i.Soil.3.6.setmaterial(phase2, sandflow.foundation)
g.i.GroundwaterFlow.BoundaryYMin[g.i.Phase.2]= "Closed"

# 3rd Phase
phase3 = g.i.phase(phase2)
phase3.Identification = "Immersion Phase"
phase3.DeformCalcType = "Plastic"
phase3.PorePresCalcType = "Phreatic"
phase3.TimeInterval = time.phase.3
phase3.Deform.IgnoreUndrainedBehaviour = True
phase3.Deform.ResetDisplacementsToZero = False
g.i.activate((g.i.Soil.3.3, "
              g.i.Soil.2.13, g.i.Soil.2.9, g.i.Soil.2.7, g.i.Soil.2.6, g.i.Soil.2.8, g.i.Soil.2.10, "
              g.i.Soil.1.8, g.i.Soil.1.5, "
              g.i.Lineload.1, g.i.Lineload.2), phase3)
g.i.Soil.3.3.setmaterial(phase3, concrete)
g.i.Soil.2.13.setmaterial(phase3, concrete)
g.i.Soil.2.9.setmaterial(phase3, concrete)
g.i.Soil.2.7.setmaterial(phase3, concrete)
g.i.Soil.2.6.setmaterial(phase3, concrete)
g.i.Soil.2.8.setmaterial(phase3, concrete)
g.i.Soil.2.10.setmaterial(phase3, concrete)
g.i.Soil.1.8.setmaterial(phase3, concrete)
g.i.Soil.1.5.setmaterial(phase3, concrete)
```

```
g.i.activate((g.i.Line.27, g.i.Line.28, g.i.Line.29, g.i.Line.30, g.i.Line.31, g.i
    .Line.32, g.i.Line.33, g.i.Line.34, g.i.Line.35, g.i.Line.36), phase3)
g.i.GroundwaterFlow.BoundaryYMin[g.i.Phase.3]= "Closed"
g.i.WaterConditions.2.3.Conditions[g.i.Phase.3] = "Dry"
g.i.WaterConditions.2.4.Conditions[g.i.Phase.3] = "Dry"
g.i.WaterConditions.2.5.Conditions[g.i.Phase.3] = "Dry"

# 4th Phase
phase4 = g.i.phase(phase3)
phase4.Identification = "Sand Backfill"
phase4.DeformCalcType = "Plastic"
phase4.PorePresCalcType = "Phreatic"
phase4.TimeInterval = time.phase.4
phase4.Deform.IgnoreUndrainedBehaviour = False
phase4.Deform.ResetDisplacementsToZero = False
g.i.activate((g.i.Soil.3.1, g.i.Soil.3.2, g.i.Soil.2.1, g.i.Soil.2.2, "
              g.i.Soil.1.6, g.i.Soil.1.7, g.i.Soil.1.4), phase4)
g.i.LineLoad.1.1.qy.start.set(g.i.Phase.4, -(ballast.water.immersion)*0.75)
g.i.LineLoad.2.1.qy.start.set(g.i.Phase.4, -(ballast.water.immersion)*0.75)
g.i.Soil.3.1.setmaterial(phase4, soil.cover)
g.i.Soil.3.2.setmaterial(phase4, soil.cover)
g.i.Soil.2.1.setmaterial(phase4, soil.cover)
g.i.Soil.2.2.setmaterial(phase4, soil.cover)
g.i.Soil.1.6.setmaterial(phase4, soil.cover)
g.i.Soil.1.7.setmaterial(phase4, soil.cover)
g.i.Soil.1.4.setmaterial(phase4, soil.topcover)
g.i.GroundwaterFlow.BoundaryYMin[g.i.Phase.4]= "Closed"

# 5th Phase
phase5 = g.i.phase(phase4)
phase5.Identification = "Ballast Concrete"
phase5.DeformCalcType = "Consolidation"
phase5.PorePresCalcType = "Phreatic"
phase5.TimeInterval = time.phase.5
g.i.LineLoad.1.1.qy.start.set(g.i.Phase.5, -(udl.operation))
g.i.LineLoad.2.1.qy.start.set(g.i.Phase.5, -(udl.operation))
g.i.GroundwaterFlow.BoundaryYMin[g.i.Phase.5]= "Closed"

# 6th Phase
phase6 = g.i.phase(phase5)
phase6.Identification = "Open For Traffic"
phase6.DeformCalcType = "Consolidation"
phase6.PorePresCalcType = "Phreatic"
phase6.TimeInterval = time.phase.6 # 75
g.i.LineLoad.1.1.qy.start.set(g.i.Phase.6, -(udl.operation + total.vehicle.load))
g.i.LineLoad.2.1.qy.start.set(g.i.Phase.6, -(udl.operation + total.vehicle.load))
g.i.GroundwaterFlow.BoundaryYMin[g.i.Phase.6]= "Closed"

# Tunnel operational time
for n in range(9):
    g.i.phase(g.i.Phases[-1])
    g.i.Phases[-1].DeformCalcType = "Consolidation"
    g.i.Phases[-1].PorePresCalcType = "Phreatic"
    g.i.Phases[-1].TimeInterval = 3650 #per 10 years
    g.i.Phases[-1].Deform.ForceFullyDrainedOnActivation = False
    g.i.GroundwaterFlow.BoundaryYMin[g.i.Phases[-1]]= "Closed"

#%% Select meshpoint for monitoring:
g.i.selectmeshpoints()
g.o.addcurvepoint('node', g.o.Soil.4.2, (0, -14.81))
g.o.addcurvepoint('node', g.o.Soil.4.2, (-13.99, -14.88))
g.o.addcurvepoint('node', g.o.Soil.4.2, (13.99, -14.88))
```

```
g_o.addcurvepoint('node', g_o.Soil_3_3, (0, -14.25))
g_o.addcurvepoint('node', g_o.Soil_4_1, (0, -14.75))
g_o.addcurvepoint('node', g_o.Soil_4_2, (0, -15.25))
g_o.addcurvepoint('node', g_o.Soil_4_5, (0, -15.50))
g_o.addcurvepoint('node', g_o.Soil_5_1, (0, -18.00))
g_o.addcurvepoint('node', g_o.Soil_6_1, (0, -28.00))
g_o.addcurvepoint('node', g_o.Soil_7_1, (0, -38.00))
g_o.addcurvepoint('node', g_o.Soil_8_1, (0, -75.00))

# Set which phase to calculate
g_i.InitialPhase.ShouldCalculate = True
phase1.ShouldCalculate = True
phase2.ShouldCalculate = True
phase3.ShouldCalculate = True
phase4.ShouldCalculate = True
phase5.ShouldCalculate = True
phase6.ShouldCalculate = True
phase7.ShouldCalculate = True
phase8.ShouldCalculate = True
phase9.ShouldCalculate = True
phase10.ShouldCalculate = True
phase11.ShouldCalculate = True
phase12.ShouldCalculate = True
phase13.ShouldCalculate = True
phase14.ShouldCalculate = True
phase15.ShouldCalculate = True
phase16.ShouldCalculate = True

# Run the calculation
g_i.calculate()
```

Listing C.8: Python code snippet for the construction stages

The following listing is the snippet of the Python code for extracting the settlement result at the specific node in PLAXIS output.

```
#Retrieve settlement at selected node
def getnodeid_result(phase, resulttype, nodeid):
    nodeindex = None
    resultLocation = 'Node'
    _resulttypeID = g_o.ResultTypes.Soil.NodeID
    _nodeids = g_o.getresults(phase, _resulttypeID, resultLocation)
    nodeindex = _nodeids[:].index(nodeid)
    if nodeindex is not None:
        _resultvalues = g_o.getresults(phase, resulttype, resultLocation)
        _requestedvalue = _resultvalues[nodeindex]
        return _requestedvalue
    print('Could not find the requested node number in the results of this phase')
    return None
def getnodeid_x(phase, nodeid):
    return getnodeid_result(phase, g_o.ResultTypes.Soil.X, nodeid)
def getnodeid_y(phase, nodeid):
    return getnodeid_result(phase, g_o.ResultTypes.Soil.Y, nodeid)
def getnodeid_uy(phase, nodeid):
    return getnodeid_result(phase, g_o.ResultTypes.Soil.Uy, nodeid)

node_number = 48021 #node selected for data extraction
uy_0 = 0 #choose the stage
print("Node -" Phase_0: uy_0 = -" m".format(node_number, uy_0))
```

Listing C.9: Python code snippet to extract settlement result in the PLAXIS output

ACRONYMS

2D Two Dimension v
CPT Cone Penetration Test v
DOFS Distributed Optical Fiber Sensor v
FEM Finite Element Method v
HS Model Hardening Soil Model v
LM 1 LM 1 52
NAP Normal Amsterdam Peil 25
OCR Over Consolidated Ratio 29
SSC Model Soft Soil Creep Model v
TS Tandem System 52
UDL Uniform Distributed Load 52
VWSG Vibrating Wire Strain Gauges 85

LIST OF SYMBOLS

a	Net area ratio
c	Soil cohesion
C_{AGE}	Aging factor
C_{α}	Creep index
C_c	Compression index
C_{OCR}	Overconsolidation factor
C_{qc}	Cone resistance correction factor
C_r	Reloading index
C_{sw}	Swelling index
D_r^2	Soil relative density
e	Void ratio
e_{max}	Maximum Void ratio
e_{min}	Minimum Void ratio
EA	Normal rigidity of plate
EI	Flexional rigidity of plate
E_{50}^{ref}	Secant stiffness in triaxial test
E_{oed}^{ref}	Tangent stiffness in Oedometer test
E_{ur}^{ref}	Stiffness in unloading/reloading
F_r	Normalized friction ratio
f_s	CPT sleeve friction
G_0	Soil small strain modulus
γ_{sat}	Soil volumetric unit weight
k	Hydraulic conductivity
λ^*	Modified compression index
μ^*	Modified creep index
κ^*	Modified swelling index
m	Power depends on the type of soil
n	Soil compressibility factor
OCR	Over consolidation ratio
ϕ'	Soil effective internal friction angle
p^{ref}	Isotropic stress level
Q_{tn}	Normalized tip resistance
$q_{c,table}$	Modified cone resistance
q_c	CPT tip resistance
q_t	Normalized cone resistance
R_f	CPT friction ratio
σ_{v0}	Total vertical stress
σ'_{v0}	Effective vertical stress
s	Standard deviation
u_2	Measured pore pressure
$\bar{x}$	Mean